Design and synthesis of chemical probes for investigations into sulforaphane metabolism

Andrei Albulescu

Submitted in partial fulfilment of the requirements of Liverpool John Moores University for the Degree of Doctor of Philosophy

March 2022

ACKNOWLEDGEMENTS

ABSTRACT

Sulforaphane (**1**: 1-isothiocyanato-4-methylsulfinylbutane), one of several isothiocyanates (ITCs) that can be isolated from vegetables of the *Brassica* family, has attracted significant interest due to its chemopreventive activity (**Fig. A.1**). Previous investigations into its activity have revealed that it can bind to Kelch-like ECH associated protein 1 (Keap1) leading to the accumulation of transcription factor nuclear factor erythroid-2 related factor 2 (Nrf2), which activates the transcription of phase II enzymes involved in conjugation reactions. **1** is also involved in a variety of other underexplored pathways, including inflammation, apoptosis and cell cycle arrest, making it an interesting candidate for therapeutic applications beyond cancer. However, due to its low stability in physiological conditions and lack of distinguishing chemical features, the full complement of biological interactions has not been determined, and few synthetic analogs have been synthesized.
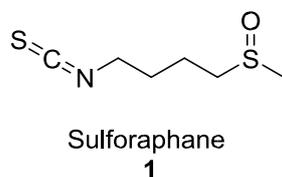
Sulforaphane
1

Fig. A.1 Sulforaphane

This thesis aims to address these challenges by designing, making and testing chemical probes that mimic the structure and activity of **1** while containing moieties that allow tracing their interactions after administration in cell systems. Furthermore, we focused on assessing whether the new derivatives of **1** show improved stability and/or activity compared to the parent compound.

Chapter 1 provides an introduction to cancer, chemoprevention and a summary of the known roles of sulforaphane. Chapter 2 describes an initial approach to introduce fluorinated reporter

groups into the sulforaphane parent molecule and related analogues to be detected using ^{19}FNMR. This work involved the synthesis of a library of fluorinated isothiocyanates (F-ITCs), bearing modifications to the oxidation state of the sulfur atom and the length of the carbon chain between the sulfur group and the isothiocyanate, in two separate series using either a trifluoroethyl or a trifluoromethyl reporter group (**Fig. A.2**). This provided the opportunity to obtain preliminary structure-activity relationships within this structural class.
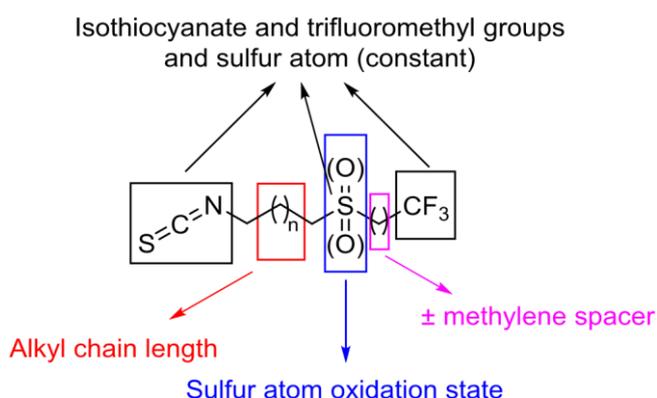
Fig. A.2 Diversity in the library of fluorinated derivatives of sulforaphane

The fluorinated compounds were synthesized in 20-42% overall yields over 3-5 steps and 1136% over 4-6 steps for the trifluoroethyl and the trifluoromethyl series, respectively. Biological testing comparing the F-ITCs with the corresponding natural ITCs sulforaphane, iberin, erucin and erysolin showed that the oxidation state of the sulfur atom is a key factor in determining pro-apoptotic activity. In the trifluoroethyl series, the 4-carbon sulfoxide **82** (**Fig. A.3**) showed improved activity compared to **1**. ^{19}F-NMR studies revealed that the compounds are detectable down to concentrations of ~2 µM, comparable to the dietary concentrations of ITCs.

82
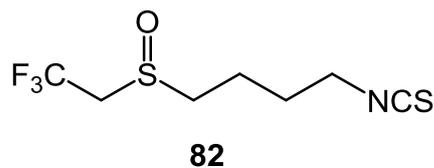
Fig. A.3 Fluorinated derivative of sulforaphane **82**

Chapter 3 explored an alternative approach, based on CuAAC "click" chemistry, and involved the synthesis of an alkyne derivative of **1**, which was able to participate in copper catalyzed alkyne-azide cycloaddition reactions with azides bearing relevant payloads. The alkyne probe **156** was synthesized in overall yield, while a mitochondria-targeting TPP$^+$ based azide was also obtained. The alkyne and the triazol **167** resulting from the "click" reaction between the alkyne and the TPP$^+$ probe were taken into biological testing. Interestingly, at 10 µM concentrations the alkyne showed improved pro-apoptotic activity compared to sulforaphane; however, the mitochondria targeting probe showed little activity, raising the possibility that the mitochondria are not the relevant organelles in **1** apoptotic activity.

156   **167**
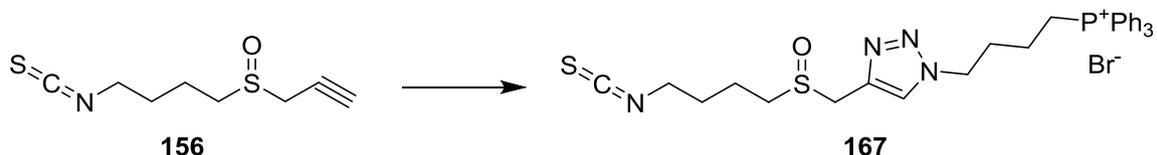
Scheme A.1 Synthesis of a triphenylphosphonium "click" probe

The alkyne probe may be a useful tool in investigating the metabolism of **1** (and related natural product isothiocyanates) and future work will focus on developing "click" reactions between azides and fluorescent or biotinylated moieties, leading to the detection, capture and identification of biomolecules that the probe binds to as well as facilitating assessment of subcellular distribution.

TABLE OF CONTENTS

LIST OF ABBREVIATIONS

AD	Alzheimer's disease
AIF	Apoptosis inducing factor
ARE	Antioxidant response element
BSE	Broccoli sprouts extract
CAD	Caspase-activated DN-ase
CDK	Cyclin-dependent kinase
CI	Combination Index
cLogP	Calculated LogP
CSC	Cancer stem cell
CuAAC	Copper-catalysed Azide-Alkyne Cycloaddition
DAST	*N,N*-diethylamino sulfur trifluoride
DIPEA	*N,N*-diisopropylethylamine
Eru	Erucin
Ery	Erysolin
FADD	Fas associated protein with death domain
FasL	(FS-7 associated surface antigen) ligand
F-ITC	Fluorinated isothiocyanate
FSC	Forward Scattered Light
GCL	Glutamate-cysteine ligase
GPCR	G-protein coupled receptor
GST	Glutathione-S-transferase
HAT	Histone acetyl transferase
HDAC	Histone deacetylase
HDI	Human development index
HIF1α	Hypoxia inducing factor 1 alpha
HO-1	Heme oxygenase 1
Ibe	Iberin
IKK	Inhibitor of kappa B kinase
IL-6	Interleukin 6
ITC	Isothiocyanate
IκB	Inhibitor of kappa B
JC-1	First J-aggregate forming cationic dye
Keap1	Kelch-like ECH associated protein 1

LC/MS	Liquid chromatography coupled with mass spectrometry
LOD	Limit of detection
LOQ	Limit of quantitation
mCPBA	3(*meta*)-chloro-perbenzoic acid
MRI	Magnetic resonance imaging
MTG	MitoTracker Green
NF-κB	Nuclear factor kappa B
NMR	Nuclear magnetic resonance
NQO-1	NAD(P)H Dehydrogenase Quinone 1
Nrf2	nuclear factor erythroid-2 related factor 2
PBS	Phosphate Buffer Saline
PET	Positron Emission Tomography
QR	Quinone reductase
QSAR	Quantitative structure-activity relationship
RA	Rheumatoid Arthritis
RPMI 1640 (media)	Rosswell Park Memorial Institute 1640
S/N	Signal to noise ratio
SF	Sulforaphane
SPAAC	Strain-Promoted Azide-Alkyne Cycloaddition
SS peptides	Szeto-Schiller peptides
SSC	Side Scattered Light
STAT3	Signal transducer and activator of transcription 3
TBTA	Tris[(1-benzyl-1*H*-1,2,3-triazol-4-yl)methyl]amine
TLC	Thin layer chromatography
TMSCF$_3$	Trifluoromethyltrimethylsilane (Ruppert-Prakash Reagent)
TNFα	Tumour necrosis factor alpha
TPP$^+$	Triphenylphosphonium
TPSA	Topological Polar Surface Area
VEGF	Vascular endothelial growth factor

CHAPTER 1

INTRODUCTION

1.1. Cancer and chemoprevention

Cancer is one of the major sources of mortality and morbidity in the world, being the main cause of premature deaths in 55 countries, including most of Western Europe, and one of the top four causes in 179 countries. With over 18 million new cases and over 9 million cancerrelated deaths in 2018 (**Fig. 1.1**), as well as an annual cost of care exceeding 1 trillion US dollars, the burden of cancer makes it one of the foremost world health priorities (Bernard & Christopher, 2020).

There are >200 distinct types of cancer, but what they have in common is the development of uncontrollable cell growth (tumours) with the potential to invade other areas in the body (Hanahan & Weinberg, 2011). The causes of cancer are often complex, with genetics and environment combining towards abnormal cell function. According to the prevalent somatic mutation theory, cancers start with a genetic change in a cell, which is then inherited by its progeny (Martincorena & Campbell, 2015). For this to occur, several important cellular systems have to fail to function properly, including DNA repair, apoptosis, senescence, and autophagy. Further, the growth of tumours requires subsuming normal cell machinery to initiate angiogenesis (Carmeliet & Jain, 2000; Otrock *et al.*, 2007), the growth of blood vessels required as a source of oxygen and nutrients, and cells also acquire the ability to migrate and invade other tissues, in a process called metastasis (Talmadge & Fidler, 2010).

Major risk factors for cancer include smoking, infectious agents, ultraviolet radiation, and chemicals, with certain types of cancer showing strong associations with specific factors (e.g.,

in melanoma and skin cancers 65-90% of the risks are attributable to sun exposure/UV radiation; human papilloma virus (HPV) may be the cause of 90% of the cases of cervical cancer, while *Helicobacter pylori* could be involved in 65-80% of gastric cancer cases)(Wu *et al.*, 2016). Diet can also influence cancer risk, with certain foods, such as processed meat products, shown to increase the risks of colorectal cancer (Baena & Salinas, 2015; Vargas & Thompson, 2012; Wiseman, 2018). In particular, the Western diet is considered one of reasons behind the increased incidence for certain cancers, including colorectal, stomach and liver cancers, in countries with a high/very high human development index (HDI), compared to that in countries with a low HDI (**Fig. 1.1**). However, a diet rich in fruit and vegetables, such as the Mediterranean diet, reduces the risks for certain cancers, an effect known as chemoprevention (Farinetti *et al.*, 2017; Mentella *et al.*, 2019; Tsao *et al.*, 2004; Wattenberg, 1985).

Chemoprevention is divided into primary, secondary, and tertiary chemoprevention. Primary chemoprevention refers to protection against cancer in a healthy person; secondary chemoprevention means preventing a pre-cancerous area from developing cancer, whereas tertiary chemoprevention refers to preventing the reoccurrence of cancer in a patient who has previously had cancer (Landis-piwowar & Iyer, 2014).
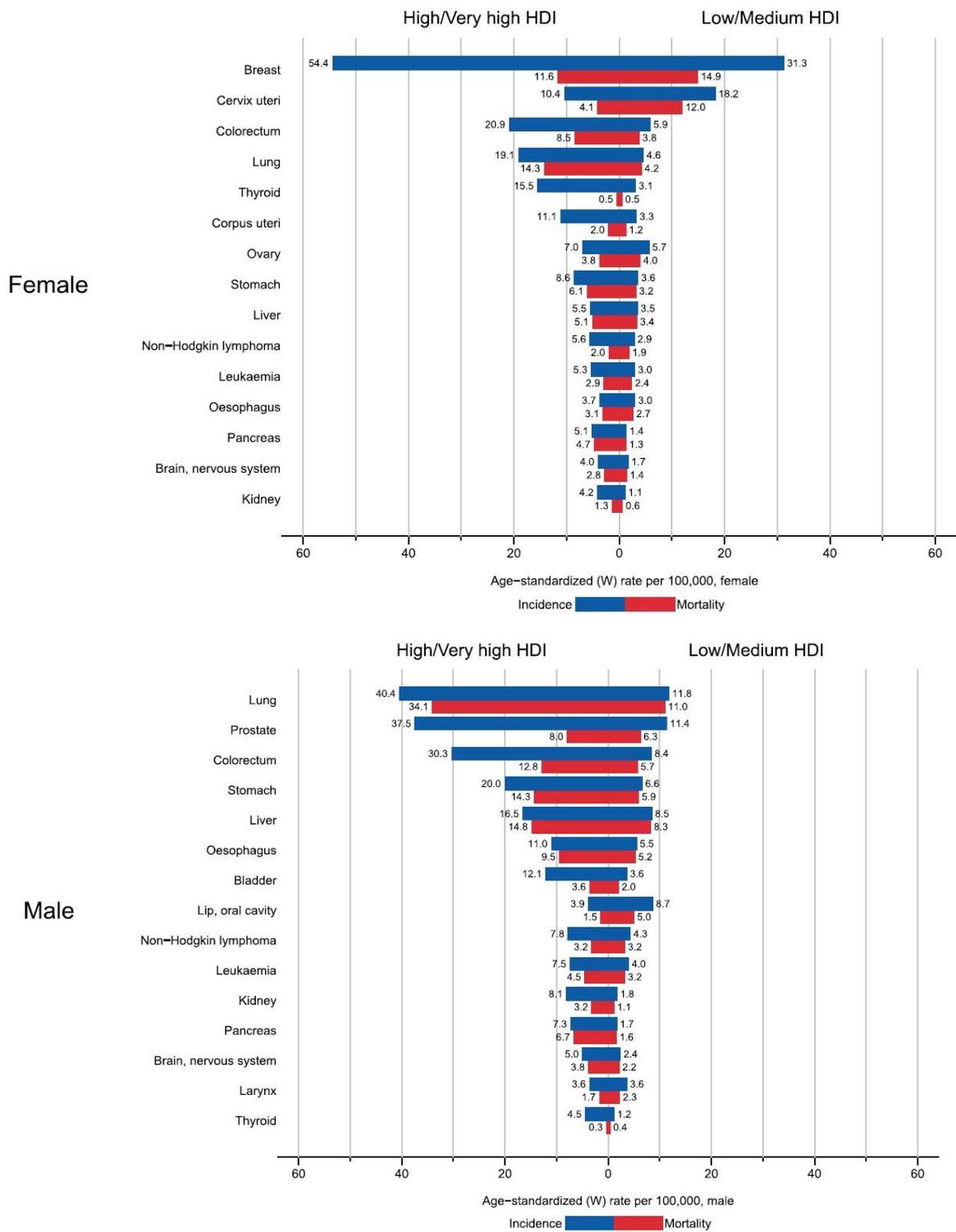
Fig. 1.1 A comparison of incidence and mortality in females and males caused by the most frequent types of cancers in countries with high/very high human development indexes (HDI) versus low and medium HDI – reproduced from (Bernard & Christopher, 2020)

Chemopreventive agents are reported to intervene at various stages in the development of cancer, affecting tumour initiation, promotion, and/or progression (**Fig. 1.2**). Those that act to prevent tumour initiation are called blocking agents, and work to prevent damage to the DNA, often through the direct metabolizing/inactivation of the carcinogens. The agents that interfere with promotion and propagation are known as suppressing agents and affect cancer cell proliferation or delay metastasis.
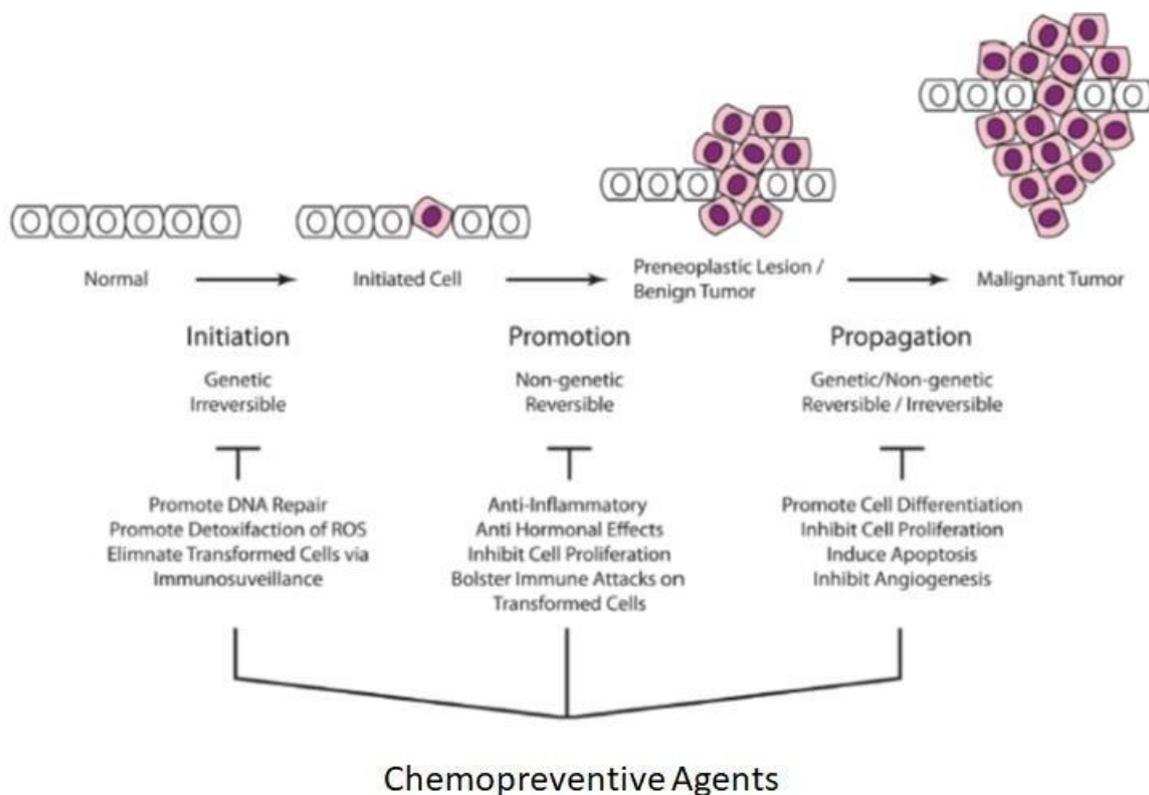
Fig. 1.2 Chemoprevention and the stages of cancer (Kotecha *et al.*, 2016)

The economic burden of cancer was estimated in the UK at 12.8 billion pounds in 2009, of which 4.66 billion pounds were cost of care expenses (Luengo-Fernandez *et al.*, 2013). To reduce these costs, cancer chemoprevention, particularly through dietary means, is increasingly suggested to provide the benefits it has shown in the treatment of cardiovascular diseases, for which death rates in England have decreased 52% between 1990 and 2013 (Ames, 1983;

Bhatnagar *et al.*, 2016; Kotecha *et al.*, 2016; Pericleous *et al.*, 2013). Dietary chemopreventive

compounds include polyphenols with antioxidant properties, such as curcumin (found in

turmeric) (Thangapazham *et al.*, 2006), 6-gingerol (found in ginger) (Poltronieri *et al.*, 2014),

resveratrol (found in the skin of red grapes) (Ko *et al.*, 2017), and epigallocatechin gallate

(found in green tea)(Du *et al.*, 2012), as well as isothiocyanates such as sulforaphane **1**, iberin

2, erucin **3,** and erysolin **4** (**Scheme 1.1 a**), benzyl isothiocyanate, phenethyl isothiocyanate or

allyl isothiocyanate (Keum *et al.*, 2004).
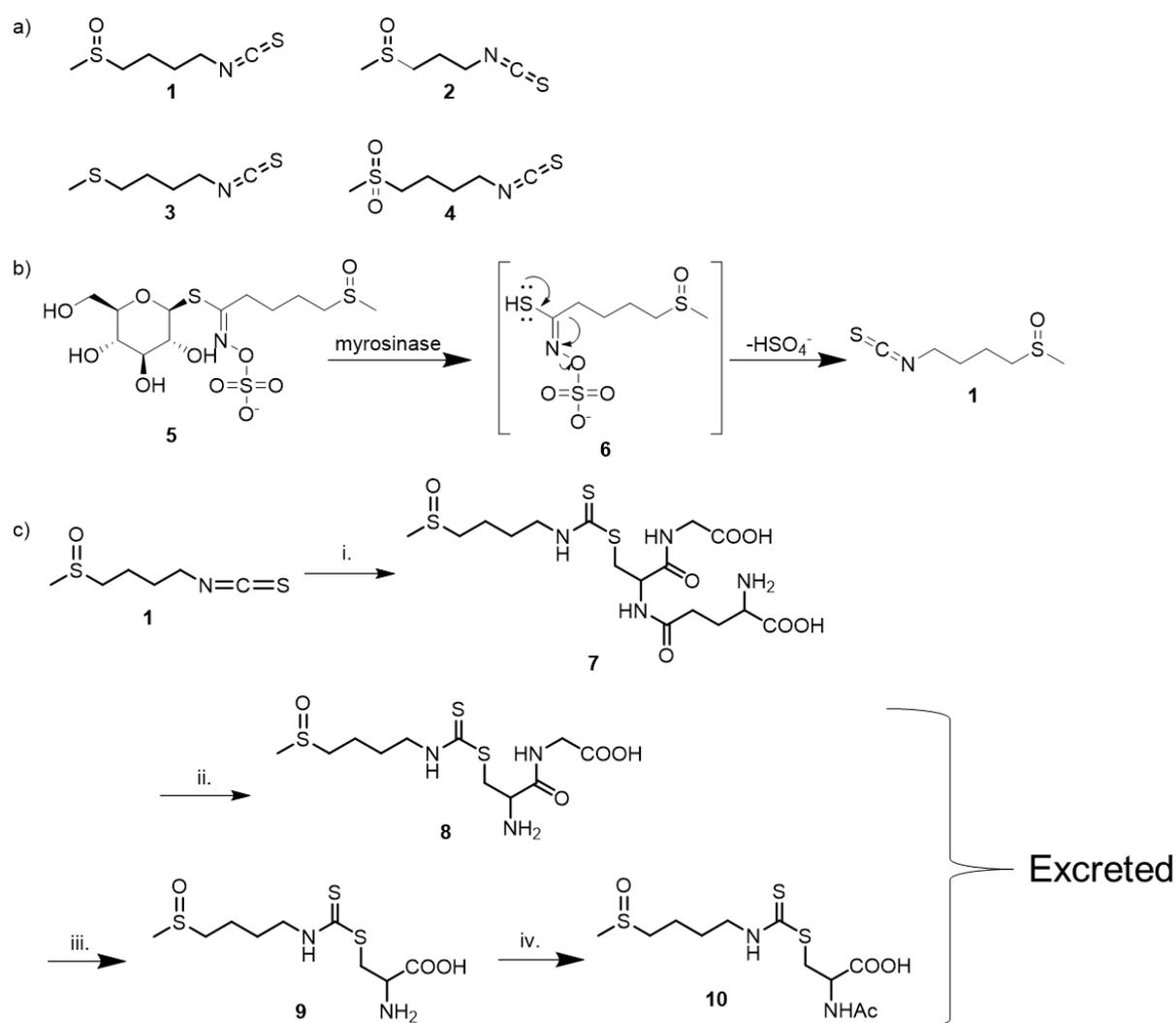
Scheme 1.1 a) Dietary isothiocyanates: sulforaphane (**1**), iberin (**2**), erucin (**3**) and erysolin (**4**); b) myrosinase-catalysed hydrolysis of glucoraphanin leading to sulforaphane; c) sulforaphane metabolism: i. conjugation with glutathione catalysed by glutathione *S*-transferase; ii. removal of glutamate catalysed by gamma-glutamyltransferase; iii. removal of glycine catalysed by dipeptidases; iv. acylation of the cysteine amino group, catalysed by *N*-acetyl transferase.

1.2. Sulforaphane

1.2.1 Natural occurrence and metabolism

Sulforaphane (SF: 1-isothiocyanato-4-methylsulfinylbutane) **1** is one of several isothiocyanate (ITC) natural products – (**Scheme 1.1 a**) that can be extracted from cruciferous vegetables of the *Brassica* family, such as cabbage and particularly broccoli. Its natural occurrence is in the form of the glucosinolate glucoraphanin **5**, which can undergo hydrolysis upon mechanical damage to the plant (**Scheme 1.1 b**), leading either to **1** (when catalysed by the enzyme myrosinase found in the plant or produced by the flora of the human colon) or to the related nitrile. **1** is subsequently metabolised (mostly through conjugation with glutathione and the mercapturic acid pathway – **Scheme 1.1 c**) (Kassahun *et al.*, 1997) and excreted, with more than 80% leaving the body via urine within 12-24h after consumption (Gasper *et al.*, 2005).

The initial interest surrounding **1** is related to evidence that it is the principal constituent facilitating the chemopreventive properties of cruciferous vegetables (Y. Zhang *et al.*, 1992). Indeed, **1** is reportedly effective in reducing the rates of a wide variety of cancer types (e.g. lung, breast, prostate and colon), with oral administration of **1** reported to protect against carcinogenesis in rodent models with a genetic predisposition, as well as in cancers induced by exposure to carcinogens such as dimethylbenz[a]anthracene (Fahey *et al.*, 1997) or benzo[a]pyrene (Fahey *et al.*, 2002). Unlike most small molecules, which tend to have single biological targets, **1** is involved in multiple pathways, which may account for its broad anticancer activity (Juge *et al.*, 2007), (Clarke *et al.*, 2008), (Liang & Yuan, 2012), (Vanduchova *et al.*, 2019).

1.2.2 Phase II enzyme induction

The best described mechanism for chemoprevention by **1** is its ability to induce phase 2 enzymes, which detoxify the organism by converting carcinogens into inactive metabolites, through the activation of the transcription factor Nrf2 (nuclear factor erythroid 2-related factor 2) – **Fig. 1.3** (Y. Zhang *et al.*, 1992)**,** (Keum, 2011)**,** (Townsend & Johnson, 2016). Under normal conditions, Nrf2 forms a complex in the cytoplasm with a dimer of its repressor, Kelch-like

ECH associated protein 1 (Keap1). The Keap1 dimer also binds to the E3 ubiquitin ligase Cullin-3-RING box 1, facilitating the ubiquitination of Nrf2 followed by proteasomal degradation, thus maintaining a low level of Nrf2 (Taguchi *et al.*, 2011), (Pandey *et al.*, 2017). Keap1, a cysteine-rich protein, acts as a chemical redox sensor, with several sulfhydryl residues available for reaction. ITCs such as **1** react with these sulfhydryl residues, determining conformational changes that destabilize the Keap1-Nrf2 complex, as well as its interaction with Cullin-3 (C. Hu *et al.*, 2011). Ubiquitination of Nrf2 is prevented and upcoming Nrf2 accumulates in the cytoplasm through depletion of Keap1. Nrf2 then translocates into the nucleus, where it binds to the antioxidant responsive element (ARE), present in the upstream regulatory sequence of several genes encoding cytoprotective proteins. Nrf2 binding to ARE activates gene expression, leading to increased production of enzymes such as epoxide hydrolase, heme oxygenase 1 (HO-1), NAD(P)H dehydrogenase (quinone) 1 (NQO1), as well as glutamate-cysteine ligase (GCL) and glutathione S- transferase (GST), key proteins in the glutathione pathway (Clarke, Hsu, Williams, *et al.*, 2011; Kensler *et al.*, 2013).
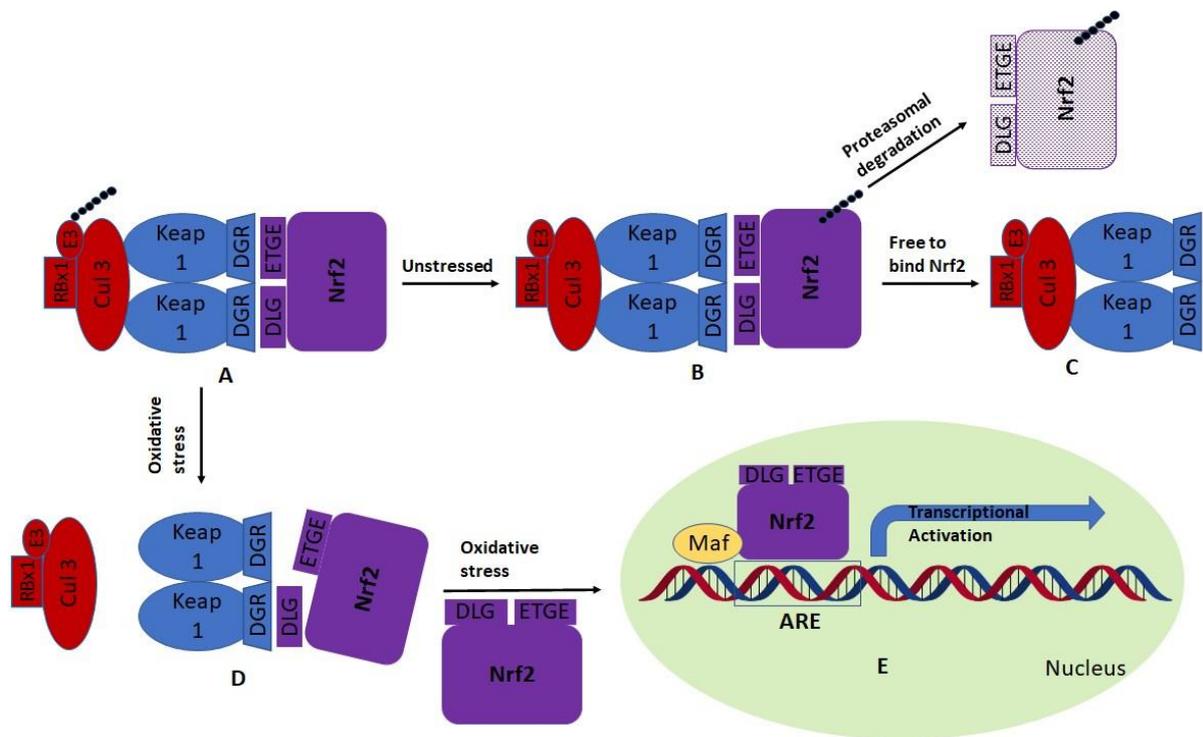
Fig. 3 The Keap1-Nrf2 pathway (adapted from (Pandey *et al.*, 2017)): A. Under normal conditions, Keap1 interacts with Nrf2 and with Cul3-Rbx1-E3, which recruit ubiquitin; B. In unstressed conditions, Nrf2 is ubiquitinated; C. Nrf2 is directed towards proteasomal degradation, while the Keap1-Cul3 complex can bind other Nrf2 molecules; D. In oxidative stress, modifications to Keap1 dissociate the complex with Cul3, and the ETGE domain of Nrf2, while the DLG domain remains attached, sequestering Keap1; E. Further Nrf2 accumulates and translocates into the nucleus where it interacts with the ARE to activate transcription to synthesise phase II enzymes/antioxidants.

1.2.3 Sulforaphane in inflammation

Interestingly, **1** is also reported to exhibit anti-inflammatory properties (Heiss *et al.*, 2001). Inflammation is a natural reaction of the organism, generally when faced with injuries or infection, that is characterized by pain, swelling, redness and heat (*dolor, tumor, rubor* and *calor*), and driven by the production of small inflammatory proteins, known as cytokines (Larsen & Henson, 1983; J. M. Zhang & An, 2007). The normal purpose of inflammation is to facilitate the removal of the cause of injury or infection and the associated damaged cells, as

well as to begin tissue repair. However, prolonged, or chronic, inflammation is mechanistically linked to carcinogenesis and a feature in very different diseases such as diabetes (Lontchi-Yimagou *et al.*, 2013), rheumatoid arthritis (RA) (Yang *et al.*, 2016), Alzheimer's disease (AD) (Holmes, 2013), (Akiyama *et al.*, 2000) or cardiovascular disease (Black & Garbutt, 2002), (Golia *et al.*, 2014). Accordingly, understanding the mechanisms underlying the antiinflammatory properties of **1** presents interest for applications reaching far beyond cancer. A mechanism through which **1** influences the inflammatory response is through inhibition of the transcription factor nuclear factor kappa B (NF-κB) (Heiss *et al.*, 2001), (Greaney *et al.*, 2016).

NF-κB is a family of transcription factors including NF-κB1 (p50), NF-κB2 (p52), RelA (p65), RelB and c-Rel (Gilmore, 2006). Active forms of NF-κB operate as a heterodimer; composed of two subunits, p50 and RelA, or p52 and RelB (**Fig. 1.4**). NF-κB is sequestered in the cytoplasm by a group of regulator proteins known as inhibitor of κB (IκBs). In the canonical pathway, phosphorylation of IκB, catalysed by inhibitor of κB kinase (IKK) leads to its ubiquitination and proteasomal degradation, freeing NF-κB for translocation to the nucleus, where it will initiate transcription of target genes. In an auto-regulatory fashion, this includes the gene for

IκB, ensuring the inactivation of excess NF-κB. In the non-canonical pathway, the NF-κB inducing kinase (NIK) activates a different IKK complex, which phosphorylates the larger p100, leading to partial proteolysis leaving behind a p52-RelB complex.
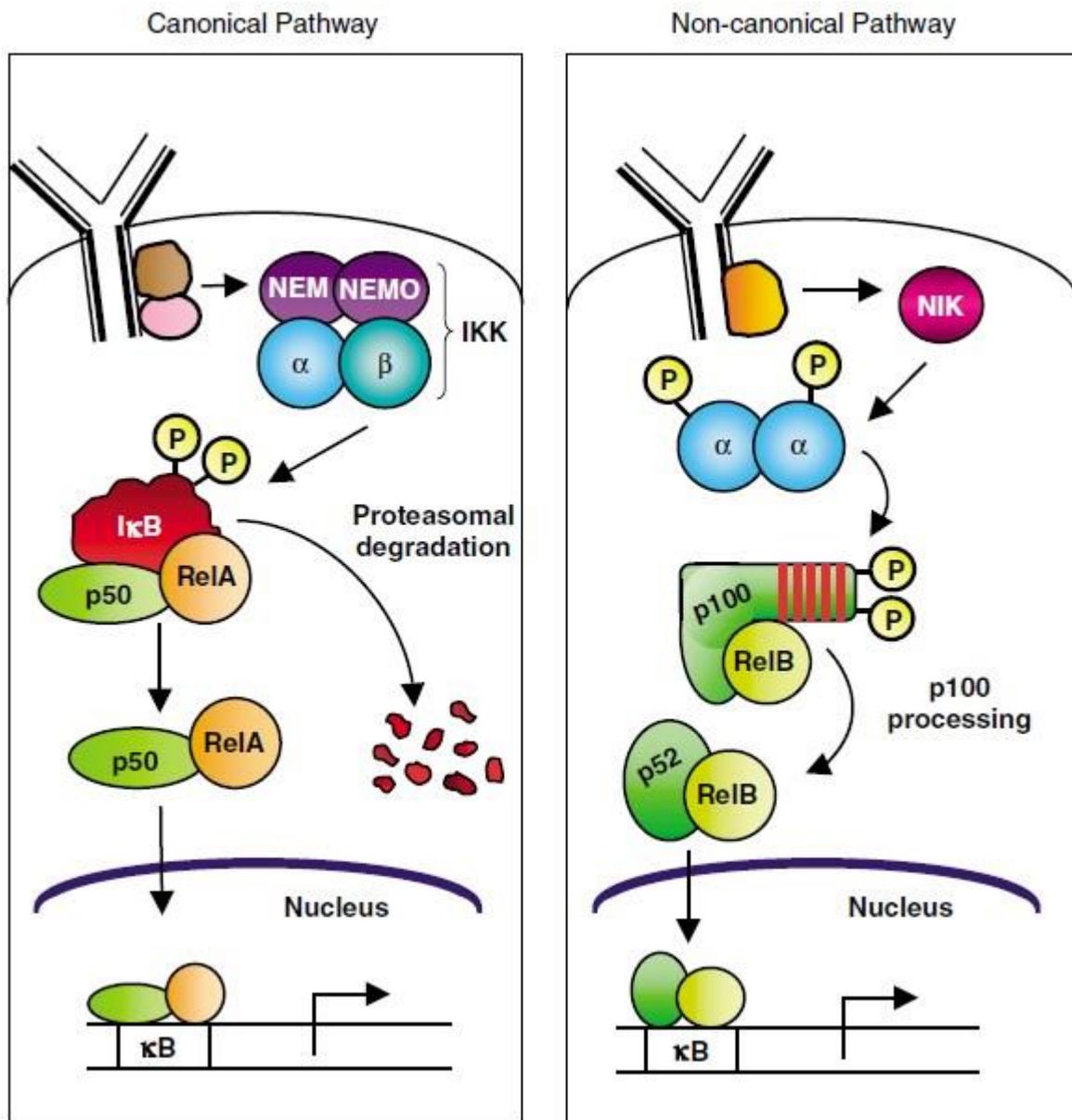
Fig. 1.4 Canonical and non-canonical pathways of NF- κB activation (reproduced from (Gilmore, 2006))

NF-κB is considered a key player in inflammation and cancer, its activation leading to the induction of genes coding for pro-inflammatory molecules such as cytokines (e.g. TNFα and IL-6), and chemokines, as well as anti-apoptotic genes like Bcl-XL. Furthermore, TNFα is itself one of the activators of NF-κB, leading to a positive feedback loop that can trigger a cytokine storm (Moon *et al.*, 2009).

It has been suggested that sulforaphane can interact directly either with the transcription factor or with its inhibitor. However, the full complement of immunologically relevant molecules **1** interacts with is likewise not known, and difficult to determine using conventional methods due to its rapid metabolism.

Downstream, sulforaphane was shown to reduce the production of pro-inflammatory cytokines TNF-α, IL-1 and IL-6(Hung *et al.*, 2014; Kensler *et al.*, 2013; Negi *et al.*, 2011), and enhance the production of anti-inflammatory cytokine IL-10 (C. Wang & Wang, 2017).

1.2.4 Cell cycle arrest induced by sulforaphane

Under normal conditions, the process of cell growth and division occurs according to a well-defined programme known as the cell cycle (**Fig. 1.5**). The cell progresses through four stages (Johnson & Walker, 1999). In the mitosis stage (M), the genetic material of the cell is divided into daughter chromosomes, usually followed by cytokinesis, the split into daughter cells. Typically, a mammalian cell only spends a small amount of time in the M stage (~1h of a 24h cycle), with much more dedicated to the other three, which together form the interphase. In the first gap stage (G_1), the cell is generally metabolically active and grows in size. Subsequently, in the Synthesis (S) stage, the cell starts to replicate the DNA. A second gap stage (G_2) between synthesis and mitosis, allows for more preparations for division, with growth and protein synthesis as hallmarks. Following mitosis, the cell can re-enter the cell cycle, or exit the G_1 stage it to remain quiescent in the G_0 stage. In the G_0 stage, the cells will continue to function normally, except that they will no longer actively prepare for mitosis until outside signalling will cause them to re-enter the G_1 stage.
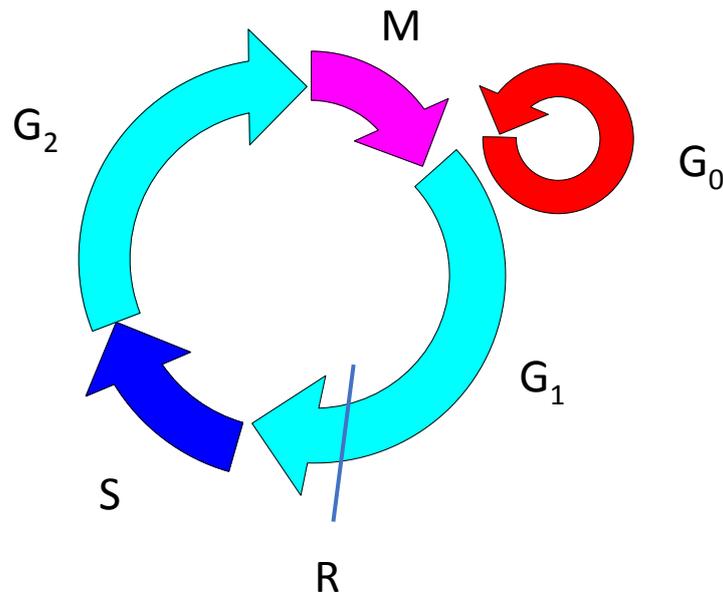
Fig. 1.5 The normal eukaryotic cell cycle. The cell progresses through four stages: Mitosis (M), two gap phases (G_1 and G_2), and a synthesis phase (S) or exits the cycle to remain quiescent (G_0). The restriction point (R) is the main checkpoint where cells are controlled for DNA damage before going into the S phase.

The transitions between stages are controlled by checkpoints, when cells detected to have damaged DNA are prevented from dividing. The main checkpoint, known as the restriction point (R), occurs towards the end of the G_1 stage, but additional checkpoints exist between G_1 and S and between the G_2 and M stages. Triggering a checkpoint usually leads to increased production of p53, a protein with a major role in DNA repair; if DNA repair fails, p53 will direct the cell towards apoptosis. Progression through these checkpoints is regulated by cyclins, which activate enzymes known as cyclin-dependent kinases (CDKs), with different CDKs responsible for specific checkpoints. (L. Gamet-Payrastre, 2006)

In cancer, an increased expression of telomerase, the enzyme that repairs the normal damage to the ends of chromosomes acquired during division, allows the cancer cells to divide far beyond the normal 40-60 divisions that a normal cell will typically undergo in its lifetime. Furthermore, one of the genes most commonly mutated in a cancer cell is the one for p53.

These mutations to p53 lead to decreased ability to repair DNA damage and to trigger apoptosis. Consequently, DNA damage continues to accumulate as cells undergo uncontrolled division, which leads to cancer cell DNA presenting major mutations compared to normal cells. Sulforaphane has been reported to induce cell cycle arrest at different stages, depending on the cell type, with quiescent cells typically arrested in the G_0-G_1 stage, and tumour cells arrested in the G_2-M stage(L. Gamet-Payrastre, 2006; Laurence Gamet-Payrastre *et al.*, 2000; Parnaud *et al.*, 2004) (**Table 1.1**). In HT29 human colon carcinoma cells, **1** was shown to induce cell cycle arrest at the G_2-M phase, with increased levels of cyclin B1 detected. Based on experiments using roscovitine, a cdc2 kinase inhibitor, it was suggested that cdc2 kinase can be a protein through which **1** achieves cell cycle arrest (Parnaud *et al.*, 2004). However, it is still unknown whether **1** interacts directly with cdc2 kinase or with other molecules upstream.

Table 1.1 Stages for cell cycle arrest induced by sulforaphane (reproduced from (Juge *et al.*, 2007))

G_0-G_1	G_2-M	S
HT29	HT29	UM-UC-3
DU-145	DU-145	
LnCap	PC-3	
T24	MCF-7	
Non-transformed T	Jurkat T cells	
lymphocytes	Caco-2	
	MIA Paca-2	
	UM-UC-3	
	F3II	

1.2.5 Induction of apoptosis by sulforaphane

1 also mediates apoptosis, one of three types of programmed cell death, a process that allows the organism to eliminate damaged or unnecessary cells in a non-inflammatory manner(Chiao *et al.*, 2002; Laurence Gamet-Payrastre *et al.*, 2000). Unlike necrosis, another process of cell death, apoptosis occurs in a controlled way, with specific features including cell shrinkage, chromatin condensation and non-lytic fragmentation of the cell into contained apoptotic bodies which are removed through autophagy (Hotchkiss & Nicholson, 2006; Kerr *et al.*, 1972; Ouyang *et al.*, 2012). Apoptosis is effected through a group of cysteine proteases (caspases) and occurs when induced by signals from inside the cell (the intrinsic pathway – **Fig. 1.6**), or by stimuli from outside the cell, activated by so-called death ligands such as Tumour Necrosis Factor α (TNFα) or Fas Ligand (FasL), (the extrinsic pathway – **Fig. 1.7**). The two pathways, while initially separated, ultimately converge downstream in the execution phase, where 'effector' caspases (3, 6, and 7) cleave and inactivate important cellular proteins, such as the DNA repair enzyme poly-(ADP-ribose) polymerase (Hotchkiss & Nicholson, 2006). **1** has been linked mainly to the intrinsic pathway (Chiao *et al.*, 2002), (L. Gamet-Payrastre, 2006), but studies have shown that, in certain tumour cells, **1** can also activate caspase-8, the initiator caspase in the extrinsic pathway (Shang *et al.*, 2017).
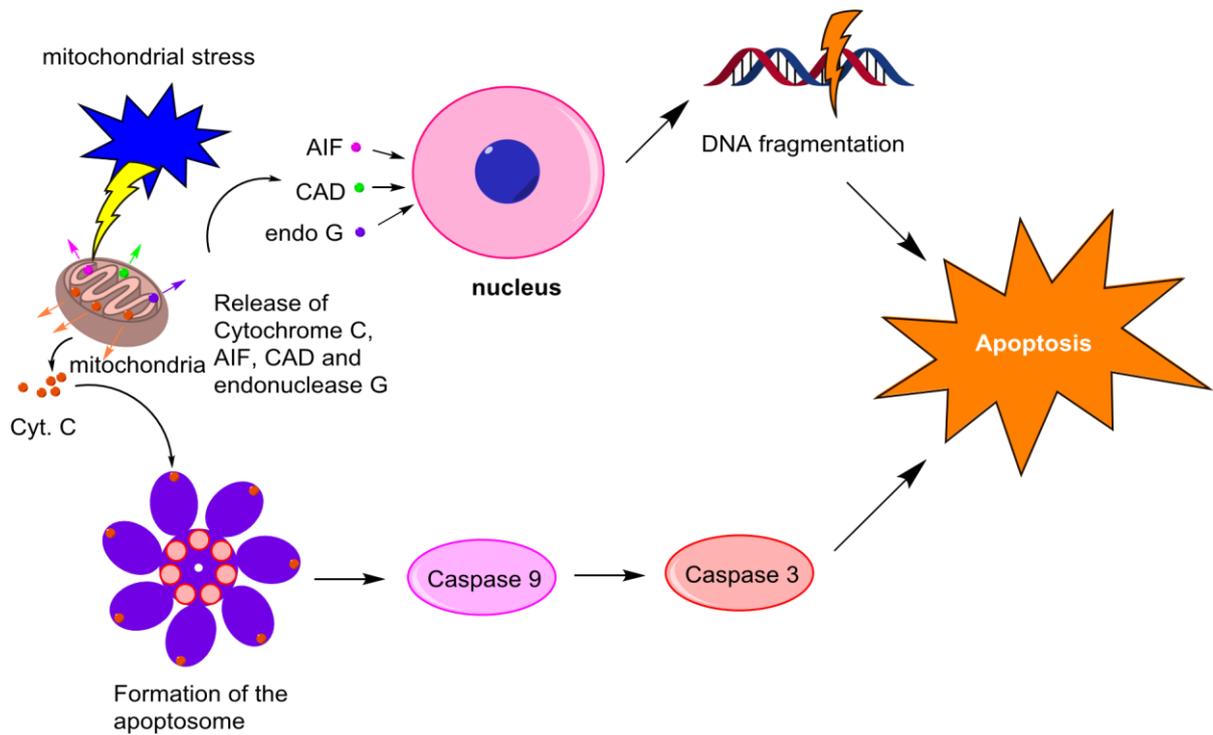
Fig. 1.6 Apoptosis, intrinsic pathway: Mitochondrial stress leads to the release of cytochrome C, as well as of apoptosis inducing factor (AIF), endonuclease G, and Caspase-activated DNase (CAD). Cytochrome C binds apoptotic protease activating factor 1 (Apaf 1) and procaspase 9, leading to the formation of the apoptosome, which in turn leads to the activation of caspase 9. Caspase 9 cleaves procaspase 3, activating the effector caspase 3, which cleaves a number of proteins resulting ultimately in apoptosis. In parallel, AIF, endonuclease G, and CAD relocate to the nucleus where they cause DNA fragmentation with the same outcome.
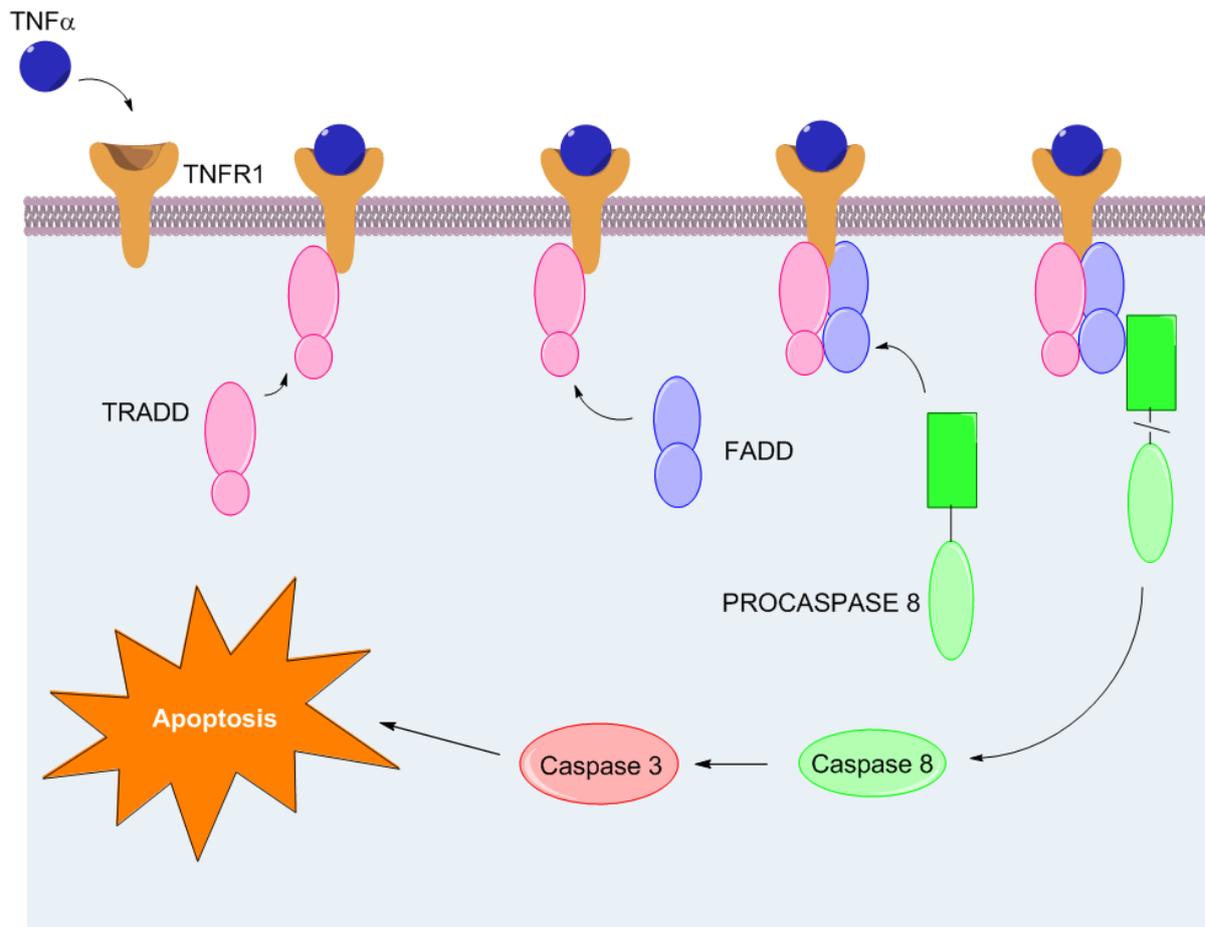
Fig. 1.7 Apoptosis, extrinsic pathway: extracellular ligands, such as TNFα or FAS-ligand bind to membrane receptors (TNFR1 and FAS-R, respectively), leading directly or indirectly to the recruitment of Fas-associated protein with death domain (FADD). The death domain of FADD binds procaspase 8, whose cleavage releases caspase 8. Caspase 8 cleaves procaspase 3, and the activation of caspase 3 begins the execution pathway of apoptosis.

1.2.6 Histone modification by sulforaphane

Sulforaphane was shown to have an effect on histone acetylation, a process with major consequences for gene expression (Clarke, Hsu, Yu, *et al.*, 2011; Mitsiogianni *et al.*, 2021; Myzak *et al.*, 2006). Histones are highly basic proteins, whose relative positive charge cause the negatively charged DNA to coil around and condense into complexes called nucleosomes, making it possible for high quantities of DNA to fit inside the nucleus. Histone acetylation is a normal post-translational modification that reduces the histones' positive charge, causing conformation shifts that uncoil the DNA, allowing access to RNA and transcription factors and

activating gene expression (Gräff & Tsai, 2013; Grunstein, 1997). Histone acetylation is reversible, and the balance between acetylated (transcriptionally active) and deacetylated forms of chromatin is maintained by the enzymes that catalyse these processes, histone acetyl transferases (HATs) and histone deacetylases (HDACs). In cancer, HDACs are typically overexpressed in order to facilitate the characteristic increased rates of gene transcription. Accordingly, they are an intriguing therapeutic target for anticancer drugs. Sulforaphane was shown to indirectly decrease HDAC activity through two of its downstream metabolites from the glutathione pathway, its conjugates with cysteine and *N*-acetyl cysteine. This led to increased levels of acetylated histones in several types of cancer cells, including prostate and colon cancer cells (Myzak *et al.*, 2006). The decrease in HDAC activity (primarily HDAC3 and HDAC6) induced by sulforaphane is more prominent in prostate cancer cells versus normal prostate cells, along with differences in levels of cell cycle arrest and apoptosis (Clarke, Hsu, Yu, *et al.*, 2011). It was suggested that **1** (through its NAC metabolites) decreases HDAC activity by hindering the interaction between HDAC and its corepressor, silencing mediator for retinoid or thyroid-hormone receptors (SMRT) (Rajendran *et al.*, 2013). Interestingly, the increase in histone acetylation was also linked with increased transcription of long terminal repeats (LTR), an off-target effect that can lead to genome instability (Baier *et al.*, 2014).

Another epigenetic modification, DNA methylation, was found to be affected by **1** through inhibition of DNA methyltransferases (DNMTs) DNMT1 and DNMT3a in human breast cancer cells.

1.2.7 Inhibition of angiogenesis

Angiogenesis, the process of stimulating the development of new blood vessels, is essential for providing the increased quantities of oxygen and nutrients required to maintain the fast growth

of tumour cells (Carmeliet & Jain, 2000; Otrock *et al.*, 2007). In its absence, the tumours are limited to dimensions that allow the cells to be supplied through diffusion. While the process through which cancer cells acquire the ability to initiate angiogenesis is not fully understood, vascular endothelial growth factor (VEGF) is known to be one of the important pro-angiogenic molecules secreted from tumour cells. Sulforaphane was shown to inhibit the expression of VEGF in hepatic cancer cells through suppressing the expression of its two important transcription activators, signal transducer and activator of transcription 3 (STAT3) and hypoxia-inducible factor-1-alpha (HIF1α) (Bertl *et al.*, 2006; Cavell *et al.*, 2011). In squamous cell carcinoma and prostate cancer cells, **1** was found to inhibit the accumulation of HIF1α through activating the phosphorylation of extracellular signal-regulated protein kinase (ERK) and c-Jun *N*-terminal Kinase (JNK) (Yao *et al.*, 2008). Interestingly, with both ERK and JNK involved in glycolysis (Papa *et al.*, 2019), this may offer a direct route through which sulforaphane can affect cell metabolism.

1.3. Clinical trials for sulforaphane

The varied biological pathways in which sulforaphane is involved, combined with the fact that it is a dietary compound (i.e. less likely to have severe side effects at dietary levels), have made SF an attractive target for clinical studies regarding its therapeutic effects. As recently reviewed (Mazarakis *et al.*, 2020), most of the clinical trials that are already completed were phase I studies targeted at healthy individuals, aiming to determine the doses required to maintain the necessary plasma levels of sulforaphane to induce the desired biological response (**Appendix 1**). Notably, the data from these clinical trials are affected by the lack of uniformity in the form that **1** is administered, from dietary consumption of broccoli, raw or steamed, to enriched variants, such as broccoli sprout extract (BSE), to various stabilized versions of sulforaphane (e.g. Sulforadex®, Prostaphane®). The form of administration can be a major source of

variability in observed biological activity, considering some require the hydrolysis of glucoraphanin to be catalysed by mirosinase from the intestinal flora. Variance in the levels of mirosinase production will affect the absorption of sulforaphane, leading to false negative results for individuals whose intestinal flora is unable to hydrolyse glucoraphanin properly.

In a clinical trial on women with abnormal mammograms (Zhang *et al.*, 2016), the intake of cruciferous vegetables was associated with a decrease in cell proliferation rate, but no significant correlations were observed for other biomarkers including levels of HDACs, acetylated histones and p21 due to the limited sample size. Sulforaphane also had a positive effect in treating patients infected with *Helicobacter pylori*, a bacterial infection which is associated with gastritis, ulcers and gastric cancers (Fahey *et al.*, 2002; Yanaka *et al.*, 2009).

With the increased interest in sulforaphane, there are also a few dozen ongoing clinical trials for using sulforaphane in a wide range of diseases, from autism and schizophrenia to diseases with an inflammatory aspect, such as diabetes, osteoarthritis and allergic airways diseases, and several types of cancer, including prostate, breast and head and neck squamous cell cancer.

1.4. Co-therapies including sulforaphane

An emerging direction in sulforaphane cancer research is the use of combination therapies, using **1** in conjunction with established chemotherapeutic drugs. A combination approach can often be useful, whether the drugs target the same cellular pathway or different pathways in synergy with each other. Synergism in drug-drug interactions is quantified through a combination index (CI) (Chou, 2010), calculated based on IC_{50} (the half maximal inhibitory concentration) values with the formula in **Eq. 1.1**

$$CI = \frac{IC_{50}A_{(A+B)}}{IC_{50}A} + \frac{IC_{50}B_{(A+B)}}{IC_{50}B} \qquad\qquad (1.1)$$

where $IC_{50}A_{(A+B)}$ refers to the concentration of A that achieves 50% inhibition in a combination with B, whereas $IC_{50}A$ is the refers to the IC_{50} for A alone. The values for CI will be between 0 and 1 for synergy, equal to 1 for additivity, and greater than 1 for antagonism.

Table 1.2 Types of cancer and drugs that have shown synergy with sulforaphane (reproduced from (Kamal *et al.*, 2020))

Cancer types	Molecules that show synergism with sulforaphane	Cell lines
Pancreatic Cancer	Gemcitabine, doxorubicin, 5-fluorouracil, 17allylamino 17-demethoxygeldanamycin, ibuprofen, aspirin and curcumin	Mia-Paca-2 and Panc-1
Breast Cancer	Paclitaxel, docetaxel, gemcitabine, clofarabine, afimoxifene, and lapatinib	SUM149, SUM159, MCF7, T47D, SKBR-3, and BT-474
Colorectal Cancer	Oxaliplatin, diindolylmethane and (-)epigallocatechin-3-gallate	Caco-2 cells, 40-16, and HT-29
Prostate Cancer	Taxol, cisplatin, and Tumor necrosis factor-related apoptosis ligand (TRAIL)	DU145 and PC3
Cervical Cancer	Eugenol	HeLa
Glioma	Resveratrol and temozolomide	U251 and LN229
Multiple Myeloma	Arsenic trioxide	PCNY-1, MM1.S, KMS-11, and ARP-1
Adenoid Cystic Carcinoma	5-Fluorouracil	ACC-M and ACC-2
Melanoma	Quercetin	B16F10

Sulforaphane has shown synergy with other chemotherapies in a wide range of cancers (**Table 1.2**). Of particular interest are the results involving pancreatic cancer, a particularly aggressive malignancy with poor prognosis. A major issue in treating pancreatic cancer is the removal of cancer stem cells (CSCs), which are responsible for tumour initiation, metastasis and

recurrence after treatment. A combination of sulforaphane and 5-fluorouracil was effective in targeting MIA-PaCa2 cells with high levels of CSCs, while the combination of **1** and gemcitabine reduced their clonogenic potential (Kallifatidis *et al.*, 2011). In another study, **1** potentiated (CI between 0.62 and 0.87) the activity of 17-allylamino 17-demethoxygeldanamycin against MIA-PaCa2 and Panc1 cells (Li *et al.*, 2011). *In vivo* tests of the combination showed reduced tumour growth in athymic mice compared to each treatment alone.

In breast cancer, minimally cytotoxic doses of 5 µM **1** improved the inhibitory activity of paclitaxel and docetaxel in vitro as well as tumour growth reduction in vivo in mice. Synergistic cytotoxic activity was also reported in colorectal (Chen *et al.*, 2013) and prostate cancers (X. Wang *et al.*, 2016), gliomas (Jiang *et al.*, 2010) and melanoma (Pradhan *et al.*, 2010). Overall, combination therapies with sulforaphane seem a promising avenue of research.

1.5. Derivatives of Sulforaphane

With the increased interest in sulforaphane, there have been several attempts at studying the activity of other related isothiocyanates.

1.5.1 Natural isothiocyanates

Among the closely related natural ITCs are erucin **3**, where the sulfoxide group is reduced to a sulfide, erysolin **4**, where the sulfoxide has instead been oxidised to a sulfone, and iberin **2**, the inferior homologue of sulforaphane, with only a three-carbon linker between the sulfoxide and the –NCS group (**Scheme 1.1 a**). All these have also been isolated from their respective glucosinolates, similar to sulforaphane, and have shown similar, though slightly reduced activity compared to **1** (Y.
Zhang *et al.*, 1992).

1.5.2 Synthetic isothiocyanates

Synthetic derivatives of sulforaphane represent a natural avenue of research into deriving structure-activity relationships. Taking inspiration from (and to some extent overlapping with) the natural isothiocyanates, Zhang *et al.* synthesised sulfides, sulfoxides and sulfones with between 3 and 5 methylene groups between the sulfur atom and the isothiocyanate in the very work that established sulforaphane as a major inducer for phase II enzymes (Zhang *et al.*, 1992). Further work investigated analogues in which the sulfoxide was replaced with various other groups (Posner *et al.*, 1994). Among the attempted substitutions, the quinone reductase (QR) induction activity was preserved at similar levels only when the sulfoxide was replaced with a ketone or a dimethylphosphine oxide, whereas ethyl, carboxylic acids, esters or thioesters exhibited reduced activity. Other avenues of research included nonaromatic cyclic and bicyclic derivatives, looking for the effect of restricted conformations on activity, and a range of aryl and benzyl isothiocyanates.

Hu *et al.* (2013) synthesised a library of sulforaphane derivatives with variability in the length of the spacer between the ITC and the sulfoxide (between 3 and 6 carbons), as well as a number of substitutions for the terminal methyl with various alkyl and aryl groups. Evaluations for cytotoxicity in several cancer cell lines identified that a benzyl replacement for the terminal methyl can lead to a more potent compound than sulforaphane, maintaining the ability to induce phase II enzymes and to cause apoptosis (K. Hu *et al.*, 2013).

Relevant to our project, Kielbasinski *et al.* (2014) synthesised fluorinated derivatives of sulforaphane (Kiełbasiński *et al.*, 2014), where the terminal methyl is replaced either by a trifluoromethyl or a trifluoroethyl group (discussed in more detail in **Chapter 2**). Other work includes some heterocyclic and water soluble derivatives (Shi *et al.*, 2016) and derivatives where the sulfoxide group was replaced by a phosphonate (Psurski *et al.*, 2017).
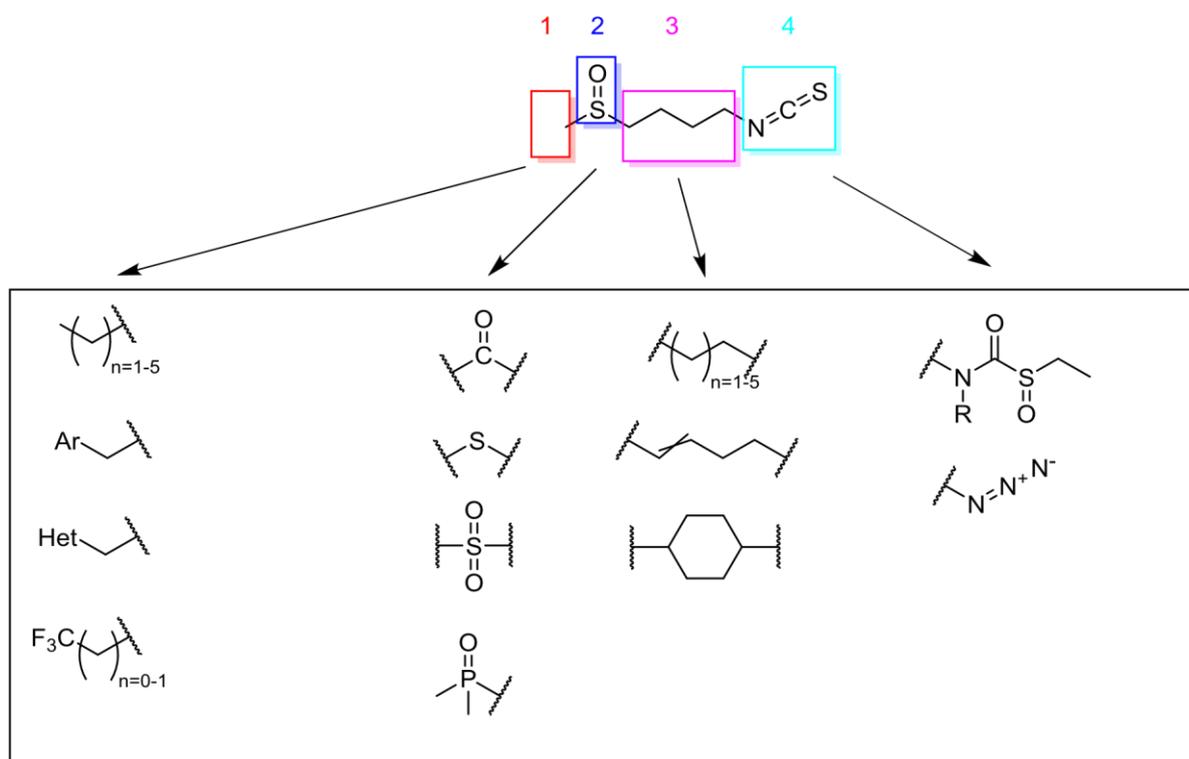
Fig. 1.8 Synthetic derivatives of sulforaphane – structure modifications: 1. Terminal methyl; 2. Sulfoxide; 3. Interior alkyl chain; 4. Isothiocyanate

A separate field of derivatives, also highly relevant to this thesis, refers to the development of sulforaphane derived chemical probes, particularly "click" probes. Ahn *et al.* developed the sulfoxythiocarbamate derivative **11** (**Fig. 1.9**) and employed it to investigate binding to the Cys residues in Keap1, identifying Cys151 as a main target (Ahn *et al.*, 2010). Clulow *et al.* compared the Ahn probe with a newly developed probe **12** and sulforaphane in a competition-based assay to identify protein targets of sulforaphane (Clulow *et al.*, 2017b). These targets included Keap1 and macrophage migration inhibitory factor (MIF), a pro-inflammatory cytokine, as well as two sub-units of NF-κB – p65 and p52. Furthermore, bio-informatic analysis of their results suggested that the major pathway affected by sulforaphane is apoptosis signalling.
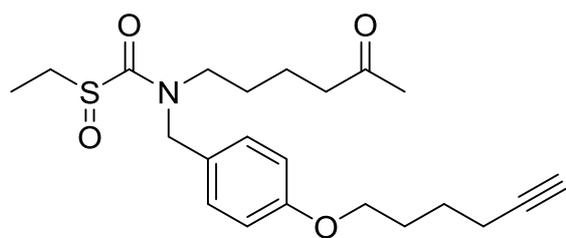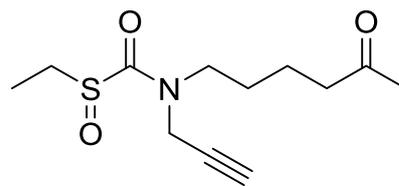
11   **12**

Fig. 1.9 Click probes derivatives of sulforaphane: sulfoxythiocarbamates **11** (Ahn *et al.*, 2010) and **12** (Clulow *et al.*, 2017a)

CHAPTER 2

FLUORINATED ANALOGUES OF SULFORAPHANE AS CHEMICAL PROBES

2.1. Introduction – fluorine in chemical biology

2.1.1 Organofluorine compounds, properties and applications in bioactive molecules

Fluorine, although the most abundant halogen in the earth's crust, is severely underrepresented in molecules created in the animal world, with only around a dozen known organofluorine compounds occurring naturally (J. Wang *et al.*, 2014). Some of the reasons behind this rarity include the fact that fluorine, the most electronegative element, tends to form insoluble salts, therefore having a low availability for the biochemistry that takes place in an aqueous environment. Moreover, fluorine has an extremely high oxidation potential, preventing its participation in the biological redox reactions common to other halogens, which are based on using hydrogen peroxide as an oxidant. The hydration energy for fluorine is also much higher than for other halogens, making it a weak nucleophile. Moreover, the C–F bond is one of the strongest bonds in organic chemistry and is, therefore, very difficult to alter under biological conditions (Gillis *et al.*, 2015; O'Hagan, 2008).

Nonetheless, since the discovery in the 1950s that 5-fluorouracil **13** has anti-tumoral activity (Cohen *et al.*, 1958), fluorinated molecules have become increasingly more common as drugs and agrichemicals, to the point where they currently represent about 20-25% of all pharmaceuticals (J. Wang *et al.*, 2014), including some of the highest selling ones, such as atorvastatin (Lipitor®) **14** and fluoxetine (Prozac®) **15** (**Fig. 2.1**). In these compounds, the fluorine atoms perform a variety of functions: Given the general strength of C–F bonds, fluorine can replace hydrogen atoms in positions that are vulnerable to degradation, increasing the biological half-life of molecules. $–CF_3$, $–OCF_3$, $–SCF_3$, as well as perfluorophenyl groups in particular are frequently used to increase a molecule's lipophilicity and, thus, its bioavailability.

Difluoromethylene (CF$_2$) groups have been used as bioisosteres for oxygen atoms, with the two fluorine atoms attached to a carbon atom mimicking the two electron pairs on an oxygen atom (Martínez *et al.*, 2016). Another major use for fluorine atoms is to direct the conformation of a molecule. One of the most common ways through which this is achieved, though by no means the only one, is the "*gauche* effect", whereby in aliphatic systems, an electronwithdrawing functional group (e.g. -F, -NR$_2$) located vicinal to a fluorine atom tends to align *gauche* (60° torsion angle) to it, due to a combination of stabilising hyperconjugation and intramolecular electrostatic interactions; as well as the avoidance of a destabilising *anti*conformation (O'Hagan, 2008; Tatum *et al.*, 2015; Thiehoff *et al.*, 2017; Verhoork *et al.*, 2018; Wiberg *et al.*, 1990; Wolfe, 1972). Fluorine atoms, due to their electronegativity (3.98), also significantly alter the pK$_a$ of acidic and basic functional groups in their vicinity (Mykhailiuk *et al.*, 2017). Interestingly, perfluorinated molecules such as perfluorodecalin are used as oxygen carrier liquids in medical applications, due to the high solubility of oxygen in perfluorocarbons (Castro & Briceno, 2010). A separate application of fluorine in medicinal chemistry is the use of ^{18}F as a medical imaging tracer e.g., ^{18}F-deoxyglucose **16** in ligands for positron emission tomography (PET) imaging and diagnostics. With a radioisotope decay half-life of 110 minutes, it is more stable than, and therefore preferable to, isotopes such as ^{15}O, ^{13}N or [11]C. Particularly relevant to this project is the use of fluorine in nuclear magnetic resonance spectroscopy – ^{19}F-NMR.

13   **14**

15　　　　　　　　　　**16**
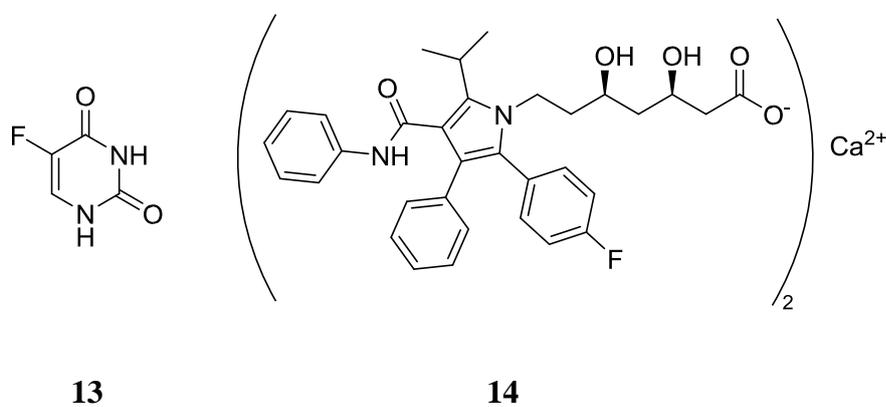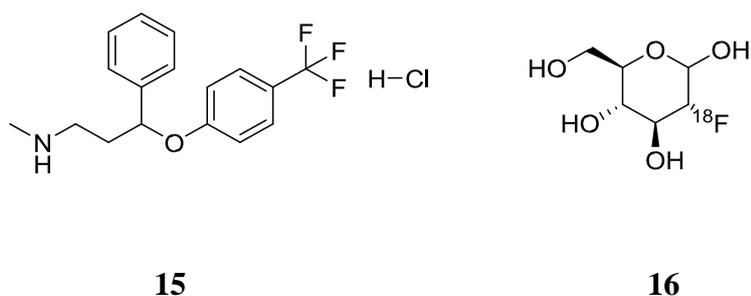
Fig. 2.1. Fluorinated drugs: 5-fluorouracil **13**, atorvastatin (Lipitor®; **14**), fluoxetine (Prozac®; **15**), and [18F]2-fluoro-2-deoxyglucose **16**

2.1.2 ^{19}F-NMR spectroscopy in chemical biology

^{19}F-NMR spectroscopy has several advantages that make it particularly suitable for biological applications: It uses the only naturally occurring isotope of fluorine, and the combination of 100% abundance and having a ratio of 9 electrons per nucleus makes it extremely sensitive (e.g. in comparison with ^{13}C-NMR, which is hampered to some extent by the low abundance of ^{13}C) and slow T1 relaxation rates in determining even minute changes in environment and chemical structure. Additionally, the lack of naturally occurring organofluorine compounds in biological samples facilitates its use as part of molecules that can be traced without background noise. Compared to ^{1}H-NMR spectra, this makes it possible to acquire ^{19}F-NMR spectra forgoing the use of more expensive deuterated solvents. Finally, ^{19}F has a spin of ½, which makes reading and interpreting spectra similar to those of spectra obtained using proton NMR. (Cobb & Murphy, 2009)

Consequently, ^{19}F-NMR spectroscopy has found a variety of applications in chemical biology. It is used in binding studies, with fluorine atoms introduced in proteins to study protein-protein, protein-ligand and protein-DNA binding (Dalvit & Vulpetti, 2019; Papeo *et al.*, 2007). [19]Flabeled-nucleosides have also been used to identify small molecules that can bind to nucleic acids (Gee *et al.*, 2016). Similarly constructed macromolecules have been employed to

determine aspects of protein folding and nucleic acid secondary structure (Mishra *et al.*, 2014).
However, given the preponderance of fluorine-containing pharmaceuticals, a major application
for ^{19}F-NMR spectroscopy is in studies of the metabolism of these compounds, as has been
done, for example, with fluorouracil. Perfluorocarbons and fluorinated gases, such as SF_6 and
C_3F_8 have been used as MRI contrast agents.

2.1.3 Introducing fluorine into organic molecules

The strategies for obtaining organofluorine compounds have changed considerably through the
years. Unlike for other halogens, fluorination using elemental fluorine is not often used, due to
a combination of extreme reactivity (leading to energetic, uncontrollable reactions), toxicity
(both fluorine and hydrogen fluoride, the main by-product of direct fluorination reactions, are
particularly toxic), and the need for special equipment (given that HF will react with glass) (Su,
2008). Following years of using inorganic fluorides in the Balz-Schiemann, Halex or Swarts
reactions (**Scheme 2.1**), a major breakthrough for fluorination reactions was the discovery of
sulfur tetrafluoride derivatives *N,N*-diethylaminosulfur trifluoride (DAST®) **23** and its more
stable derivative *bis*(2-methoxyethyl)aminosulfur trifluoride (deoxo-fluor®) **24** (Middleton,
1975). These nucleophilic reagents can transform alcohols into monofluoroalkanes and
aldehydes or ketones into *gem*-difluoroalkanes (**Scheme 2.2 a**) via deoxy-fluorination.
Similarly, electrophilic fluorination strategies have benefited from the development of the
reagent selectfluor® **33** (1-chloromethyl-4-fluorodiazoniabicyclo[2.2.2]octane
bis(tetrafluoroborate)), which can fluorinate e.g. substituted aromatic substrates, alkenes or
alpha to carbonyl groups (**Scheme 2.2 b**) (Nyffeler *et al.*, 2004).

Most of the fluorine in organofluorine compounds appears either as single atoms or as a
trifluoromethyl (–CF$_3$) moiety. The synthesis of –CF$_3$ containing molecules was significantly
facilitated by the availability and versatility of the Ruppert-Prakash reagent **40**

(trifluoromethyltrimethylsilane, or TMSCF$_3$) (Liu *et al.*, 2015). Used in a variety of nucleophilic reactions (e.g. with aldehydes and ketones, aryl nitriles, imines, Weinreb amides, etc.), TMSCF$_3$ allows synthetic access to both aliphatic and aromatic trifluoromethyl derivatives (**Scheme 2.3 a**). Furthermore, TMSCF$_3$ has been used to create in situ an electrophilic reagent used for the trifluoromethylation of indoles.
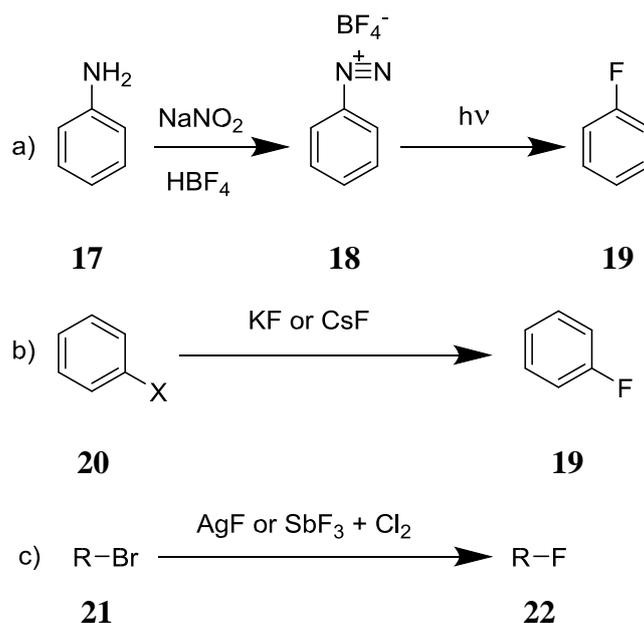
Scheme 2.1 Fluorination using inorganic fluorides: a) Balz-Schiemann reaction; b) Halex reaction; c) Swarts reaction
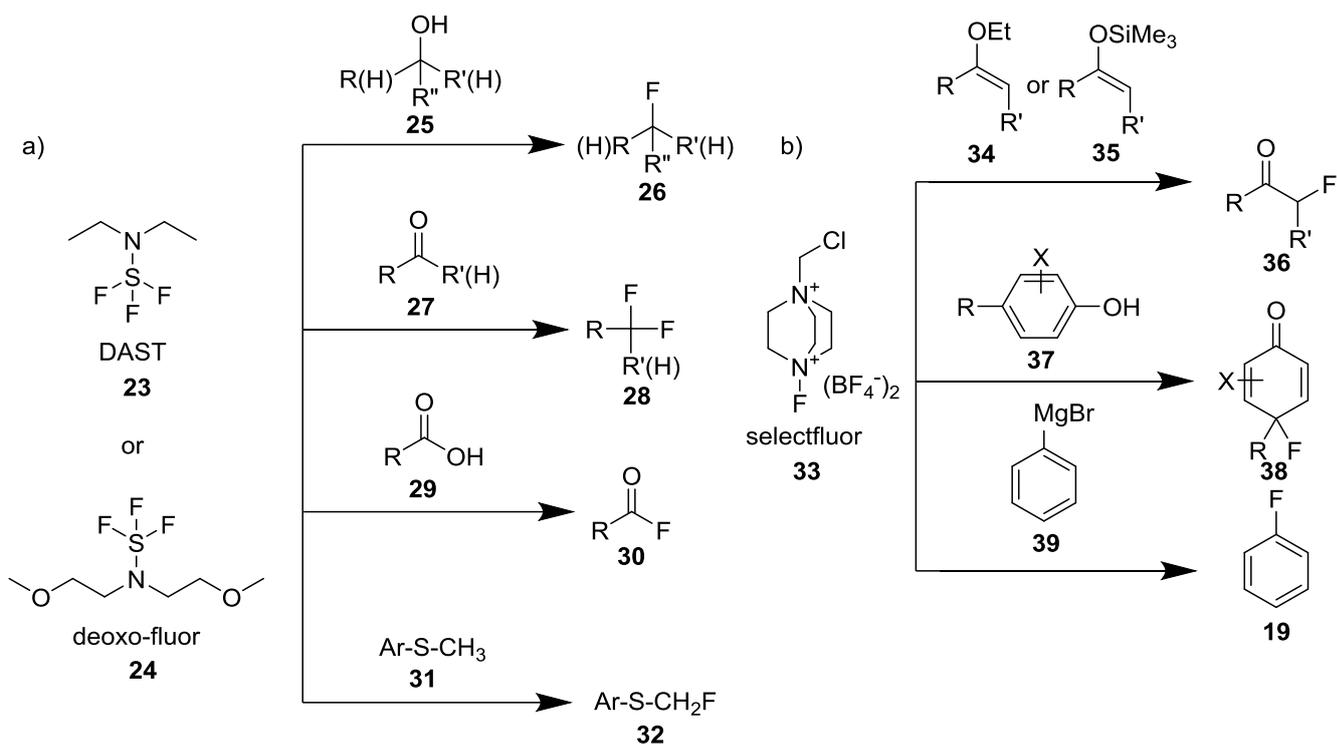
Scheme 2.2 a) Nucleophilic deoxy-fluorinations using DAST® **23** and deoxo-fluor® **24**; b) Electrophilic fluorinations using selectfluor® **33**

Among electrophilic reagents, several have been obtained where the trifluoromethyl group is bound to a heteroatom such as sulfur or iodine. Notably, Togni's reagents (3,3-dimethyl-1(trifluoromethyl)-1,2-benziodoxole **16** and 1-trifluoromethyl-1,2-benziodoxol-3(1*H*)-one **17**) have been used for the trifluoromethylation of alkenes, terminal alkynes, alcohols, and thiols, as well as aromatic and heteroaromatic substrates (**Scheme 2.3 b**) (Charpentier *et al.*, 2015).
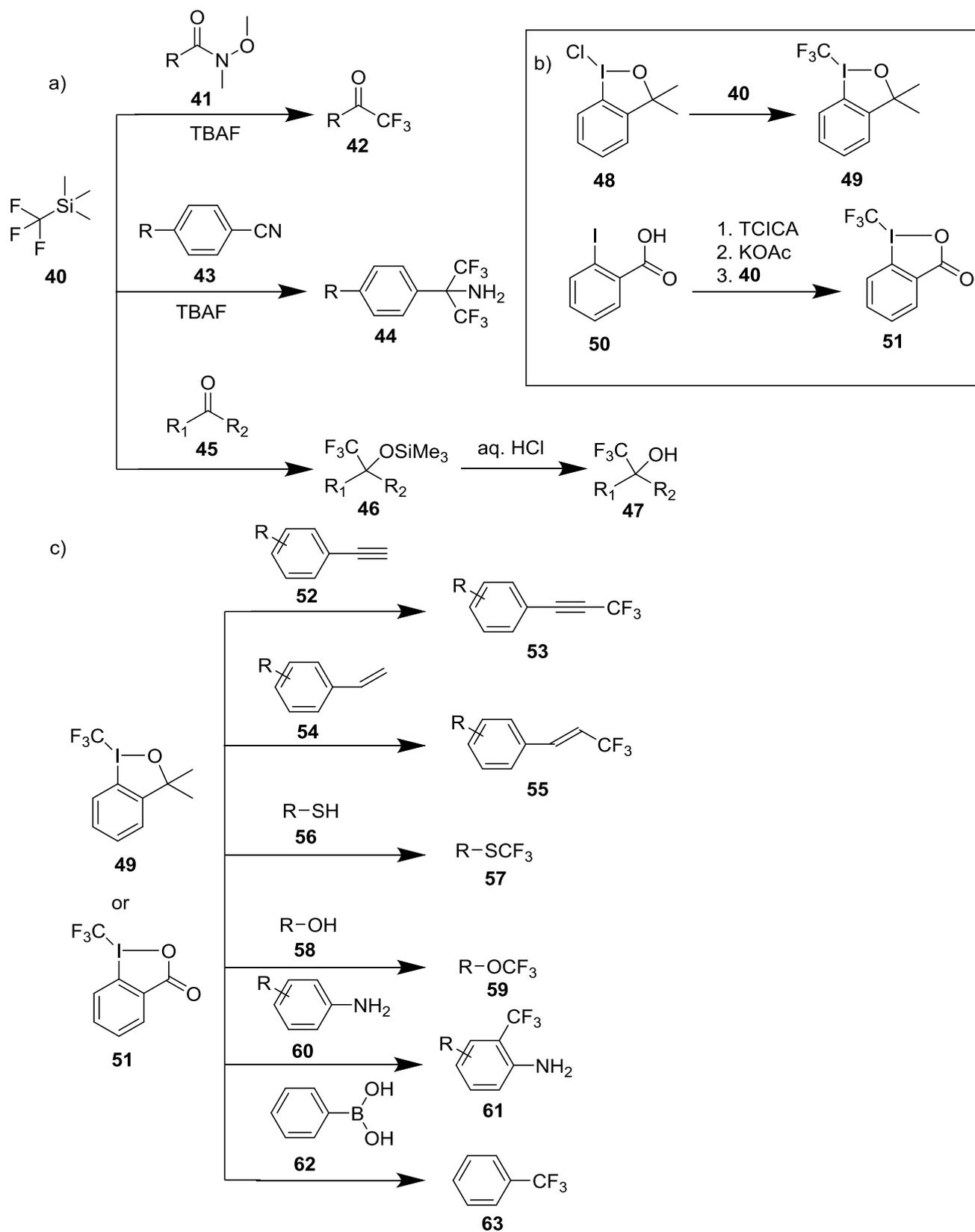
Scheme 2.3. Trifluoromethylation reactions: a) trifluoromethylation reactions using Ruppert's reagent **40**; b) Ruppert's reagent **40** is used in the synthesis of Togni's reagents **49** and **51**; c) electrophilic trifluoromethylation reactions using Togni's reagents **49** and **51**.

2.1.4 Fluorinated derivatives of natural compounds

Fluorinated derivatives of natural compounds currently in use include the above mentioned fluorouracil **13**, used in the treatment of various cancers, and (^{18}F)2-fluoro-2-deoxy-D-glucose **16**, which is the most commonly used imaging agent in PET. Fluoroacetate, one of the few naturally occurring organofluorine compounds, is a pesticide.

2.2. Synthesis of trifluoromethylated isothiocyanate probes

2.2.1 Library design

Given that naturally occurring ITCs have a range of different structures, the first aim of the project was to synthesise a library of fluorinated isothiocyanate (F-ITC) chemical probes, allowing the use of ^{19}F-NMR for investigations into ITC metabolism. Based on existing work (Kiełbasiński *et al.*, 2014), the reporter group was selected in order to meet the following criteria: i) ease of synthesis, ii) increased signal to noise ratio, and iii) minimal disruption to the molecular features compared to the parent molecules. The trifluoromethyl group presents three equivalent fluorine atoms, allowing a three-fold signal increase over using a single fluorine atom, and is more inert chemically, thus, it was chosen as a reporter group for our library. Additionally, the library was diversified to allow for the investigation of three parameters of structural variation: As related natural ITCs (**Scheme 1.1 a**) can occur as either sulfide (e.g. erucin **3**), sulfoxide (e.g. sulforaphane **1** and iberin **2**), or sulfone (e.g. erysolin **4**), one aspect that we varied was the oxidation level of the sulfur atom. Secondly, we investigated the influence of length of the alkyl chain between the sulfur-carrying group and the isothiocyanate − (four carbon long in sulforaphane **1**, erucin **3**, and erysolin **4**, and three in iberin **2**), varying it between two and five carbon atoms. Finally, the presence or absence of a methylene spacing group between the trifluoromethyl group and the sulfur atom was

investigated, as the strong electron-withdrawing effect of the trifluoromethyl group can modify the availability of sulphur electrons.
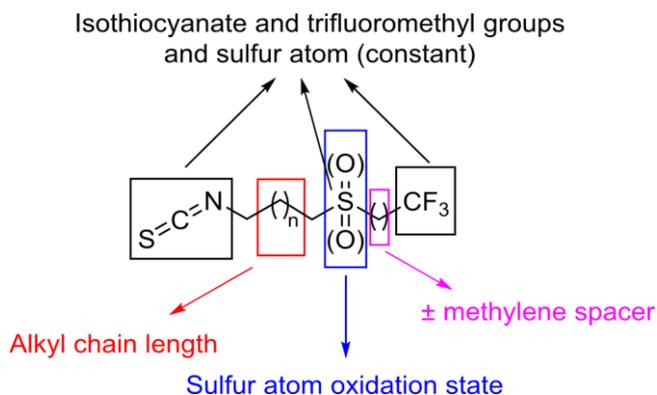
Fig. 2.2 Diversifying the library of fluorinated isothiocyanates (F-ITCs): four different lengths of alkyl chains (n = 0-3), three different oxidation states for the sulphur atom, and two different fluorinated reporter groups yields 24 different F-ITCs.

2.2.2 Computational predictions

To determine to what extent the compounds in the library were expected to mimic the properties of natural ITCs, we performed a computational analysis using the free Molinspiration® cheminformatics software (www.molinspiration.com). This software was used to calculate values for molecular properties important for quantitative structure-activity relationship (QSAR) (**Table 2.1**), and to predict how "drug-like" a molecule is, with additional scores assigned for similarity to active compounds in several categories of ligands or inhibitors (**Table 2.2**). The molecular properties include cLogP, a theoretical calculation of the coefficient of partition between layers of 1-octanol and water, and thus an indicator of molecule lipophilicity, molecular weight, and topological polar surface area (TPSA). The 'druglikeness' of a small molecule is often evaluated based on its conformance to "Lipinski's rule of five" – molecular weight below 500 Da, LogP < 5, total number of hydrogen bond donors no greater than 5, and number of hydrogen bond acceptors no greater than 10.

Cmpd. No.	Molecule	Type	cLogP	TPSA	MW	H-Bond Donors/Acceptors	Lipinski Conformance
100	$CF_3SCH_2CH_2NCS$	S	5.68	12.36	187.21	0/1	No – LogP
104	$CF_3SOCH_2CH_2NCS$	SO	4.15	29.43	203.21	0/2	Yes
108	$CF_3SO_2CH_2CH_2NCS$	SO_2	4.56	46.51	219.21	0/3	Yes
76	$CF_3CH_2SCH_2CH_2NCS$	S	3.06	12.36	201.24	0/1	Yes
80	$CF_3CH_2SOCH_2CH_2NCS$	SO	1.53	29.43	217.24	0/2	Yes
84	$CF_3CH_2SO_2CH_2CH_2NCS$	SO_2	1.93	46.51	233.24	0/3	Yes
101	$CF_3SCH_2CH_2CH_2NCS$	S	5.95	12.36	201.24	0/1	No – LogP
105	$CF_3SOCH_2CH_2CH_2NCS$	SO	4.42	29.43	217.24	0/2	Yes
109	$CF_3SO_2CH_2CH_2CH_2NCS$	SO_2	4.83	46.51	233.24	0/3	Yes
77	$CF_3CH_2SCH_2CH_2CH_2NCS$	S	3.33	12.36	215.26	0/1	Yes
81	$CF_3CH_2SOCH_2CH_2CH_2NCS$	SO	1.8	29.43	231.26	0/2	Yes
85	$CF_3CH_2SO_2CH_2CH_2CH_2NCS$	SO_2	2.2	46.51	247.26	0/3	Yes
102	$CF_3SCH_2CH_2CH_2CH_2NCS$	S	6.22	12.36	215.26	0/1	No – LogP
106	$CF_3SOCH_2CH_2CH_2CH_2NCS$	SO	4.69	29.43	231.26	0/2	Yes
110	$CF_3SO_2CH_2CH_2CH_2CH_2NCS$	SO_2	5.1	46.51	247.26	0/3	No – LogP
78	$CF_3CH_2SCH_2CH_2CH_2CH_2NCS$	S	3.6	12.36	229.29	0/1	Yes
82	$CF_3CH_2SOCH_2CH_2CH_2CH_2NCS$	SO	2.07	29.43	245.29	0/2	Yes
86	$CF_3CH_2SO_2CH_2CH_2CH_2CH_2NCS$	SO_2	2.47	46.51	261.29	0/3	Yes
103	$CF_3SCH_2CH_2CH_2CH_2CH_2NCS$	S	6.73	12.36	229.29	0/1	No – LogP
107	$CF_3SOCH_2CH_2CH_2CH_2CH_2NCS$	SO	5.2	29.43	245.29	0/2	No – LogP
111	$CF_3SO_2CH_2CH_2CH_2CH_2CH_2NCS$	SO_2	5.6	46.51	261.29	0/3	No – LogP
79	$CF_3CH_2SCH_2CH_2CH_2CH_2CH_2NCS$	S	4.1	12.36	243.32	0/1	Yes
83	$CF_3CH_2SOCH_2CH_2CH_2CH_2CH_2NCS$	SO	2.58	29.43	259.32	0/2	Yes
87	$CF_3CH_2SO_2CH_2CH_2CH_2CH_2CH_2NCS$	SO_2	2.98	46.51	275.32	0/3	Yes
3	$CH_3SCH_2CH_2CH_2CH_2NCS$ (Erucin)	S	2.67	12.36	161.29	0/1	Yes
1	$CH_3SOCH_2CH_2CH_2CH_2NCS$ (SF)	SO	1.15	29.43	177.29	0/2	Yes
4	$CH_3SO_2CH_2CH_2CH_2CH_2NCS$ (Erysolin)	SO_2	1.55	46.51	193.29	0/3	Yes
2	$CH_3SOCH_2CH_2CH_2NCS$ (Iberin)	SO	0.88	29.43	163.27	0/2	Yes
	$FCH_2SOCH_2CH_2CH_2CH_2NCS$	SO	1.43	29.43	195.28	0/2	Yes
	$(CF_3)_3CSOCH_2CH_2CH_2CH_2NCS$	SO	3.98	29.43	381.29	0/2	Yes
	CH_2CHCH_2NCS (Allyl Isothiocyanate)	No S	2.25	12.36	99.16	0/1	Yes
	$C_6F_5CH_2SOCH_2CH_2CH_2CH_2NCS$	SO	3.27	29.43	343.34	0/2	Yes
	$C_6H_5CH_2NCS$	No S	3	12.36	149.22	0/1	Yes
156	$HCCCH_2SOCH_2CH_2CH_2CH_2NCS$	SO	1.3	29.43	201.32	0/2	Yes
167	$TPP^+(CH_2)_4C_2N_3HCH_2SO(CH_2)_4NCS$	SO	4.54	60.15	561.74	0/2	No – MW

Table 2.1 Calculated molecular properties and conformance with Lipinski's rule of 5 for fluorinated isothiocyanate probes and for some natural isothiocyanates (calculated using Molinspiration® software)

Some trends emerge when comparing these molecules. The values for TPSA and numbers of hydrogen bond acceptors are both dictated predominantly by the oxidation state of the sulphur atom, with constant values for each of the three categories of compounds. The values for cLogP show that in every series the sulfide is the most lipophilic, oxidation to the sulfoxide considerably reduces lipophilicity, while adding the second oxygen atom to make a sulfone increases lipophilicity again to an intermediate value, although closer to that of the sulfoxide than to that of the sulfide. Lipophilicity likewise increases with molecular weight, since the difference comes from adding methylene groups. It is particularly interesting to compare the trifluoromethyl ($-CF_3$) and the trifluoroethyl ($-CH_2CF_3$) derivatives, though. The $-CH_2CF_3$ compounds in a series share the same MW as the $-CF_3$ derivatives of the series with the immediate superior alkyl length (e.g. the $-CH_2CF_3$ derivatives in the 2 carbon series **76**, **80** and **84** have the same MW as the $-CF_3$ derivatives in the 3 carbon series **101, 105,** and **109** respectively). However, the direct attachment of the $-CF_3$ moiety to the sulphur atom considerably increases cLogP, to the extent that the lowest cLogP in the TFM series (4.15 for the two carbon sulfoxide **104**) is higher than the highest cLogP in the $-CH_2CF_3$ series − (4.1 for the five carbon sulphide **79**). This is likely due to the electronwithdrawing effect of the directly attached $-CF_3$ group reducing the availability of sulphur electrons. The natural sulfoxides, sulforaphane **1** and iberin **2**, have the lowest cLogP values (0.88 and 1.15, respectively), but the $-CH_2CF_3$ sulfoxides (**80-83**), with cLogP values between 1.53 and 2.58, come reasonably close. With a cLogP > 5, none of the sulfides in the $-CF_3$ series (**100-103**) conform to Lipinski's rule of five; furthermore, the 4 and 5 carbon sulfones (**110, 111**) and the 5 carbon sulfoxide **107** were also calculated to be too lipophilic.

Table 2.2 Heatmap of Molinspiration® bioactivity scores for the fluorinated isothiocyanate probes and for some natural isothiocyanates (Green shows better activity). (*Continued on next page.*)

ID No	Molecule	GPCR ligand	Ion Channel Modulator	Kinase inhibitor	Nuclear receptor ligand	Protease inhibitor	Enzyme inhibitor
100	$CF_3SCH_2CH_2NCS$	-0.65	-0.5	-1.99	-1.41	-1.4	-0.13
104	$CF_3SOCH_2CH_2NCS$	-0.47	-0.33	-1.4	-1.01	-1.08	0.24
108	$CF_3SO_2CH_2CH_2NCS$	-0.53	-0.54	-1.39	-1.03	-0.9	0.01
76	$CF_3CH_2SCH_2CH_2NCS$	-0.63	-0.56	-1.84	-1.19	-1.15	-0.02
80	$CF_3CH_2SOCH_2CH_2NCS$	-0.45	-0.65	-1.34	-0.86	-0.98	0.25
84	$CF_3CH_2SO_2CH_2CH_2NCS$	-0.45	-0.83	-1.31	-0.89	-0.73	0.04
101	$CF_3SCH_2CH_2CH_2NCS$	-0.43	-0.2	-1.72	-1.09	-0.96	0.01
105	$CF_3SOCH_2CH_2CH_2NCS$	-0.22	-0.09	-1.38	-0.63	-0.61	0.31
109	$CF_3SO_2CH_2CH_2CH_2NCS$	-0.37	-0.14	-1.22	-0.78	-0.55	0.12
77	$CF_3CH_2SCH_2CH_2CH_2NCS$	-0.41	-0.27	-1.59	-0.91	-0.75	0.1
81	$CF_3CH_2SOCH_2CH_2CH_2NCS$	-0.21	-0.4	-1.32	-0.51	-0.54	0.31
85	$CF_3CH_2SO_2CH_2CH_2CH_2NCS$	-0.3	-0.44	-1.15	-0.66	-0.41	0.15
102	$CF_3SCH_2CH_2CH_2CH_2NCS$	-0.33	-0.19	-1.54	-0.89	-0.79	0.16
106	$CF_3SOCH_2CH_2CH_2CH_2NCS$	-0.13	-0.09	-1.23	-0.46	-0.47	0.43
110	$CF_3SO_2CH_2CH_2CH_2CH_2NCS$	-0.27	-0.14	-1.09	-0.61	-0.41	0.25
78	$CF_3CH_2SCH_2CH_2CH_2CH_2NCS$	-0.31	-0.26	-1.43	-0.72	-0.6	0.24
82	$CF_3CH_2SOCH_2CH_2CH_2CH_2NCS$	-0.12	-0.38	-1.18	-0.36	-0.4	0.43
86	$CF_3CH_2SO_2CH_2CH_2CH_2CH_2NCS$	-0.21	-0.42	-1.03	-0.5	-0.29	0.26
103	$CF_3SCH_2CH_2CH_2CH_2CH_2NCS$	-0.22	-0.12	-1.36	-0.72	-0.64	0.23
107	$CF_3SOCH_2CH_2CH_2CH_2CH_2NCS$	-0.04	-0.03	-1.07	-0.33	-0.34	0.48

111	CF$_3$SO$_2$CH$_2$CH$_2$CH$_2$CH$_2$CH$_2$NCS	-0.17	-0.08	-0.95	-0.47	-0.29	0.31
79	CF$_3$CH$_2$S(CH$_2$)$_5$NCS	-0.2	-0.19	-1.25	-0.57	-0.46	0.3
83	CF$_3$CH$_2$SO(CH$_2$)$_5$NCS	-0.03	-0.31	-1.03	-0.24	-0.28	0.47
87	CF$_3$CH$_2$SO$_2$(CH$_2$)$_5$NCS	-0.11	-0.36	-0.9	-0.38	-0.18	0.31
3	CH$_3$SCH$_2$CH$_2$CH$_2$CH$_2$NCS (Erucin)	-2	-1.64	-3.48	-2.67	-2.2	-0.88
1	CH$_3$SOCH$_2$CH$_2$CH$_2$CH$_2$NCS (Sulforaphane)	-0.35	-0.59	-1.98	-0.84	-0.72	0.44
4	CH$_3$SO$_2$CH$_2$CH$_2$CH$_2$CH$_2$NCS (Erysolin)	-0.71	-0.59	-1.51	-1.27	-0.77	0.01
2	CH$_3$SOCH$_2$CH$_2$CH$_2$NCS (Iberin)	-1.44	-1.63	-3.19	-2.04	-1.88	-0.69
	FCH$_2$SOCH$_2$CH$_2$CH$_2$CH$_2$NCS	-0.46	-0.38	-1.65	-0.5	-0.61	0.44
	(CF$_3$)$_3$CSOCH$_2$CH$_2$CH$_2$CH$_2$NCS	0.23	-0.05	-0.41	0.14	0.14	0.42
	CH$_2$CHCH$_2$NCS	-3.68	-3.67	-3.99	-3.8	-3.85	-3.22
	C$_6$F$_5$CH$_2$SOCH$_2$CH$_2$CH$_2$CH$_2$NCS	0.07	-0.28	-0.61	-0.21	-0.05	0.36
	C$_6$H$_5$CH$_2$NCS	-0.95	-0.28	-1.62	-1.57	-1.49	-0.22
156	HCCCH$_2$SOCH$_2$CH$_2$CH$_2$CH$_2$NCS	-0.41	-0.54	-1.57	-0.79	-0.78	0.34
167	TPP$^+$(CH$_2$)$_4$C$_2$N$_3$HCH$_2$SO(CH$_2$)$_4$NCS	0.27	-0.29	-0.25	-0.25	-0.05	0.4

The Molinspiration® bioactivity prediction calculates a druglikeness score for six important
drug classes, with higher scores suggesting increased likelihood of druglike activity in these
classes. With scores above 0.2 being considered a positive result, sulforaphane was predicted
to only have activity as inhibitor of other enzymes (see heat-map in **Table 2.2**). Notably
however, the scores for the other natural isothiocyanates included in the comparison (iberin **2**,
erucin **3**, erysolin **4**, allyl isothiocyanate and benzyl isothiocyanate) were negative, suggesting
a low likelihood of activity as enzyme inhibitors. On the positive side, all the sulfoxides in the
library were also predicted to show some enzyme inhibitor activity, with both 4-carbon

sulfoxides (**82** and **106**) showing almost identical scores to **1**, and the 5-carbon sulfoxides (**83** and **107**) having the highest overall scores.

Overall, the computational predictions suggested a good similarity between the designed library of fluorinated isothiocyanates and the natural ITCs. The –CH$_2$CF$_3$ derivatives, despite their slightly higher molecular weight, were predicted to more closely resemble the natural ITCs than the –CF$_3$ derivatives.

2.2.3 Synthetic approach

To modify the alkyl chain length, four different commercially available phthalimide-protected amino-bromoalkanes, **64-67** were chosen as starting materials, having an alkyl chain length between two and five carbon atoms. To vary the oxidation state of the sulfur atom, some of the initially synthesised sulfides were oxidized stepwise to sulfoxide and then to sulfone. However, the modification from trifluoroethyl to trifluoromethyl required adopting completely different fluorination strategies. The first set of fluorinated derivatives, carrying the 2,2,2-trifluoroethyl moiety, was synthesised based on existing work (Kiełbasiński et al. 2014) (**Scheme 2.4**). 2,2,2-Trifluoroethanethiol was used as source for the fluorine atoms, through an intermediary sodium thiolate (**68**-**71)**, which was reacted with the brominated *N*-alkyl-phthalimide starting materials. The phthalimide protecting group was removed from the resulting sulphides using the standard method of hydrazinolysis in ethanol at reflux. The newly formed amines (**72**-**75**) were telescoped and treated with thiophosgene, with cooling and neutralization of the formed HCl, forming the isothiocyanate group. The resulting compounds (**76-79**) were the sulfides, the first set of compounds that would be part of the library. After "flash" chromatography purification,

successive oxidations using 3-chloro-perbenzoic acid (mCPBA) gave access to sulfoxides **80-83** and sulfones **85** and **86**. Sulfones **84** and **87** were not synthesized due to a low amount of sulfoxide starting material.

64-67 (n=1-4)   **68-71** (n=1-4)   **72-75** (n=1-4)

76-79 (n=1-4)   **80-83** (n=1-4)   **84-87** (n=1-4)
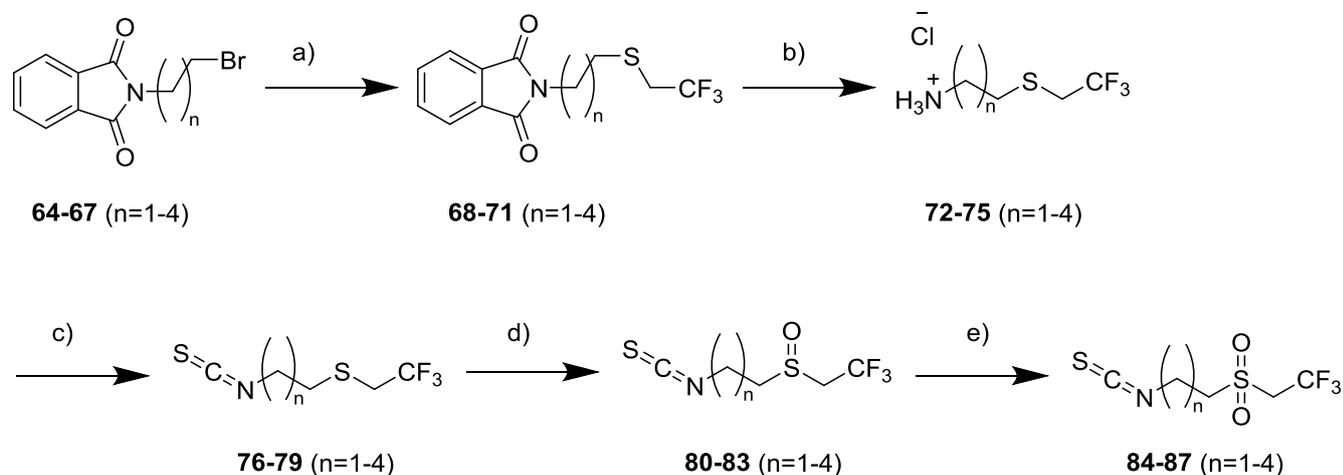
Scheme 2.4. Synthesis of trifluoroethylated isothiocyanates. Reagents and conditions: a) Na, CF$_3$CH$_2$SH, dimethoxyethane, 0 ºC to rt; b) NH$_2$NH$_2$·H$_2$O, EtOH, reflux then HCl, reflux; c) CSCl$_2$, *aq* NaOH (5%), CHCl$_3$, 0-5 ºC; d) *m*CPBA, CH$_2$Cl$_2$, 0 ºC; e) *m*CPBA, CH$_2$Cl$_2$, rt.

Table 2.3 Isolated yields for trifluoroethyl derivatives

Number of carbons	Trifluoroethanethiolation		Phthalimide deprotection + ITC assembly		Oxidation to sulfoxide		Oxidation to sulfone	
	Entry	**Yield (%)**	**Entry**	**Yield (%)**	**Entry**	**Yield (%)**	**Entry**	**Yield (%)**
2	**68**	76	**76**	37	**80**	88	**84**	—
3	**69**	70	**77**	53	**81**	83	**85**	65
4	**70**	86	**78**	49	**82**	85	**86**	72
5	**71**	71	**79**	42	**83**	80	**87**	—

The synthesis of a second group of trifluoromethylated derivatives, while starting from the same phthalimide-protected amino bromo alkanes (**64**-**67**), required a different fluorination approach (**Scheme 2.5**). Trifluoromethanethiol, which could theoretically be used as a

homologue for 2,2,2-trifluoroethanethiol in the reaction used for the first set of F-ITCs, is unstable, decomposing to release hydrofluoric acid, while its stabilized forms – copper or tetramethylammonium salts, are expensive. Thus, instead of attaching the –SCF$_3$ group, to the existing carbon skeleton, we chose to create the S-CF$_3$ bond.

The usual strategy for substitution on the sulphur atom, using thiols or thiolates as nucleophiles (RS$^-$ + X-CF$_3$), fails due to the negative polarization caused by the three fluorine atoms in trifluoromethyl groups. For this reason, we used a method (Matheis et al. 2015) that avoids this issue by changing the polarity of the sulfur atom by placing it in a thiocyanate group (SCN). In a one pot reaction, treatment of our starting materials with inexpensive sodium thiocyanate led to the required organic thiocyanates. Ruppert's reagent **40** was added, with trifluoromethylation occurring under basic conditions (Cs$_2$CO$_3$), with the trifluoromethyl group attacking the partial positive charge of the sulfur atom (**Scheme 2.6**). Following this key step, subsequent hydrazinolysis, ITC assembly and oxidation reactions occurred in a similar fashion compared to the trifluoroethyl series, with a notable mention that sulphur oxidation was predictably slowed by the direct adjacency of the trifluoromethyl group.

64-67 (n=1-4)   **92-95** (n=1-4)   **96-99** (n=1-4)

100-103 (n=1-4)   **104-107** (n=1-4)   **108-111** (n=1-4)
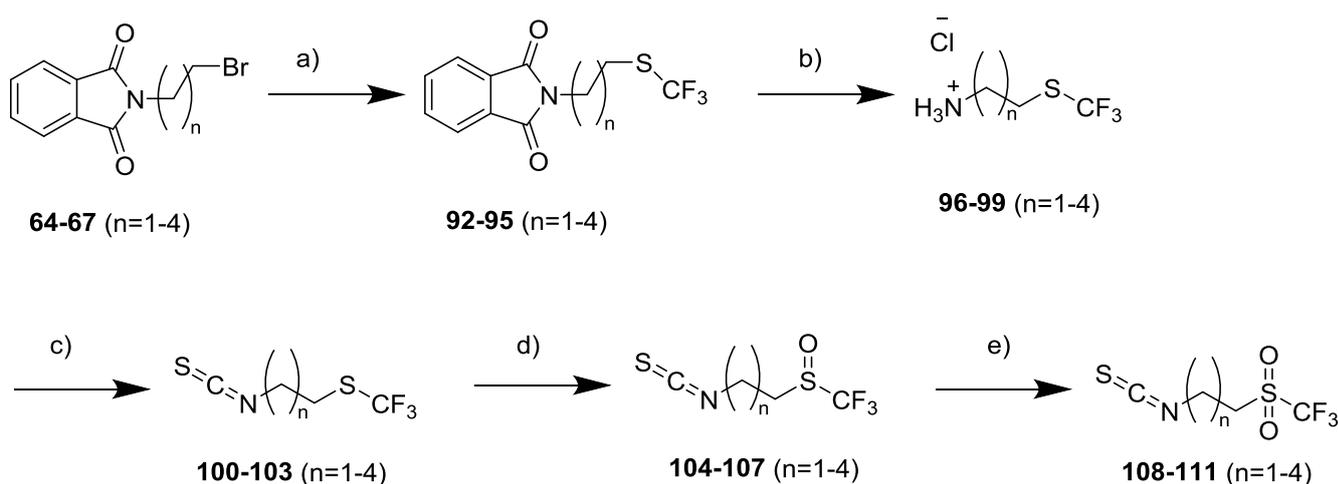
Scheme 2.5 Synthesis of trifluoromethylated isothiocyanates. Reagents and conditions: a) NaSCN, Cs$_2$CO$_3$, TMSCF$_3$, CH$_3$CN, 60 °C; b) NH$_2$NH$_2$·H$_2$O, EtOH, reflux then HCl, reflux; c) CSCl$_2$, *aq* NaOH (5%), CHCl$_3$, 0 °C; d) *m*CPBA, CH$_2$Cl$_2$, 0 °C; e) *m*CPBA, CH$_2$Cl$_2$, rt.
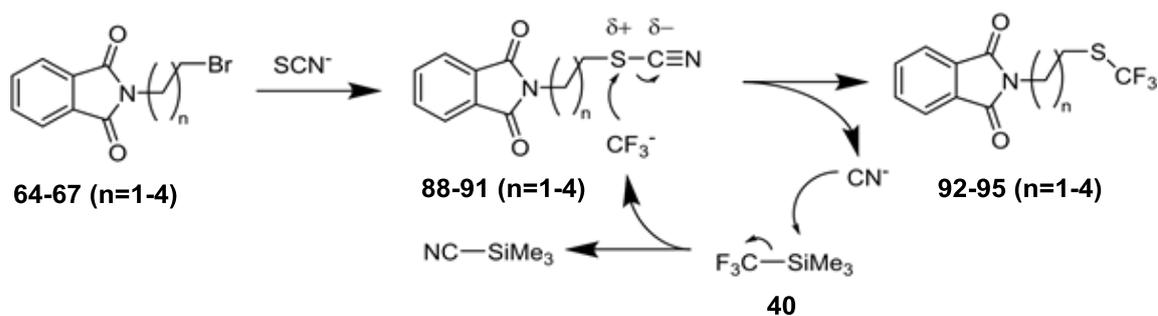
Scheme 2.6 Mechanism for the trifluoromethylation reaction using sodium thiocyanate and Ruppert-Prakash reagent **40**

Table 2.4 Isolated yields for trifluoromethyl derivatives

Number of carbons	-SCF₃ formation		Phthalimide deprotection + ITC assembly		Oxidation to sulfoxide		Oxidation to sulfone	
	Entry	**Yield (%)**	**Entry**	**Yield (%)**	**Entry**	**Yield (%)**	**Entry**	**Yield (%)**
2	**92**	81	**100**	38	**104**	68	**108**	—
3	**93**	75	**101**	20	**105**	73	**109**	—
4	**94**	82	**102**	44	**106**	78	**110**	65
5	**95**	80	**103**	39	**107**	75	**111**	—

2.3. Biological testing

The initiation of apoptosis is associated with changes in the polarity of the mitochondrial membrane, as they allow the release of cytochrome c. The proapoptotic effects of the ITCs were determined using flow cytometry. Flow cytometry is a technique in which a suspension of cells is guided by a narrow sheath of exterior fluid, separating them and allowing them to be

counted individually. Lasers emitting at specific wavelengths are used to illuminate the cells, with light detectors able to measure two types of scattered light as well as fluorescence. Forward scattered light (FSC) is typically considered to indicate cell size (with larger cells leading to more FSC), while side scattered light is associated with cell granularity (with more granular cells increasing SSC), though there can be exceptions with both.

The mitochondrial changes were assessed both dependent and independent of mitochondrial depolarisation (using the JC-1 and MitoTracker Green dyes, respectively). In the JC-1 assay, apoptosis was determined based on the ratio between green and yellow fluorescence. In normally-polarised cells, JC-1 is absorbed in mitochondria where it forms yellow fluorescent aggregates (**Fig 2.3**, see also **Chapter 3.2.2**). In apoptotic cells, depolarisation of the mitochondrial membrane leads to diffusion and dissociation of the aggregates into monomers with green fluorescence.
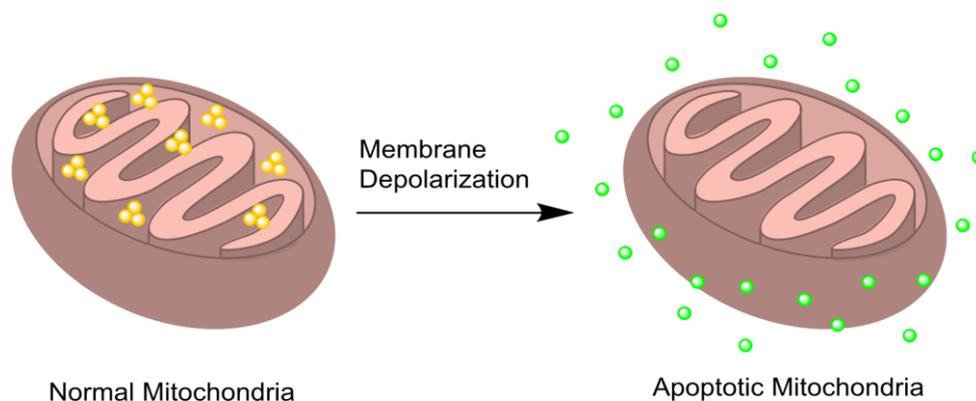

Fig. 2.3 JC-1 staining based on mitochondrial membrane potential: Yellow fluorescent aggregates inside the mitochondria (in normal functioning mitochondria) exit and disperse into green fluorescent monomers upon membrane depolarization characteristic of apoptosis.

Additionally, the initiation of apoptosis is associated with decreasing cell size and increasing granularity, resulting in a shift up and to the left on the side scatter vs forward scatter plot (**Fig. 2.4 a-c**). At high concentrations (40-80 µM), there was a clear reduction in normal aspect cells

compared to untreated, or cells treated only with PBS or vehicle. At low concentrations (up to 10 µM), changes in apoptotic state, as detected by means of the JC-1 dye were more evident than changes in aspect. (**Fig. 2.4 d-f**, **Fig. 2.4** and **Table 2.5**).
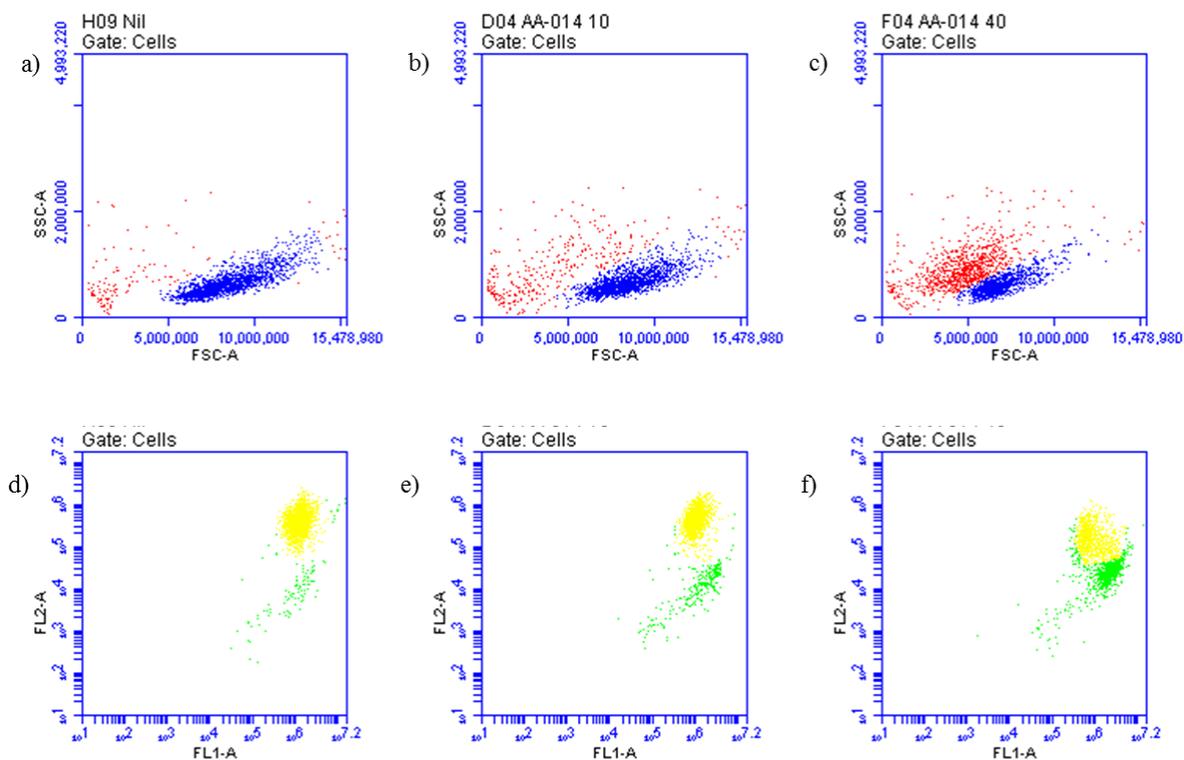

Fig. 2.4 Effect of fITCs on THP1 cell viability Representative dot plots show the effect of one candidate fITC, **83**, on the human monoblastic cell line, THP1, versus untreated cells. a-c depict side scatter vs forward scatter plots, a measure of granularity and cell size, respectively, and reveal a dose-dependent decrease in size and increase in granularity which is indicative of morphologically identifiable apoptosis (red dots) compared to normal presenting cells (blue dots). d-f depict mitochondrial membrane polarisation ($\Delta\Psi$m) using JC-1 dye. Polarised membranes in viable cells form JC-1 polymers that fluoresce at 585 nm (yellow dots), whereas apoptotic cells show depolarised membranes (green dots) that have higher green fluorescence and lower fluorescence. a, d – untreated cells; b, e: cells treated with 10 µM **83**; c, f: cells treated with 40 µM **83**. Data obtained on a BD Accuri C6. FL-1 (λ_{Ex} 488 nm; λ_{Em} 533/30 nm) FL-2 (λ_{Ex} 488 nm; λ_{Em} 585/40 nm).

A second emerging trend was the increased proapoptotic activity of sulfoxides compared to sulfides – erucin **3**, itself a sulfide, as well as **76-79** all showed considerably lower proapoptotic activity. Sulforaphane **1** and iberin **2**, as well as the fluorinated isothiocyanate sulfoxides **80-**

83 all had a higher proapoptotic activity (**Fig. 2.5**). Importantly, the apoptosis levels induced by F-ITCs were very similar in all cases to those of their natural counterparts, suggesting that their apoptotic activity occurs through similar mechanisms. This goes towards confirming the initial hypothesis that the F-ITCs can be used as reliable models for the activity of natural ITCs. The influence of alkyl chain length was not consistent between sulfides and sulfoxides, though the derivative with 4 carbon atoms **82** (i.e. the fluorinated sulforaphane analogue) had the highest proapoptotic activity.
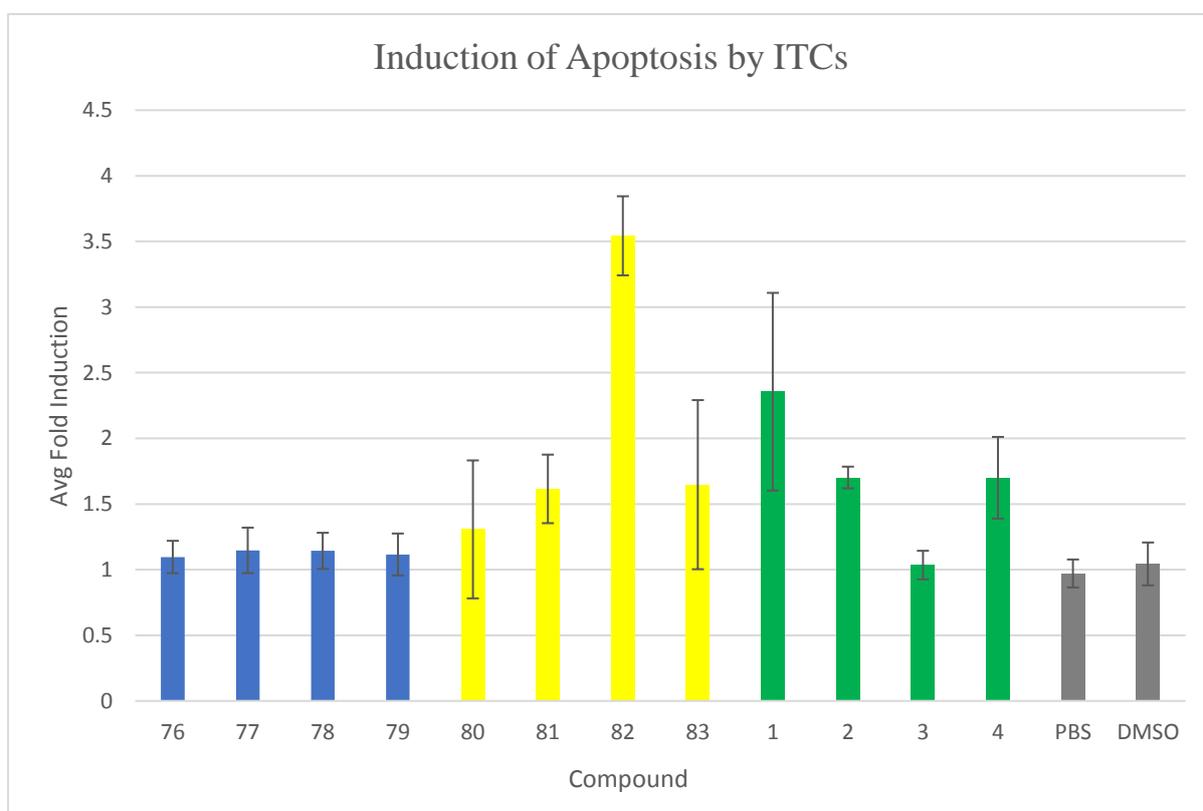

Fig 2.5 Apoptotic cells as detected using the JC-1 dye for four sulfides (**76-79**) (blue), four sulfoxides (**80-83**) (yellow) and four natural isothiocyanates (sulforaphane – SFN, iberin – IBE, erucin – ERU, and erysolin – ERY) (green) used at 10 µM concentration, compared to vehicle (DMSO/PBS), normalized versus untreated cells.

2.4. ¹⁹F-NMR studies of fluorinated isothiocyanates

2.4.1 Limit of detection and limit of quantification

A first step in determining whether ¹⁹F-NMR could be used as a chemical probe to follow metabolic changes in cells treated with the fluorinated isothiocyanates was to determine the limits of detection (LOD) and quantification (LOQ) for the F-ITCs and whether they were compatible with the concentrations used in the biological testing. The limit of detection is considered the lowest concentration at which the analyte can be reliably distinguished from the noise – in this case, the LOD required a minimum signal to noise (S/N) ratio of 2:1. The limit of quantification is the lowest analyte concentration that exhibits the S/N ratio required for reaching an acceptable precision, based on the method. For our purposes, a S/N ratio of 10:1 was sufficient for LOQ.

Since signal intensity increases in proportion to the number of NMR acquisition scans, a larger number of scans would ensure improved S/N ratios, with a correlated increase in experiment duration. For the purposes of this analysis, for lower concentrations of analyte we chose a number of scans of 512, which allowed for an acceptable duration of around 15 minutes per NMR experiment, while 128 scans were sufficient for the more concentrated solutions. Spectra of serial dilutions of 1, 0.1, 0.01, and 0.001 mg/mL of compound **82** (examples in **Fig. 2.6**), corresponding to concentrations of 4.6 mM, 0.46 mM, 0.046 mM and 4.6 µM, respectively, were taken and S/N ratios were calculated. Using the data in **Table 2.5**, the LOD using 512 scans was determined to be 5.3 µM, while the LOQ was 26.7 µM. Qualitative studies could, therefore, be performed at concentrations of 10 µM, the lower concentrations used in the biological testing, while quantitative studies could be performed at concentrations of 40 µM.

Table 2.5: Determination of the limit of detection (LOD) and the limit of quantification (LOQ) for fluorinated isothiocyanate **82**

Concentration (mg/mL)	Concentration (mmol/L)	No. Scans	Peak Intensity	Noise Intensity	S/N Ratio
1	4.6	128	5344	6.2	862
0.1	0.46	128	442	4.7	94
0.01	0.046	512	128	8	16
0.001	0.0046	512	11.2	8.1	1.38
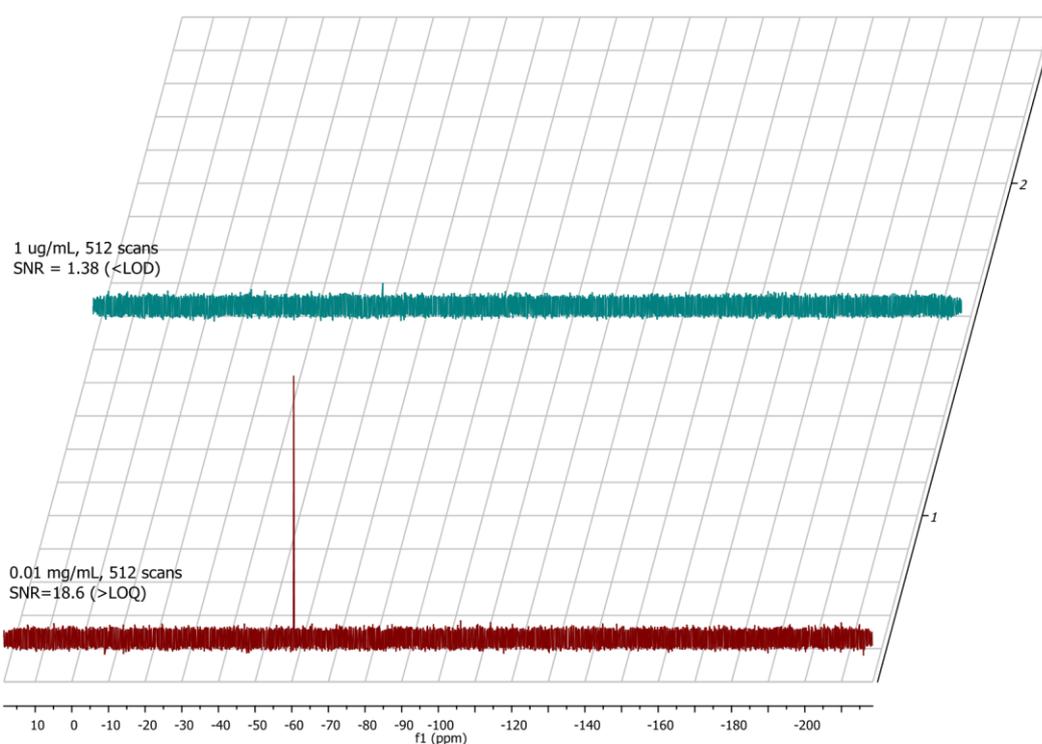
**Fig 2.6** ^{19}F-NMR spectra of lowest concentrations of the serial dilutions of compound **82**. Top: 1 µg/mL, SNR = 1.38; Bottom, 10 µg/mL, SNR = 16.

2.4.2 Stability studies

As mentioned above, sulforaphane is relatively unstable: pure sulforaphane is normally stored under a protective atmosphere and at cold temperatures, and it decomposes faster in an aqueous environment and at higher temperatures, so it would be beneficial to create derivatives that mimic its activity while having improved stability. Using ^{19}F-NMR, we performed some initial studies into the stability of our F-ITCs, focusing on the pure compounds, as well as solutions in water, PBS, and RPMI 1640 cell media.

2.4.2.1 Solid compound stability

The pure compounds were stored as solids in glass vials at room temperature. Repeated NMR acquisitions in CDCl$_3$ indicated that the compounds remained constant over more than a year.

2.4.2.2 Stability in solution

According to ^{19}F-NMR analysis, sulfides and sulfoxides behaved differently when dissolved in biologically relevant media. At a concentration of 40 µM, the sulfides remained stable in water and PBS (sharp signal at -66.2 ppm), whereas in RPMI 1640 media, the characteristic fluorine signal vanished immediately (**Fig. 2.7**). Only at much higher concentrations (1 mM, incompatible with biological testing), could we observe a new broad signal at around -65.6 ppm along with remaining intact starting sulfide at -66.2 ppm. This may represent the formation of a new fluorinated product. Together with the cLogP data (**Table 2.1**), this suggests that the increased lipophilicity of the sulfides makes them more available for reaction with one or more components of the media. This reaction could be the reason for their lack of biological activity – for the most part, the sulfides may not manage to reach the interior of the cell to have a noticeable effect.
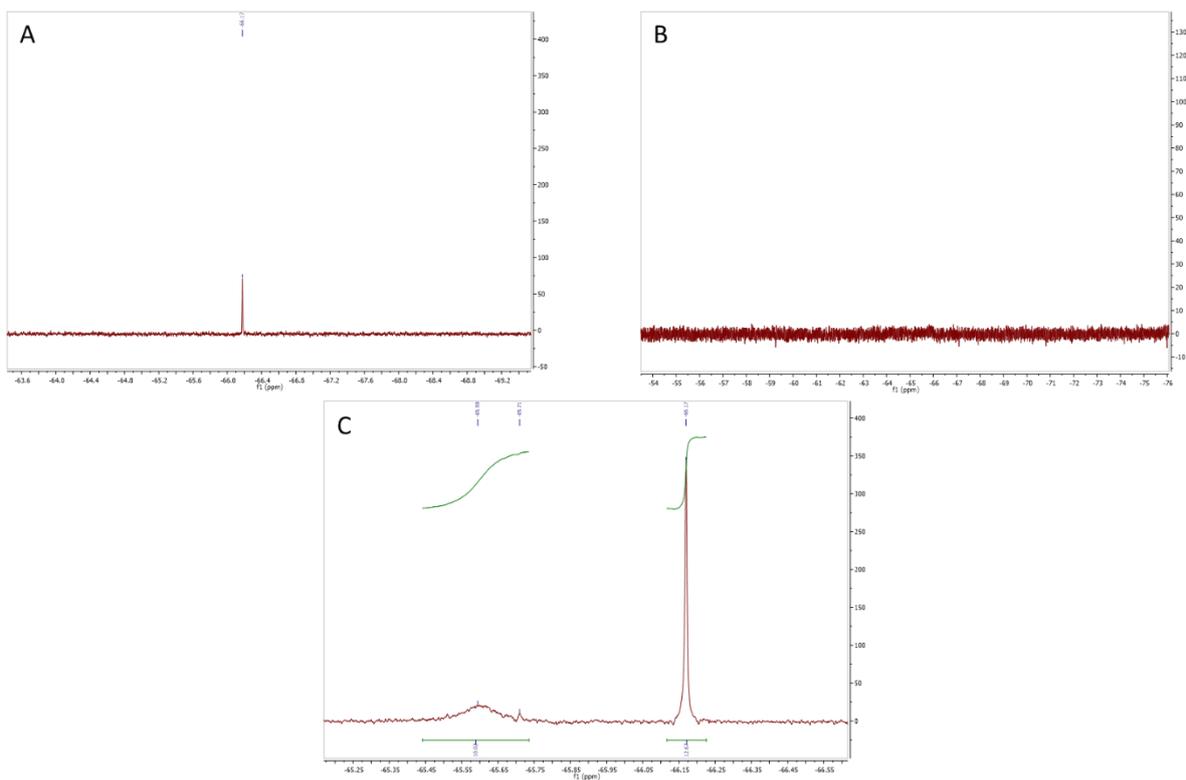
Fig. 2.7 Sulfide stability in PBS and RPMI 1640 media: A. 40 µM sulfide in PBS shows the characteristic sharp peak in proton decoupled ^{19}F-NMR (565 MHz); B. 40 µM sulfide in media shows no noticeable fluorine peak; C. 1 mM sulfide in media shows some starting sulfide, and a new broad peak.

Unlike the sulfides, the sulfoxides did not appear to undergo an immediate reaction with the RPMI media, with the sharp fluorine signal observable in media as well as in water and in PBS. A longer study at a higher concentration (500 µM) in water revealed a slow gradual change.
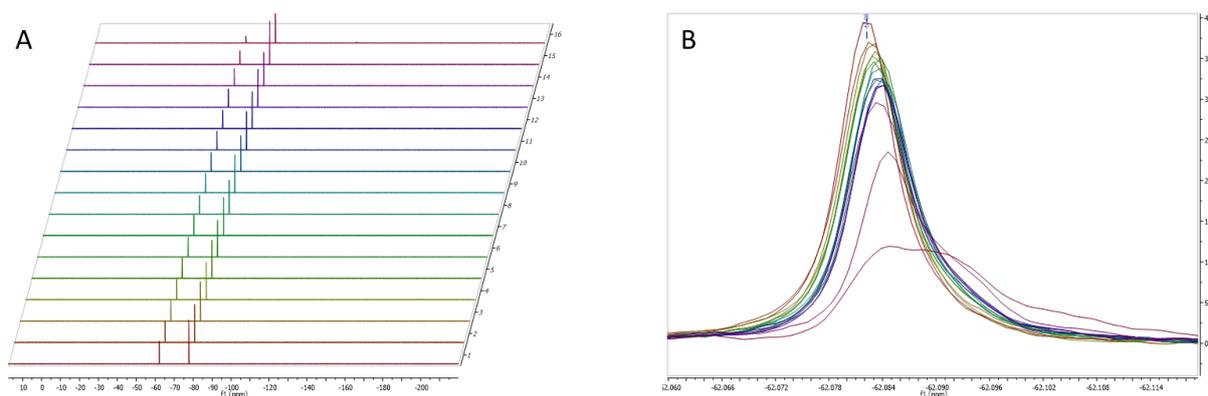
Fig. 2.8 Sulfoxide stability in RPMI media: A. Stacked view of ^{19}F-NMR spectra of sulfoxide in media over 3 days with a new fluoride peak; B. Overlap view of the fluorine peak shows a gradual broadening and shift upfield in the fluorine peak.

Another feature we observed was the surprising appearance of a new peak at -120.5 ppm, in an area characteristic for free fluoride (**Fig 2.8**). This new signal, noticeable only after >24 h, suggested that the trifluoroethyl sulfoxides may undergo a slow hydrolysis to afford the carboxylic acid (**Scheme 2.7**). Indeed, while most trifluoromethyl groups are stable to hydrolysis, some can react in the presence of strong acids

(e.g. when adjacent to aryl groups) or in the presence of aqueous bases (Buxton, Stacey and Tatlow, 1954). Basic hydrolysis seems in most cases to require a methylene group situated α to the TFM, as well as an activating group in the β position (e.g. a carbonyl, carboxyl, or aryl group). Examples containing sulfur in the activating group have thus far been limited to sulfonates and sulphonamides (King & Gill, 2002; Yearn & Katzenellenbogen, 1993) we propose that this is the first description of a sulfoxide undergoing the same hydrolysis reaction.
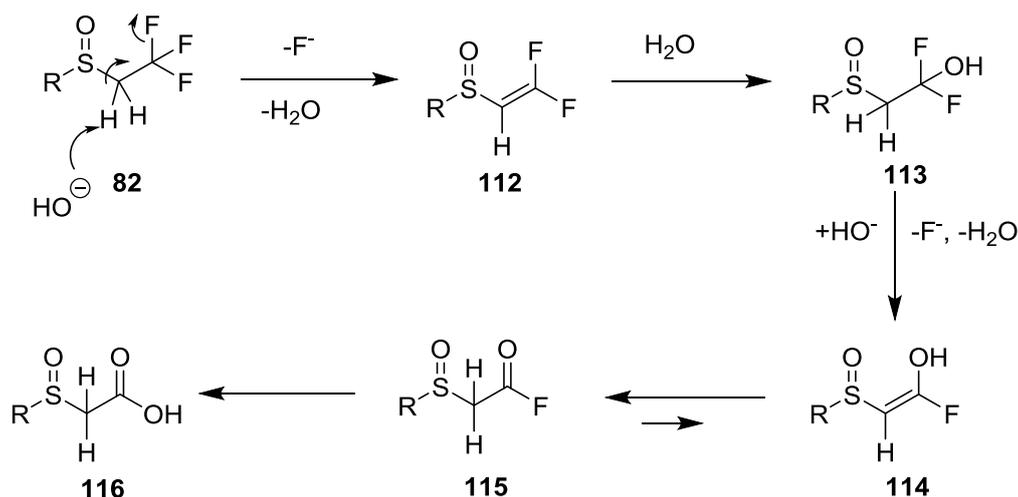
Scheme 2.7 Proposed mechanism for the basic hydrolysis of trifluoroethyl sulfoxides.

To verify this, we dissolved a sulfoxide in an aqueous sodium hydroxide solution. LC-MS analysis confirmed the formation of the carboxylate (m/z for [M+H$^+$] $C_7H_{12}NSO_3$: calculated 222.02531, found 222.02644).

The mechanism for the hydrolysis requires an attack of the hydroxide on the acidified proton of the methylene group, concomitant with the elimination of the fluoride anion (**Scheme 2.7**), leading, via conjugate addition of water to the difluoro species (**113**) and eventually affording an intermediate acyl fluoride **115** that is further hydrolysed to the carboxylic acid. It is probable that the rate limiting step in this transformation is the initial base catalyzed elimination, since the only visible new peak is that for free fluoride. Interestingly, the resulting carboxylic acid **116**, owing to the activating sulfoxide in the beta position, could theoretically undergo decarboxylation, producing a stable carbanion alpha to the sulfur and reprotonating to form natural sulforaphane, similarly to the pathway that transforms tresylates into mesylates (Yearn & Katzenellenbogen, 1993)

While this hydrolysis of trifluoroethyl sulfoxide isothiocyanates suggests that caution should be exercised if these compounds were used for treatment, it is notable that at concentrations used in biological testing this reaction is too slow to be noticeable.

2.4.2.3 Kinetics

Fig. 2.9 Determination of the first order reaction rate constant

To determine the reaction rate constant, we used a graph of the natural logarithm of the concentration versus time (**Fig. 2.9**); the absolute value of the slope of the trendline corresponds to the reaction rate constant. In this case, the rate constant was determined to be 0.0067 h^{-1}, with an R^2 value of 0.9284.

2.5. Conclusions

Expanding on existing work, we designed a library of fluorinated derivatives of sulforaphane to work as probes, covering three oxidation states on the sulfur atom (sulfide, sulfoxide and sulfone). Using Molinspiration®, the trifluoroethyl derivatives were predicted to more closely resemble the natural isothiocyanates than the trifluoromethyl derivatives. The trifluoroethyl derivatives were synthesised in – overall yields over 3-5 stages. The trifluoromethyl derivatives

were synthesised using a SCN to SCF_3 transformation and obtained in – overall yields over 46 stages.

Investigations into the biological activity of F-ITCs followed the computational predictions, with the sulfoxides showing similar activity to sulforaphane, with µM concentrations able to induce apoptosis. ^{19}F-NMR studies suggested that the F-ITCs are detectable at these concentrations, with a limit of detection around 2 µM.

The NMR studies also provided some insight into F-ITC stability in water, PBS and RPMI media. We observed a high instability of sulfides in RPMI media, possibly due to their higher lipophilicity. This may prevent the sulfides from reaching the cells intact, offering a reason for their lower activity in the induction of apoptosis. Furthermore, the studies revealed a hitherto unknown hydrolysis reaction for the sulfoxides. However, this reaction was slow, which allows the fluorinated sulfoxides to function as probes into isothiocyanate metabolism. Future work will examine this reaction in greater detail (more information in future work section).

CHAPTER 3

"CLICK" PROBES TO STUDY SULFORAPHANE METABOLISM

3.1. Introduction – "Click" chemistry

Introduced by Sharpless in 2001 (Kolb *et al.*, 2001), the concept of "click" chemistry refers to reactions that satisfy the following criteria: they are modular and wide in scope, give very high yields, generate innocuous byproducts, which can be removed by nonchromatographic methods, and are stereospecific. They use no solvents, or water, or easily removed solvents, and the reaction conditions must be simple and not sensitive to either water or oxygen. Consequently, these reactions allow the building of great diversity from a small number or products, making them ideal for the development of expansive libraries of products.

To meet the above criteria, "click" reactions require a high thermodynamic driving force, usually above 20 kcal/mol, which is often achieved based on high energy double and triple bonds or highly strained cyclic reactants. Among the reactions initially reviewed as "click" chemistry were the ring opening reactions of three-membered rings, including epoxides and especially aziridines (**Scheme 3.1 A**), "protective group" reactions forming acetal-like compounds (**Scheme 3.1 B**), and 1,3-dipolar cycloadditions, including the ones that have become basically synonymous with "click" reactions, the Huisgen cycloadditions of alkynes and azides (**Scheme 3.1 C**) (Kolb *et al.*, 2001).
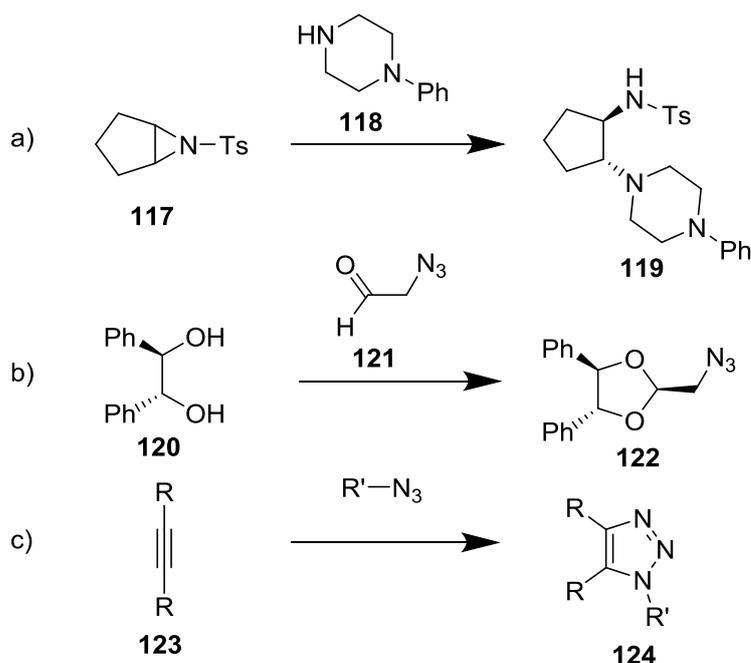
Scheme 3.1 Types of "click" reactions: A) aziridine ring opening; B) acetal formation; C) 1,3-dipolar alkyne-azide cycloaddition.

3.1.1 Regioselectivity in the 1,3-dipolar cycloaddition – Cu and Ru catalyzed reactions

Discovered in the 1960s (Huisgen, 1963; Huisgen *et al.*, 1967), the Huisgen 1,3-dipolar cycloaddition of alkynes and azides to form 1,2,3-triazoles remained relatively ignored for almost forty years. While the reaction is highly exothermic, the high activation energy (20-25 kcal/mol) leads to high temperature requirements and low reaction rates even at higher temperatures. Combined with the lack of regioselectivity (**Scheme 3.2 A**), this significantly reduced the scope of the reaction for "click" purposes to symmetric non-terminal alkynes. In 2002, Sharpless *et al.* showed that Cu(I) can catalyze the reaction for terminal alkynes, not only allowing it to occur at room temperature, but also directing it preferentially towards a 1,4disubstituted 1,2,3-triazole (**Scheme 3.2 B**) (Rostovtsev *et al.*, 2002). Cu(I) salts, such as

CuI or CuOTf·C_6H_6 can be used for catalysis though they may require an oxygen-free environment.

They can be formed *in situ*; variants include the reduction of a Cu(II) salt solution, like the inexpensive $CuSO_4 \cdot 5H_2O$, using ascorbate or ascorbic acid, or the oxidation of Cu(0) (Beckmann & Wittmann, 2007; Presolski *et al.*, 2011).

The discovery of the CuAAC reaction and the regioselectivity afforded by the Cu(I) catalyst suggested there may be a way to direct the reaction towards the opposite 1,5-disubstituted triazole. Indeed, a series of cyclopentadienyl ruthenium complexes were found to catalyze the cycloaddition and preferentially form the 1,5-disubstituted triazole (**Scheme 3.2. C**).
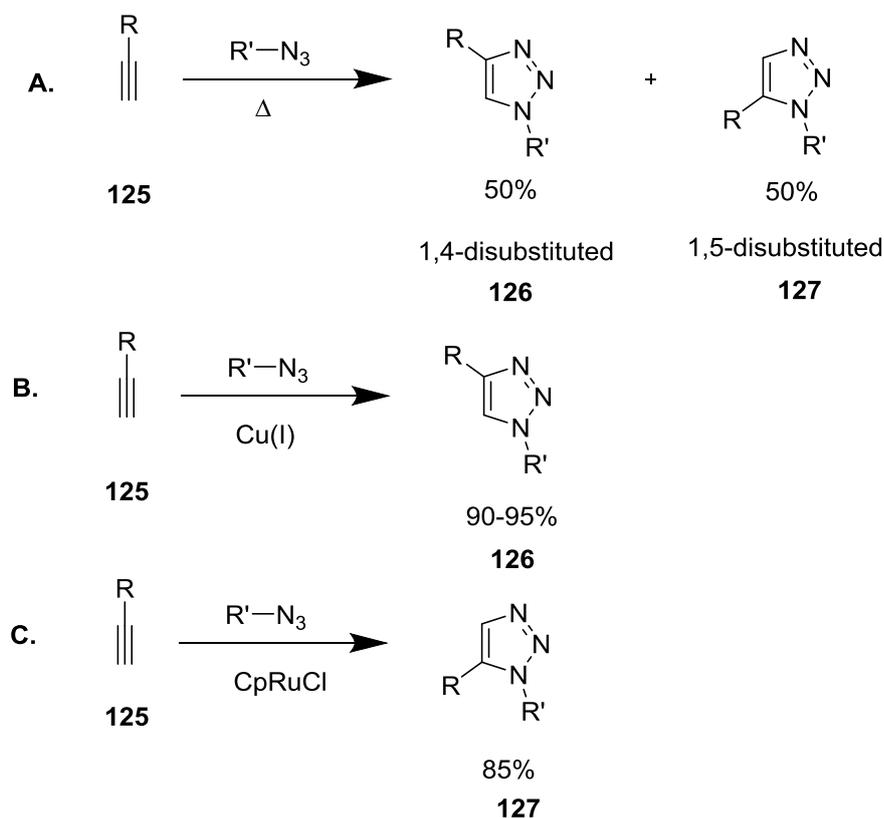
Scheme 3.2 Regioselectivity in the 1,3-dipolar alkyne azide cycloaddition. A. Huisgen's original conditions lead to no regioselectivity B. Cu(I) salts preferentially lead to 1,4

disubstituted triazoles. C. Cp*RuCl and other Ru complexes direct the reaction towards 1,5disubstituted triazoles.

The proposed mechanism (**Scheme 3.3**) involves the terminal carbon from the alkyne and subsequently the internal nitrogen from the azide bonding to two Cu ions, which allows the terminal nitrogen atom to form a bond with the other carbon in the alkyne triple bond. After the metal ions are removed, this leads to the preferential formation of the 1,4-disubstituted triazole.
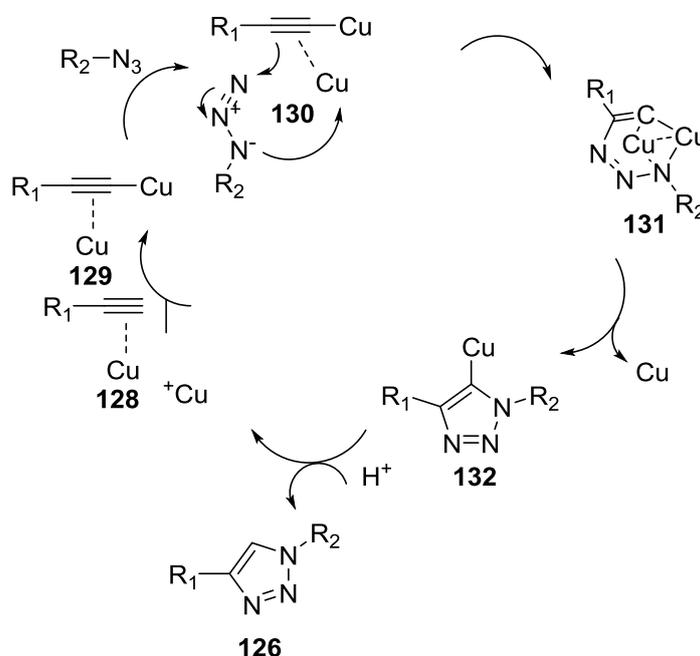
Scheme 3.3 Mechanism of the Cu(I) catalyzed alkyne azide cycloaddition (Rostovtsev *et al.*, 2002)

The copper catalyzed 1,3-dipolar alkyne-azide cycloaddition (CuAAC) was shown to be a robust reaction, able to offer access to a great diversity of compounds. Consequently, it has gained prominence in material science and particularly in chemical biology.

3.1.2 Click chemistry in chemical biology

Importantly, azide and alkyne groups are bioorthogonal, not reacting with any of the functional groups commonly found in biological molecules, which opened the door for an enormous variety of applications in chemical biology. In drug discovery, the "click" approach allows putting together large libraries of compounds for high throughput screenings and fragmentbased drug discovery (**Fig. 3.1**).
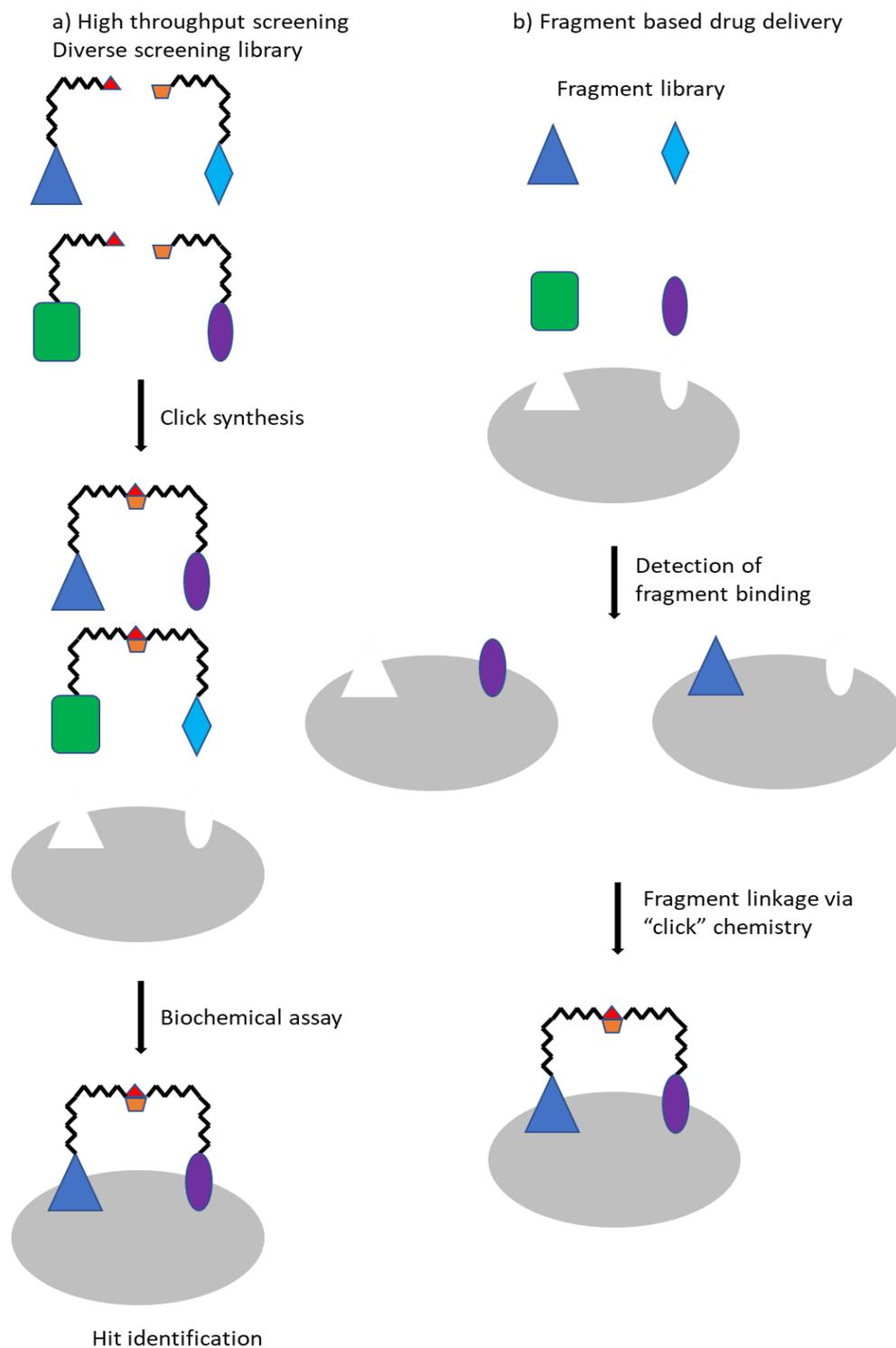
Fig. 3.1 "Click" reactions applied in drug discovery: a) High throughput screening: a screening library is created by "clicking" pairs of compounds; products are then assessed to identify hits; b) fragmentbased drug discovery: fragments are initially tested for binding with the target; probes based fragments that show binding are created and "clicked" to assemble compounds with increased activity (based on (Thirumurugan *et al.*, 2013)).

The modularity implied by "click" reactions makes them particularly useful for assembling fragments to create improved enzyme inhibitors, with examples including inhibitors for, e.g., protein phosphatases, protein kinases, metalloproteinases, cysteine and serine proteases.

Arguably though, the greater improvements allowed by the "click" reaction came in the field of bioconjugation. Here, using reliable "click" reaction (**Fig. 3.2 A**), one can attach a desired tag (or even multiple tags) in a bioorthogonal fashion, at sites modified for this purpose. These tags can therefore be universally used, making some of the most common of them commercially viable and easily accessible. This removes the necessity to rely on reactions that target specific functional groups in biological molecules (e.g. thiols, alcohols, phenols or free amines – **Fig. 3.2 B**), which are more likely to be accompanied by off-target reactions.
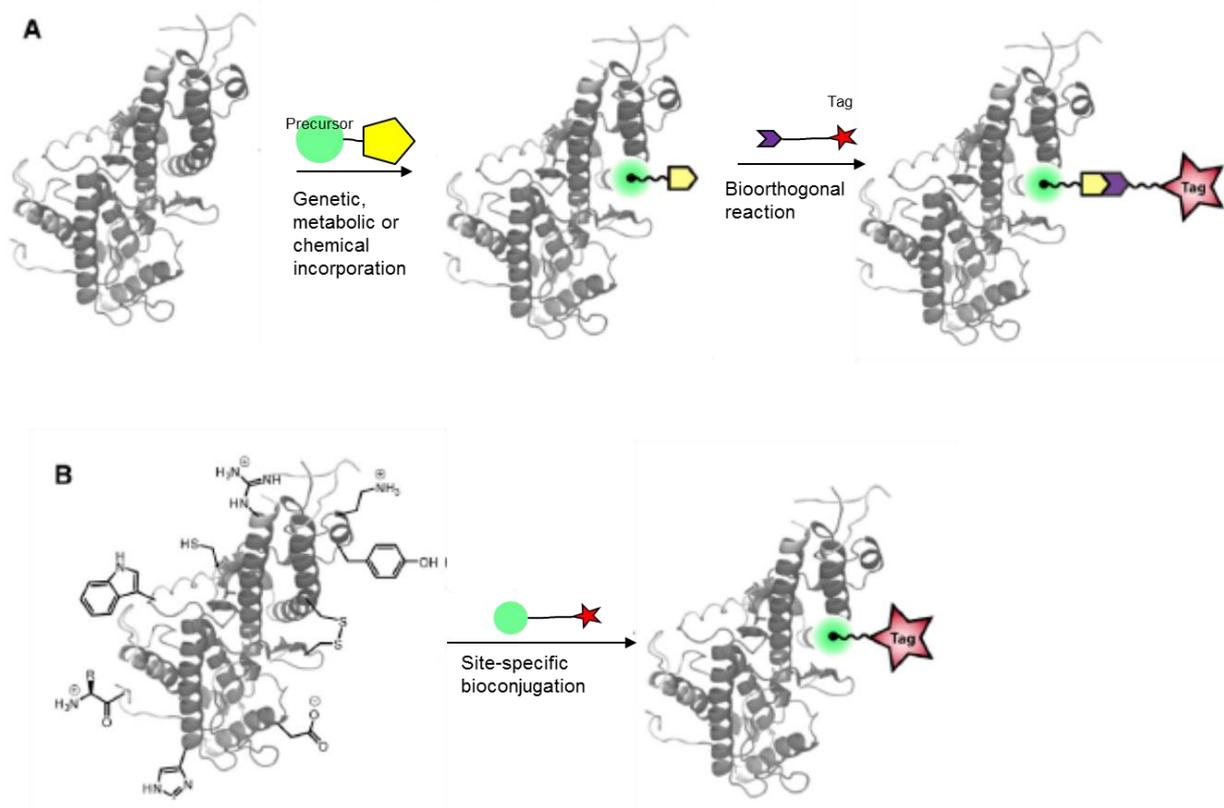

Fig. 3.2 Strategies for bioconjugation: A. "Click" strategy: a precursor with a "clickable" group is incorporated at the desired site in the biomolecule, followed by a "click" reaction to attach the tag; B. Site-specific bioconjugation, where the tag molecule reacts directly with a functional group in a biomolecule.

3.1.3 Strain promoted "click" reactions

The rapid development of applications of CuAAC in chemical biology also highlighted one of its inherent drawbacks – the use of metal catalysts reduced the scope of these applications by preventing their use in live cells. Cu (I) is unstable under physiological conditions and will undergo oxidation to Cu(II), a process associated with the production of reactive oxygen species such as superoxide and hydroxyl radicals which in turn lead to cellular damage. Furthermore, the reducing agent (e.g. ascorbate) can react with amino acid side chains including lysine, arginine and cysteine, leading to protein crosslinking (Jewett & Bertozzi, 2010; McKay & Finn, 2014).

Various approaches were made to avoid the use of metal ions in the "click" reactions, searching for conditions that would allow the reactions to occur as reliably as in their presence. One approach that has gained prominence is the use of strained cyclic alkynes (in strain promoted azide-alkyne cycloaddition – SPAAC) and alkenes (**Scheme 3.4**).
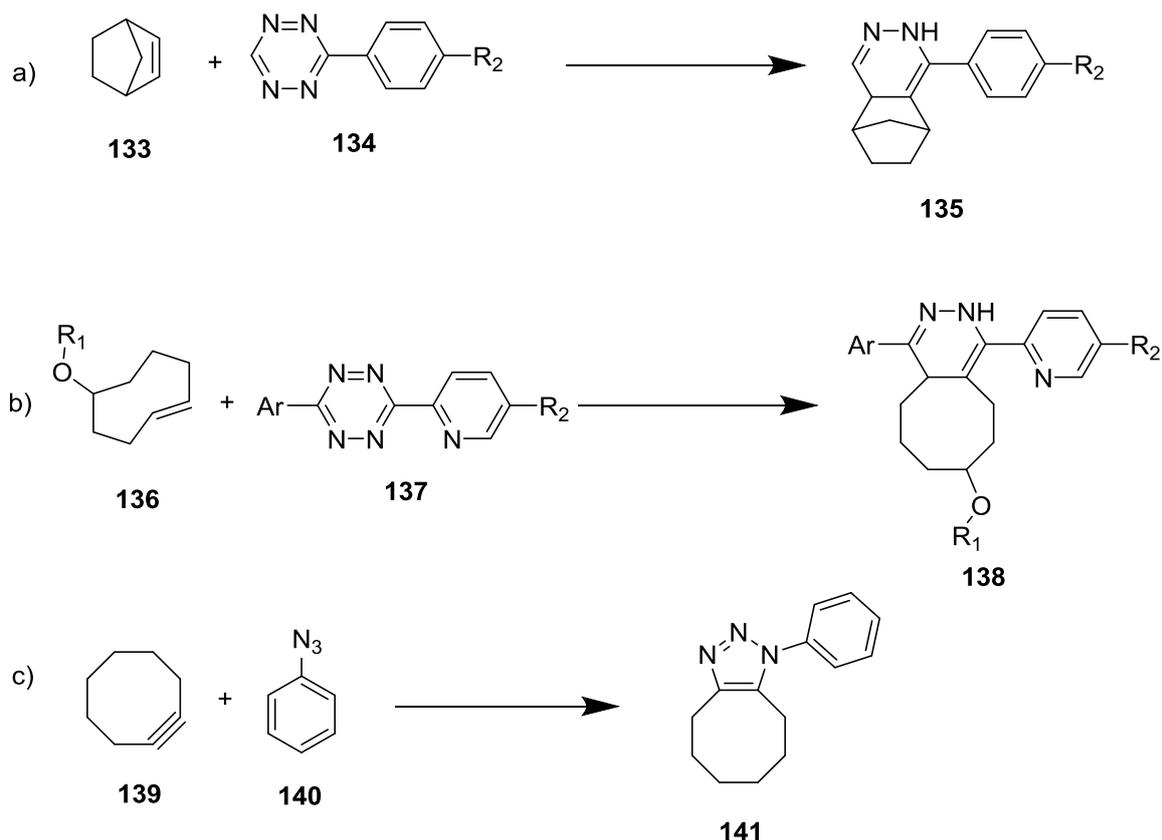
Scheme 3.4 Bioorthogonal strain promoted "click" reactions: A. norbornene and B. *trans*-cyclooctene reactions with tetrazines; C. cyclooctyne and phenyl azide react in a strain promoted azide alkyne cycloaddition (SPAAC).

For alkenes, strategies for inducing strain include *trans*-cycloalkenes and bicyclic alkenes. The strained alkynes used in SPAAC are based on cyclooctyne – cycloalkynes with less than eight carbons are too strained and unstable, while the strain in cyclononyne is insufficient, leading to reduced reactivity. A number of substituted derivatives of cyclooctyne have been synthesized to modify the lipophilicity and improve the reactivity and regioselectivity in the SPAAC reaction, increasing the scope of applications. Typical modifications include mono- or difluorination α to the triple bond, increasing the strain by fusing additional rings (benzene, cyclopropyl), or replacing a carbon in the eight-membered ring with a nitrogen, followed by substitution.

3.1.4 Previous "click" probes based on sulforaphane

In a previous attempt at a sulforaphane inspired "click" probe", Ahn *et al.* developed the sulfoxythiocarbamate derivative **11** and employed it to investigate binding to the Cys residues in Keap1, identifying Cys151 as a main target (Ahn *et al.*, 2010). Clulow *et al.* resynthesized the Ahn probe and compared it with a new developed probe **12** and sulforaphane in a competition-based assay to identify protein targets of sulforaphane (Clulow *et al.*, 2017a).
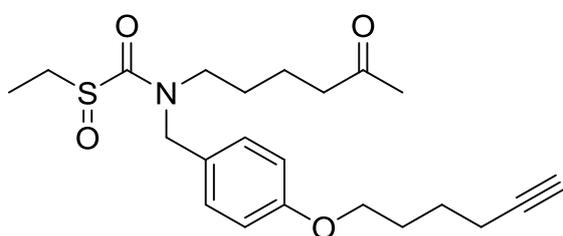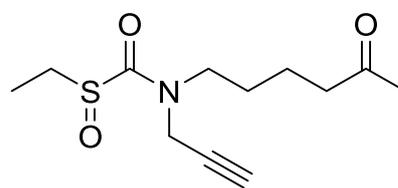
Ahn "click" probe **11**   Clulow "click" probe **12**

3.2. Mitochondria targeted probes

3.2.1 Mitochondria structure

Mitochondria are the cell organelles that are responsible for producing most of the cellular energy in the form of adenosine triphosphate (ATP) (Picard *et al.*, 2011) generating reactive oxygen species in the process. Furthermore, they regulate apoptosis through the mitochondrial permeability transition pore. Consequently, they are particularly relevant in the progression of many diseases, including cancer. However, they are less important for energy production in cancerous cells, where an 'aerobic glycolysis' is activated (Brandon *et al.*, 2006).

The mitochondrion has two membranes, an inner and an outer membrane, delimitating two interior compartments, the internal matrix and the intermembrane space (**Fig. 3.3**). While both membranes consist of a lipid bilayer, the outer membrane contains large amounts of a protein

called porin, which forms aqueous channels in the bilayer that allow small molecules (below 5000 Da) to enter the intermembrane space. Conversely, the inner membrane is much more impermeable, with about 20% of all lipids consisting of cardiolipin, a phospholipid that contains four fatty acid residues and adopts a cone-shaped structure (Chicco & Sparagna, 2007; Houtkooper & Vaz, 2008). This structure was shown to cause bends in the membrane and is considered essential for the formation of cristae, invaginations of the inner membrane greatly increase its surface area by protruding into the matrix. The inner membrane contains the enzymes that catalyze the reactions in the process of oxidative phosphorylation, while the matrix contains enzymes involved in the citric acid cycle.
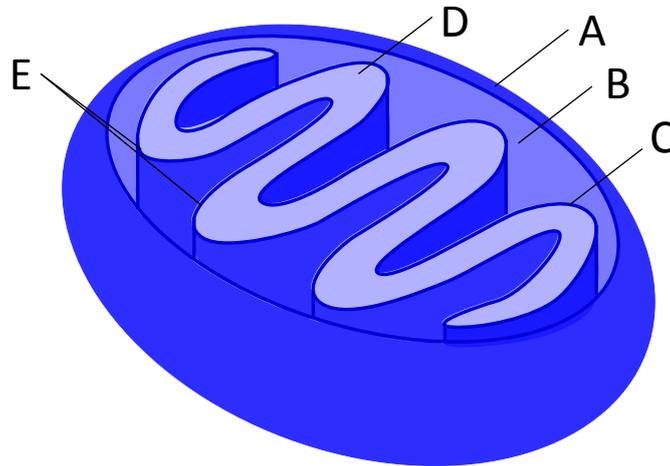

Fig. 3.3 Structure of the mitochondrion: A. Outer membrane; B. Intermembrane space; C. Inner membrane; D. Matrix; E. Cristae

A feature of oxidative phosphorylation is the outward transfer of electrons through the proteins in the respiratory chain in association with pumping protons from the matrix to the intermembrane space. This results in both a pH and a voltage gradient (membrane potential), with a higher pH in the matrix associated with a negative charge on the inside of the inner membrane, and a lower pH, similar to that of the cytosol, in the intermembrane space, and a positive charge on the outer side of the inner membrane.

3.2.2 Heterocyclic fluorescent probes

Based on the structural features of the mitochondria presented above, a natural approach is to target the mitochondria using positively charged, lipophilic compounds. This was identified early on, beginning with the first dyes that were found to accumulate in the mitochondria, such as Janus green B **142**, introduced in 1900 for mitochondria staining (**Fig. 3.4 a**) (Zielonka *et al.*, 2017).


142

143
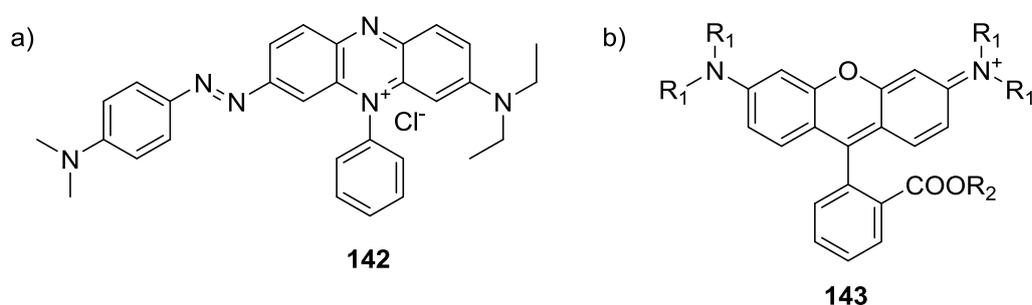
Fig. 3.4 Janus green (a) and the rhodamine scaffold (b)

More recent generations of fluorescent mitochondrial probes continue to be based on cationic heterocyclic moieties. A commonly used scaffold is that of rhodamine (**Fig 3.4 b**), which is readily taken up to the mitochondria with low cytotoxicity. Other heterocyclic cations include berberin, indolium, and tetraguanidinium.

The MitoTracker series are commercially available fluorescent probes covering a range of bands in the visible spectrum, built on either a cyanine or a rosamine skeleton. After being taken up in the mitochondria, they attach to thiols of mitochondrial proteins using a benzylic chloromethyl moiety (**Fig. 3.5**).
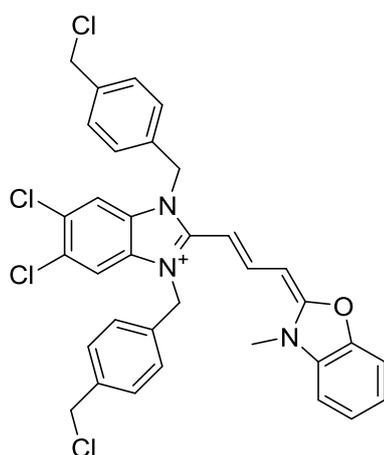
MitoTracker Green

144
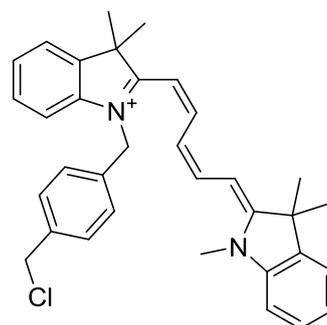
MitoTracker Deep Red

145
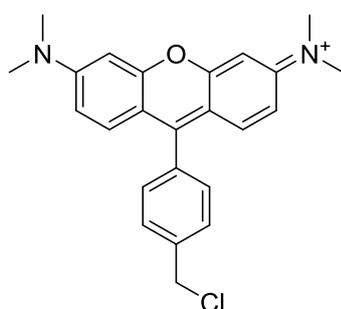
MitoTracker Orange

146
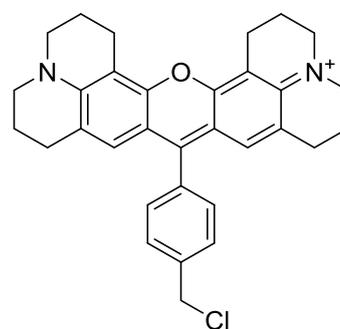
MitoTracker Red

147

Fig. 3.5 The MitoTracker series of mitochondria binding probes.

5,5',6,6'-Tetrachloro-1,1,3,3'-tetraethylbenzimidazolylcarbo-cyanineiodide, named JC-1 (as the first J-aggregate forming cationic dye identified to be sensitive to membrane potential), mentioned in **Chapter 2**, is also built on a carbocyanine skeleton. Like other carbocyanine dyes, it forms multimers named J-aggregates (thus named based on Jelley, who first described them) (Jelley 1936), which accumulate in the mitochondria. These aggregates show a shift in fluorescence to yellow-orange (590 nm), compared to the green peak (527 nm) characteristic for the monomer. Changes in mitochondrial membrane potential (e.g. triggered by apoptosis) lead to the dispersal of the J-aggregates formed by JC-1 **148** (**Fig. 3.6**). Accordingly, JC-1 has become one of the most widely used probes for mitochondrial membrane potential, including

our flow cytometry assays to determine levels of apoptosis (**Chapter 2.7**) and further work

below (**Chapter 3.5**)
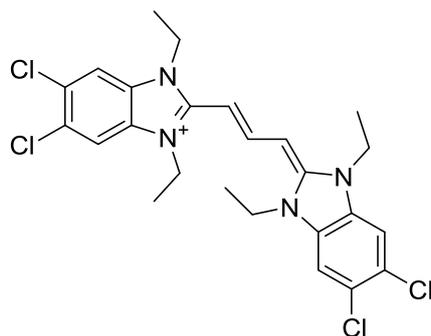
JC-1

148

 Fig. 3.6 Mitochondrial probe JC-1

3.2.3 Peptide-based approaches

Similar to cell penetrating peptides, mitochondria penetrating peptides (**Fig. 3.7**) contain

sequences using positively charged residues (Arg, Lys) and hydrophobic residues (Ile, Phe,

Tyr). Examples include the Szeto-Schiller (SS) peptides, a series of 31 different tetrapeptides

containing D-Arg to prevent enzymatic cleavage (Szeto and Schiller 2011), and peptides

containing the unnatural amino acid cyclohexyl alanine like the (Fx,r)$_3$ sequence. The SS

peptides have been used to deliver antioxidant cargoes such as tyrosine or dimethyltyrosine to

the mitochondria, while the (Fx,r)$_3$ sequence was able to deliver the antitumor agent

doxorubicin.
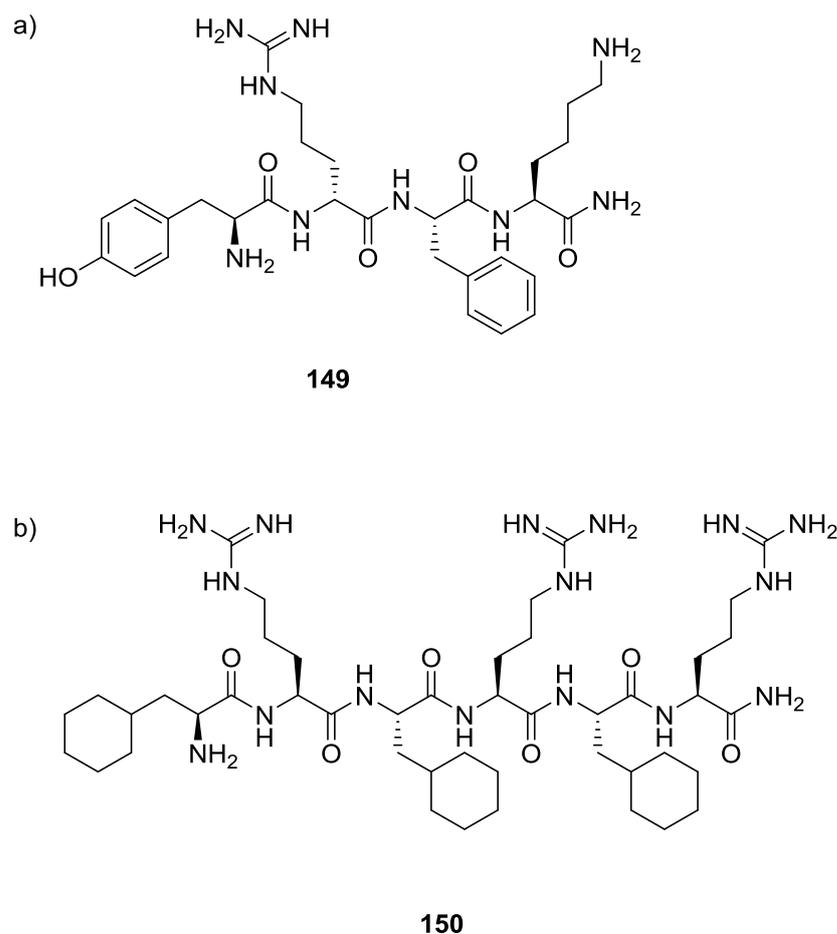
Fig. 3.7 Mitochondria targeting peptides. a) Szeto-Schiller peptide sequence 01; b) Mitochondria penetrating peptide sequence $(Fx,r)_3$

3.2.4 Triphenylphosphonium probes

While the strategy of using of fluorescent lipophilic cations has many advantages, including good mitochondrial uptake, opportunities for imaging, and generally low cytotoxicity, there are some drawbacks related to availability, complexity, and ease of derivatization. When the payload that needs to be delivered to the mitochondria is different from the dye itself, it is preferable to use less complex mitochondria targeting moieties that allow for simpler synthetic pathways and limit the possibilities for side-reactions with biological molecules. Developed from methyl triphenylphosphonium, initially used for studies of mitochondrial function and membrane potential, the triphenylphosphonium cation (TPP$^+$) became the most widely used

mitochondria-targeting moiety (Zielonka et al. 2017). Due to the relative simplicity with which it can be attached to a molecule through reactions with triphenylphosphine, TPP$^+$ has been used to create an incredible variety of mitochondria-targeted derivatives of biologically active molecules (**Fig. 3.8**), including antioxidants (e.g. mitoquinone, tocopherol, resveratrol, vitamin C) (Kelso et al. 2000; Kovarova et al. 2014; Biasutto et al. 2008; Finichiu et al. 2015), antitumor agents (e.g. geldanamycin, doxorubicin) (Kang et al. 2010; Han et al. 2014), contrast agents for MRI and PET (Zhao et al. 2014), as well as agents for "click" chemistry (MitoOctyne and MitoAzido) (Hoogewijs et al. 2016; Logan et al. 2016).
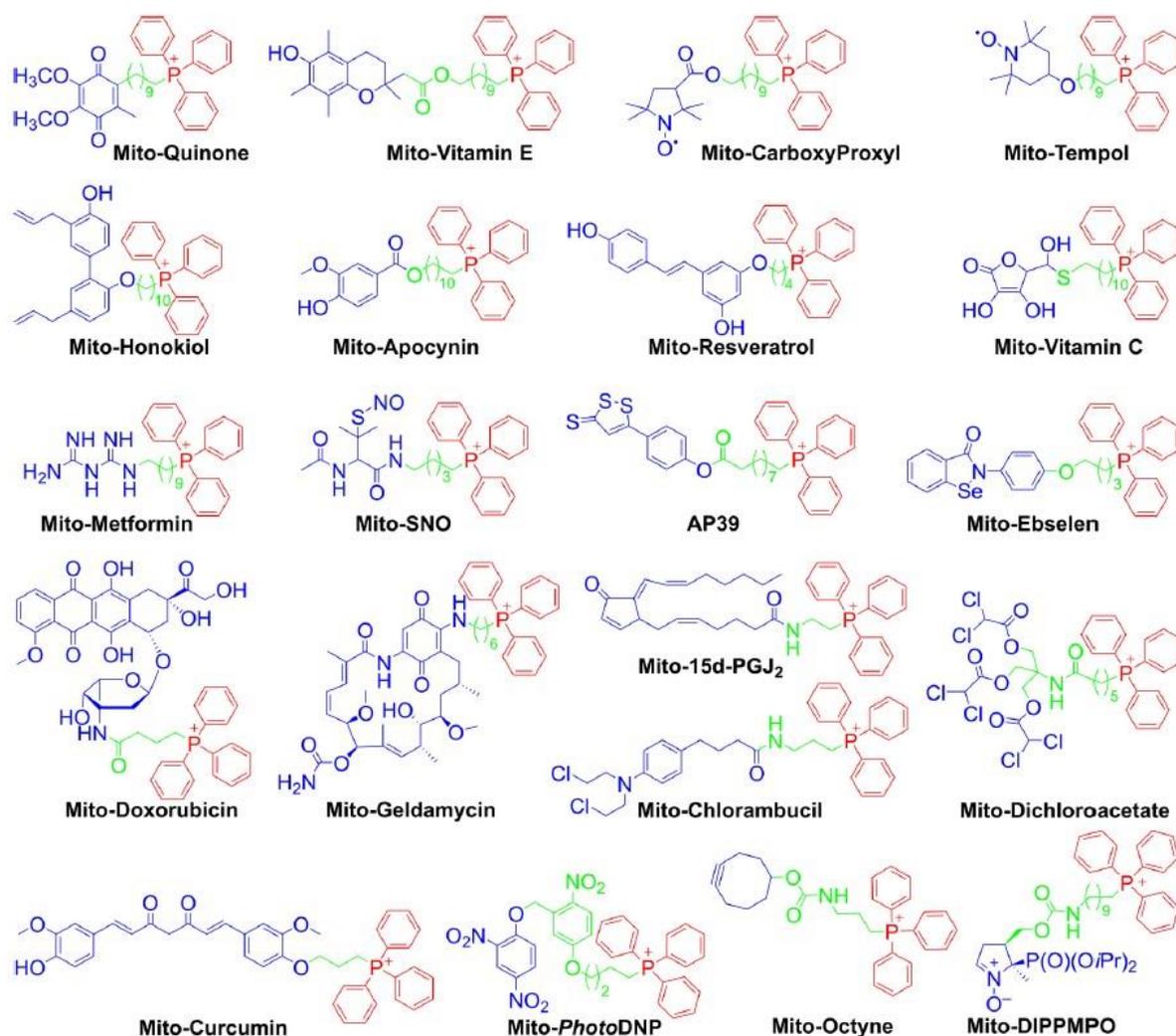

Fig. 3.9 Examples of molecules using the triphenylphosphonium for targeting mitochondriaRed is used for the mitochondria targeting moiety, green for the linker, and blue for the functional moiety (reproduced from (Zielonka *et al.*, 2017)).

3.3. Design and synthesis of sulforaphane-based click probes

3.3.1 "Click" probe design

In a parallel approach to the fluorinated probes, we decided to create "click" probes with a structure close to that of sulforaphane that make use of the 1,3-dipolar alkyne-azide cycloaddition to investigate their protein interactions. For synthetic tractability, the design we chose used one alkyne derivative of SF (**66**) that can react with a variety of azides (either newly synthesized or commercially available). Replacing the methyl in **1** with a propargyl would afford a synthetically feasible alkyne while maintaining the key moieties in **1**, while the synthetic azides could all be accessed through a common reaction from amine groups, using imidazolyl sulfonyl azide hydrosulphate, a reagent synthesized for this purpose (Goddard-Borger & Stick, 2007).

Sulforaphane **1**   Alkyne **156**
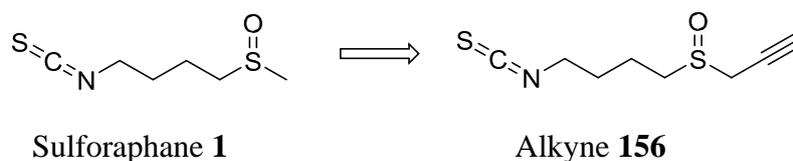
Scheme 3.5 Alkyne probe derivate of sulforaphane

The alkyne was envisioned to be used in two ways. One involves direct administration in cells, followed by cell lysis and "click" reaction in cell lysate. This would allow the biomolecule conjugates of alkyne **156** to be "clicked" with azides having fluorescent tags (bodipy, rhodamine) for imaging, or biotin tags for the biotin-streptavidin affinity purification. The second approach involves pre-synthesised "click" probes, aimed to improve the bioactivity compared to **1**. Among these, rhodamine and triphenylphosphonium were chosen as potential mitochondria-targeting probes, while "click" reactions with amino acids can be one method of obtaining peptides with a **1**-like moiety. Applications could include combining **1** with specific

organelle targeting peptide sequences, or potentially masking derivatives of **1** as a prodrug to be released upon peptide cleavage.

Table 3.1 Structures and potential applications for "click" probe azides. Azides marked with * are obtained from commercial sources.

"Click" probe azide	Structure	Potential applications
Triphenyl phosphonium		Mitochondria targeting
Rhodamine		Fluorescent, lipophilic, mitochondria targeting
Bodipy*		Fluorescent
Biotin*		Streptavidin pulldown
Azidohexanoic acid		Peptides with ITC moieties
Lysine azide		Peptide with ITC moieties
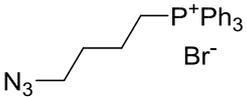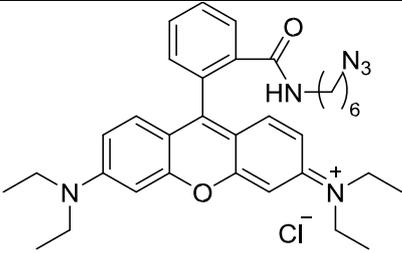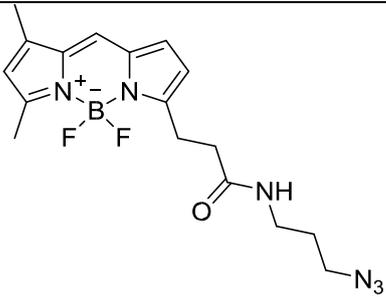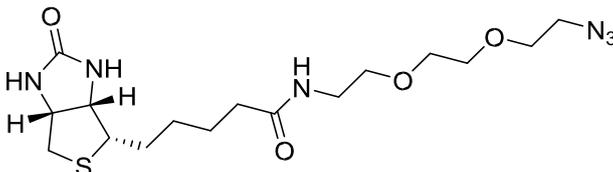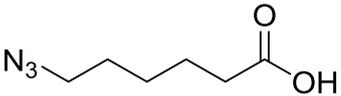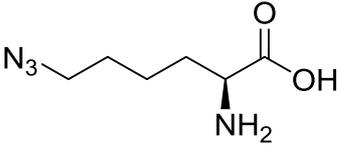
3.3.2 Computational analysis

To determine to what extent the "click" probes were expected to mimic the properties of natural ITCs, we again employed computational analysis using the free Molinspiration® cheminformatics software (www.molinspiration.com). This software was used to calculate values for molecular properties important for quantitative structure-activity relationship (QSAR) (**Table 3.2**), and to predict how "drug-like" a molecule is, with additional scores assigned for similarity to active compounds in several categories of ligands or inhibitors (**Table 3.3**).

Table 3.2 Comparison of calculated molecular properties and conformance with Lipinski's rule of 5 for sulforaphane, our designed probes and for existing "click" probes based on **1**

Cmpd. No.	Molecule	Type	cLogP	TPSA	MW	H-Bond Donors	H-Bond Acceptors	Lipinski Conformance
1	Sulforaphane	SO	1.15	29.43	177.29	0	2	Yes
156	Alkyne	SO	1.3	29.43	201.32	0	2	Yes
167	TPP$^+$ probe	SO	4.54	60.15	561.74	0	2	No – MW
	Rhodamine probe	SO	4.49	108.63	769.07	1	10	No – MW
11	Ahn probe	CO	2.83	63.69	405.56	0	5	Yes
12	Clulow probe	CO	0.46	54.45	237.30	0	4	Yes

As can be seen from **Tables 3.2** and **3.3**, the alkyne derivative is predicted to very closely mimic **1** in all categories, with smaller differences in all scores compared to the two previously synthesized "click" probes. Both the TPP$^+$ and the rhodamine probe are considerably larger molecules with higher lipophilicity, typical for compounds designed to target the mitochondria.

Table 3.3 Molinspiration® bioactivity scores for sulforaphane, designed probes, and for existing SF based "click" probes

Molecule	GPCR ligand	Ion Channel Modulator	Kinase inhibitor	Nuclear receptor ligand	Protease inhibitor	Enzyme inhibitor
Sulforaphane	-0.35	-0.59	-1.98	-0.84	-0.72	0.44
Alkyne	-0.41	-0.54	-1.57	-0.79	-0.78	0.34
TPP+ probe	0.27	-0.29	-0.25	-0.25	-0.05	0.4
Rhodamine probe	-1.22	-2.54	-2.14	-2.20	-1.09	-1.39
Ahn probe	0.08	-0.03	-0.5	0.3	0.15	0.24
Clulow probe	-0.22	-0.19	-0.79	-0.3	0.05	0.48

3.3.3 Synthetic approach towards the 'click' probes
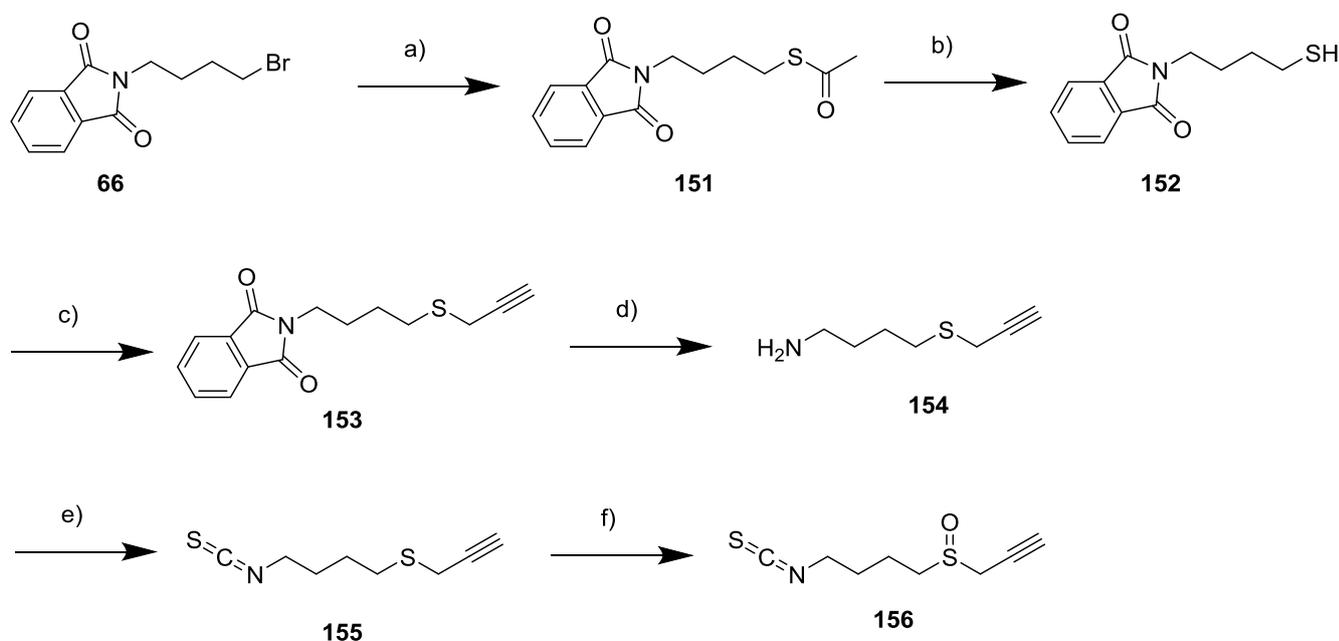
Scheme 3.6 Synthetic pathway for the sulforaphane based alkyne. Reagents and conditions: a) CH₃COSK, THF, reflux, 4h; b) 36.5% HCl, CH₃OH, MW 100ºC, 3x5 min; c) NaOH, propargyl bromide, CH₃OH, 0ºC to RT, overnight; d) NH₂NH₂, CH₃NH₂, EtOH, MW 120-160ºC 3x10 min, then HCl, MW 2x5 min; e) CSCl₂, NaOH, CHCl₃, 0ºC, 2h; f) mCPBA, NaHCO₃, DCM, 0ºC, 3h

Given that in our previous work with fluorinated probes, the probes with a 4-carbon linker most closely resembled sulforaphane in the biological testing, and that the probe would have to be used in several CuAAC reactions, we decided to focus solely on the 4-carbon probes analogous

to **1**. Using the same phthalimide-protected amino-bromoalkane **66** as a starting material, the steps in our synthesis (**Scheme 3.6**) required: a) the installation of a thiol group instead of the bromine atom; b) addition of the alkyne, under the form of a propargyl group attached to the thiol; c) amine deprotection and formation of isothiocyanate; and d) oxidation from sulphide to sulfoxide.

3.3.3.1 Thiol synthesis and propargylation
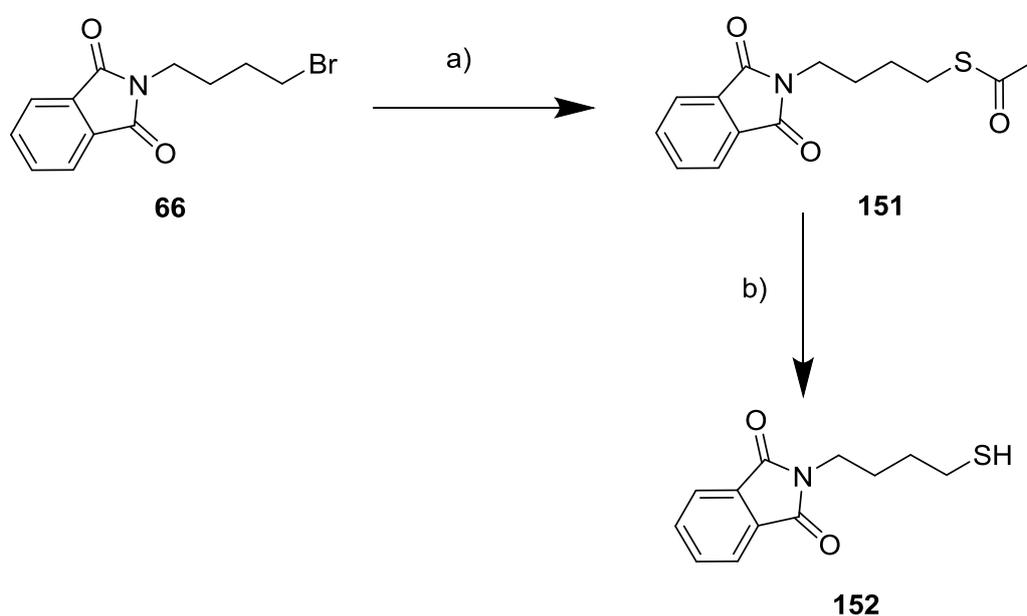
Scheme 3.7 Thiol synthesis. Reagents and conditions: a) CH₃COSK, THF, reflux, 4h; b) 36.5% HCl, CH₃OH, MW 100ºC, 3x5 min.

The thiol group could have been obtained by reacting the N-(4-bromobutyl)phthalimide **66** with sodium hydrosulfide NaSH. However, NaSH is a hygroscopic compound that is sensitive to water and oxygen and can release toxic H₂S gas (https://www.sigmaaldrich.com/GB/en/sds/sigald/161527), so we chose to avoid its use by taking an indirect approach towards the thiol (Hu et al. 2013). Treatment of *N*-(4-bromobutyl)phthalimide with potassium thioacetate in THF at reflux (4 h) gave a thioacetate

derivative **151**. This was used without purification in a subsequent microwave hydrolysis using concentrated (36.5%) HCl allowed the isolation of the free thiol **152** following "flash" chromatography (20% ethyl acetate in hexanes) in 96% yield over two steps.
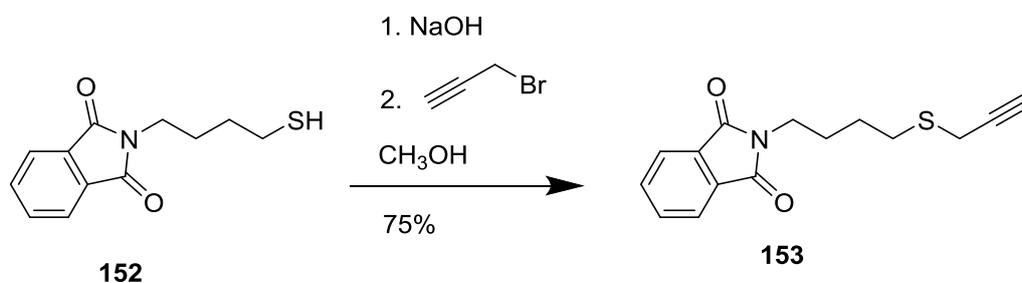
Scheme 3.8 The propargylation reaction. Reagents and conditions: NaOH, propargyl bromide, CH₃OH, 0°C to RT, overnight

To add the alkyne group to the molecule, propargyl bromide was chosen to react with the thiol **152**. the degassed thiol was treated with sodium hydroxide to form a thiolate, whose reaction with propargyl bromide gave the propargyl sulfide **153** in 75% yield following "flash" chromatography (20% ethyl acetate in hexanes).

3.3.3.3 Microwave hydrazinolysis

As the removal of the phthalimide protecting group had been the lowest yielding step in the synthesis of the fluorinated derivatives of **1**, we tried to improve the hydrazinolysis reaction using a microwave heating method and investigated the influence of several factors on its outcome. The variables that we followed included stoichiometry (using either 1:1 or a 4:1 hydrazine excess), temperature (120 – 160 ℃), and the use of methylamine as adjuvant.

Reaction mixtures were heated under microwave irradiation for 10 minutes, then samples were

analyzed using LC/MS. Peaks were identified and their peak areas were used to quantify the

amounts of starting material, intermediaries and product in each reaction (**Table 3.4**).
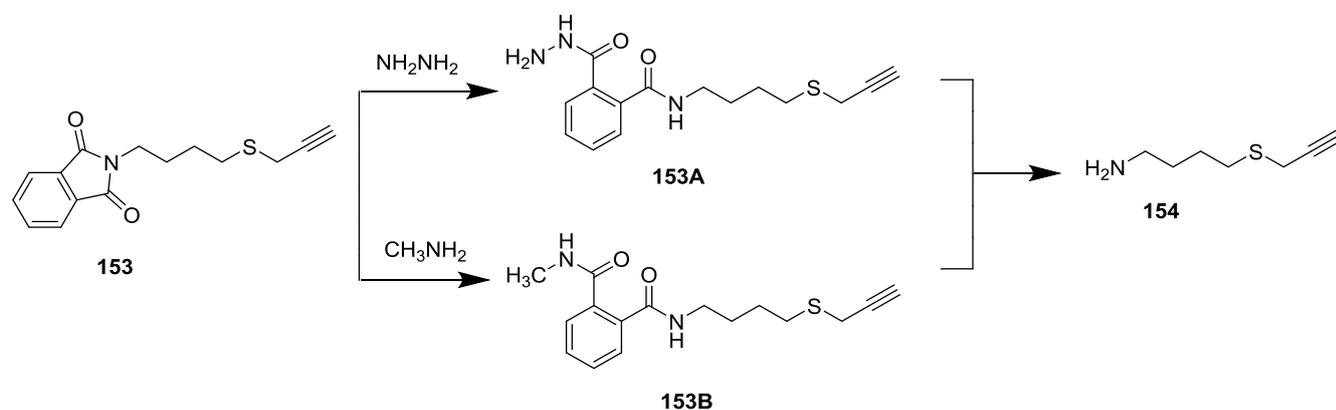
Scheme 3.9 Hydrazinolysis including observed intermediaries formed with hydrazine and methylamine

Table 3.4 Composition of the reaction mixture in the hydrazinolysis reaction as determined by analysis of peak areas of UV absorbance peaks (254 nm) in LC-MS chromatogram.

Entry	Temperature (ºC)	Molar Ratio	Methylamine	Phthalimide 153 (%)	Intermediate 153A (%)	Intermediate 153B (%)	Amine 154 (%)
MW-H1	120	1:1	NO	94.1	0.0	0.0	5.9
MW-H2	120	4:1	NO	74.5	16.5	0.0	9.0
MW-H3	140	1:1	NO	87.5	0.0	0.0	12.5
MW-H4	140	4:1	NO	47.5	28.9	0.0	23.6
MW-H5	160	1:1	NO	94.3	0.0	0.0	5.7
MW-H6	160	4:1	NO	47.4	12.3	0.0	40.3
MW-H7	120	1:1	YES	54.1	11.0	25.7	9.2
MW-H8	120	4:1	YES	51.9	20.3	11.3	16.5

MW-H9	140	1:1	YES	33.1	10.3	34.9	21.7
MW-H10	140	4:1	YES	31.3	18.8	14.0	35.9
MW-H11	160	1:1	YES	74.5	0.0	12.1	13.4
MW-H12	160	4:1	YES	6.0	3.5	27.6	62.8

3.3.3.3.1 Influence of stoichiometry on the hydrazinolysis reaction

In the literature, the hydrazinolysis reaction can be run either in 1:1 ratio of hydrazine to phthalimide (focusing on efficiency), or using an excess of hydrazine, looking to improve conversion, at the expense of having higher quantities of highly toxic hydrazine waste (Vermeulen et al. 2003). As can be seen in **Fig 3.8**, using a 4:1 ratio of hydrazine to phthalimide has improved the conversion rate towards both intermediates and products compared to the reactions occurring at 1:1 ratio, regardless of other factors. Interestingly, in the absence of methylamine, a stoichiometric ratio led to no intermediate being observed in the reaction mixture regardless of temperature. Focusing strictly on the desired amine product, increasing the amount of hydrazine led to an increase in the conversion rate varying between 1.5 and 7-fold.
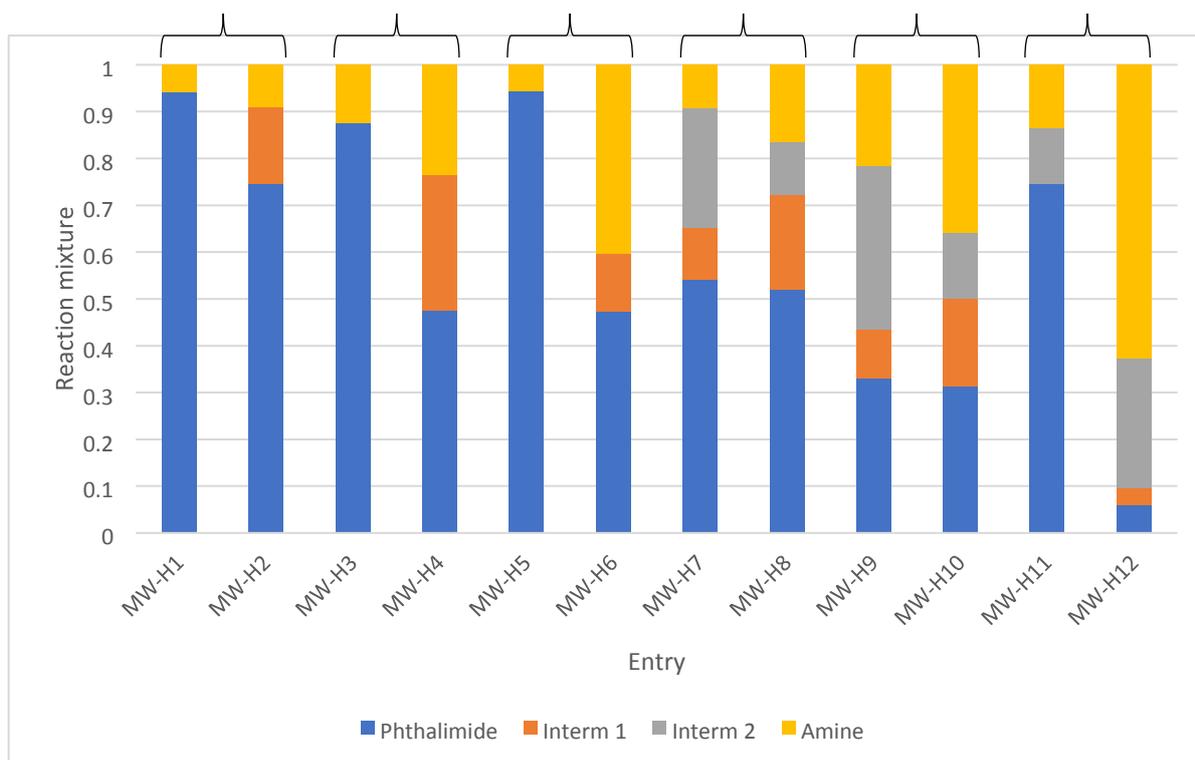
Fig. 3.8 Conversion in the hydrazinolysis reaction. Parentheses group experiments that differ only in molar ratio (phthalimide:hydrazine 1:1 vs 1:4).

3.3.3.3.2 Influence of methylamine on the hydrazinolysis reaction

The addition of methylamine has a moderate effect in increasing the amount of product observed in the reaction mixture (increases varied between 1.52 and 2.34-fold compared to the reaction in the absence of methylamine). However, grouping both intermediates together as a category allows to identify that the main effect of methylamine seems to be vastly increasing the presence of overall intermediary compounds (**Fig. 3.9**). It seems likely that the methylamine, a stronger base than hydrazine (pKa = 10.6 compared to 8.1) , will attack and open the phthalimide protecting group easier than hydrazine. Supporting this idea, in all reactions where hydrazine was used in a stoichiometric ratio, the predominant intermediary that was observed was the methylamine derivative. While the hydrazine is still required for forming the insoluble dihydrophthalazine dione, the use of methylamine clearly improves the outcome of the hydrazinolysis reaction.
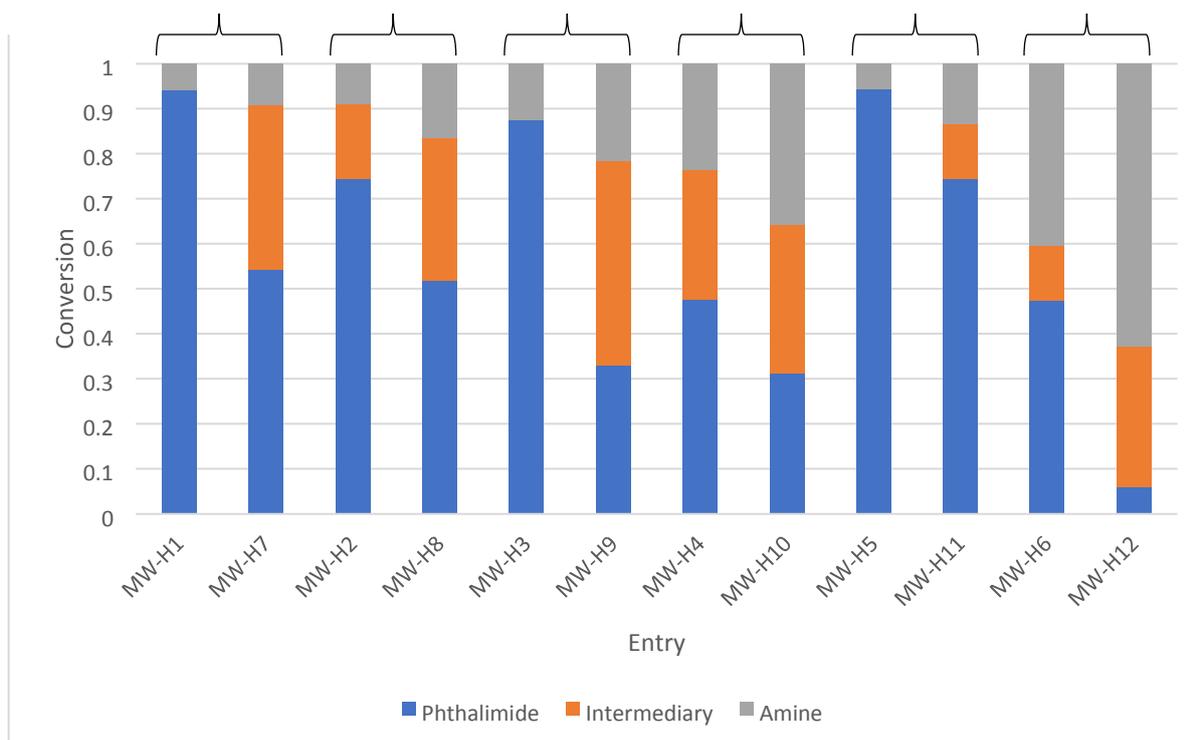
Fig. 3.9 Conversion in the hydrazinolysis reaction, focusing on the addition of methylamine; parentheses group experiments that differ only based on the absence/presence of methylamine

3.3.3.3.3 Influence of temperature on the hydrazinolysis reaction

Unlike with the other factors, the effect of temperature (**Fig. 3.10**) cannot be described independently, but in relation to the use of excess or stoichiometric amounts of hydrazine. When using a 4:1 hydrazine:phthalimide ratio, conversion increases almost linearly with a higher temperature, regardless of the presence or absence of methylamine. When using a stoichiometric amount of hydrazine, the best conversion occurs at 140 ℃, with a decrease at 160 ℃. Considering the absence of hydrazine intermediary in the presence of methylamine, a plausible explanation is that at the higher temperature some of the hydrazine is consumed, possibly by evaporation, and is therefore, less available for the reaction. However, if using excess amounts of hydrazine, the best conversion correlates with the highest temperature.
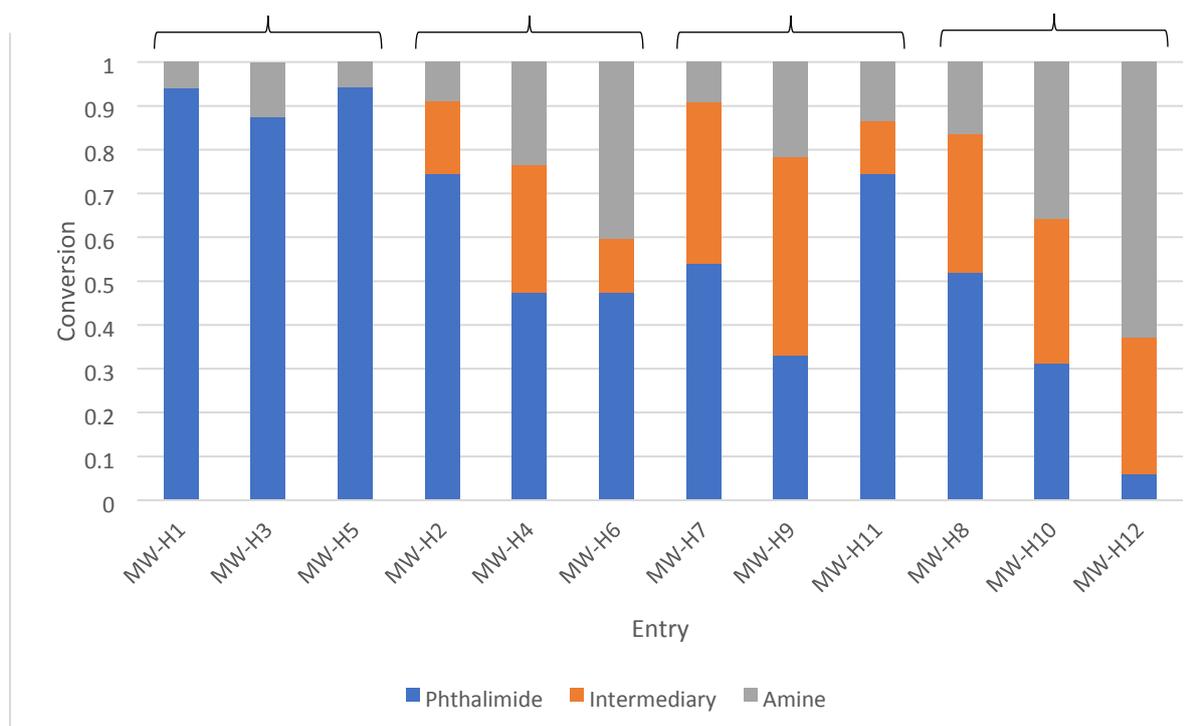
Fig. 3.10. Conversion in the hydrazinolysis reaction, focusing on the effect of temperature. Parentheses group experiments that differ only in reaction temperature.

Overall, the most favorable identified conditions for the microwave hydrazinolysis reaction included the addition of methylamine, using excess hydrazine, and the higher temperature. Proportionally, the largest favorable effect on conversion was found to stem from increasing the hydrazine:phthalimide ratio.

3.3.3.4 Isothiocyanate assembly and oxidation to sulfoxide

The poorly soluble amine **154** was treated with thiophosgene at 0 ℃ to assemble the isothiocyanate, neutralizing the released HCl with dilute NaOH. The isothiocyanate sulfide **155** was purified using "flash" chromatography (2% CH$_3$OH in DCM), giving a 65% yield over two steps including hydrazinolysis. Subsequent oxidation with *m*CPBA in DCM at 0-5 ℃ for 3 h afforded the sulfoxide **156** in 85% yield.
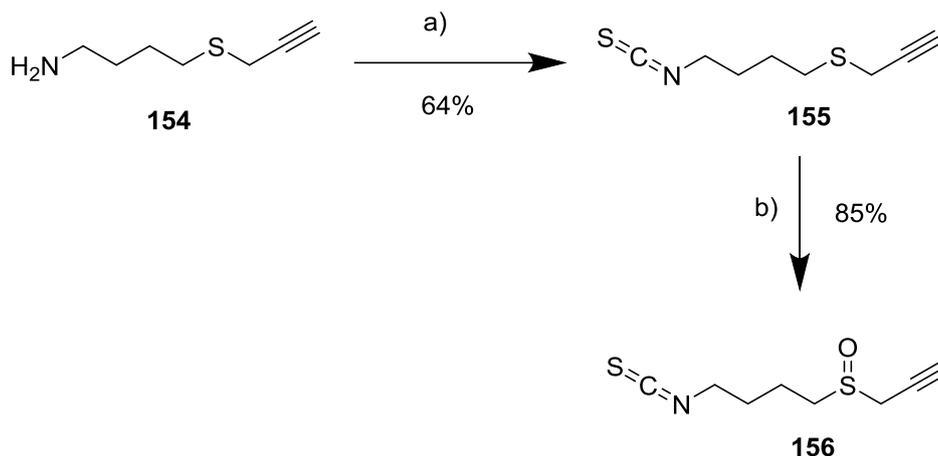
Scheme 3.10 Isothiocyanate synthesis and oxidation to sulfoxide. Reagents and conditions: a) CSCl₂, NaOH, CHCl₃, 0 ℃; b) mCPBA, DCM, 0-5 ℃

3.4. "Click" reactions

3.4.1 Azides

A unifying theme in our approach to the synthesis of azides is the transformation of amine groups into azides. For this purpose, an azidation reagent, imidazolyl sulfonyl azide hydrosulphate **160** was synthesized based on existing literature (Goddard-Borger and Stick 2007; Potter et al. 2016).

3.4.1.1 Synthesis of imidazolyl sulfonyl azide hydrosulphate
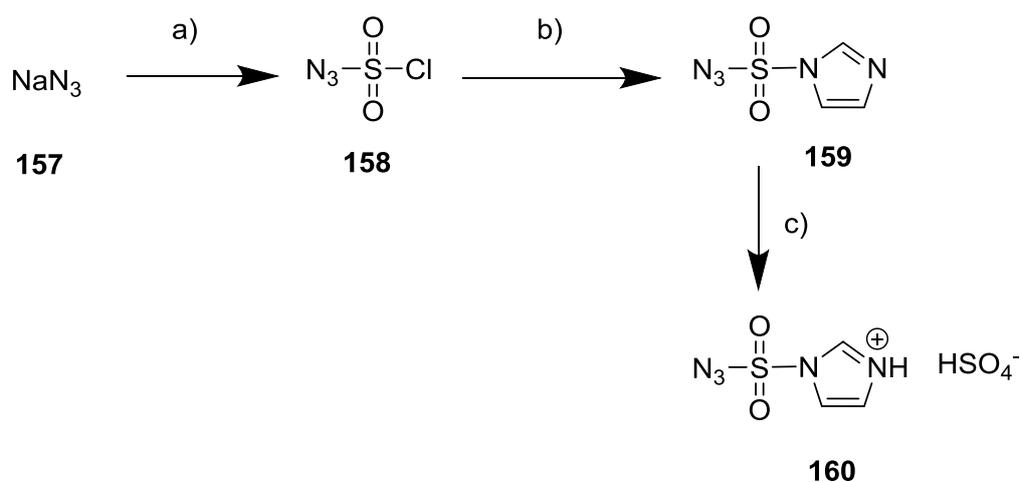
Scheme 3.11 Synthesis of imidazolyl sulfonyl azide hydrosulphate. Reagents and conditions: a) SO_2Cl_2, CH_3CN, 0ºC to RT, overnight; b) imidazole, CH_3CN, 0ºC, 3.5h; c) conc. H_2SO_4 (98%), EtOAc, 0ºC to RT, 2h.

Azidation reagents can be highly unstable, owing to the large amounts of energy stored in the azide group. Sodium azide **157**, a readily available source of N_3^-, was treated with sulfonyl chloride in equimolar ratios, and the resulting azido sulfonic chloride **158** reacted with imidazole. For increased stability, the imidazolyl sulfonyl azide **159** was crystallized as a hydrosulphate salt **160** by treatment with sulfuric acid. The resulting white crystals, obtained in 88% overall yield, were used for subsequent azidation reactions.

3.4.1.2 Test azidations and "click"

Using azidation reagent **160**, we first attempted to test a simple azidation of benzylamine. Additionally, we also decided to try to achieve a one-pot azidation plus "click" reaction, following a similar approach that has been made using triflic azide. For an initial test we also synthesized an alternate alkyne.
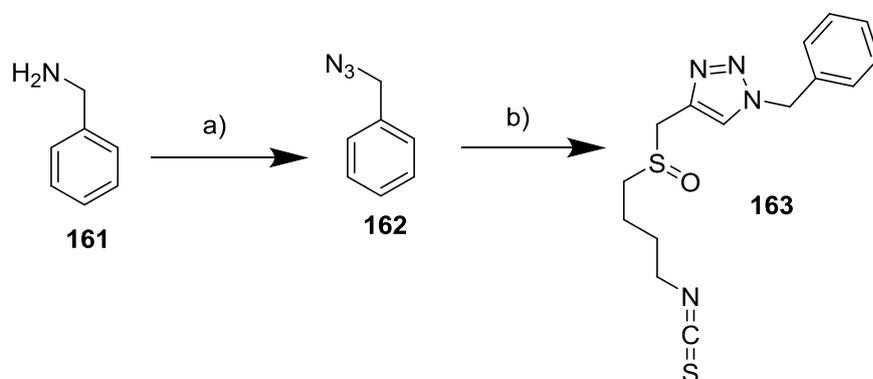
Scheme 3.12 Test azidation + "click". Conditions and reagents: a) **160**, CH_3OH, rt, 2h; b) **156**, $CuSO_4$, $NaHCO_3$, TBTA, sodium ascorbate, CH_3OH, MW 80 ºC, 30 min.

3.4.1.3 Synthesis of mitochondria targeting TPP⁺ azide
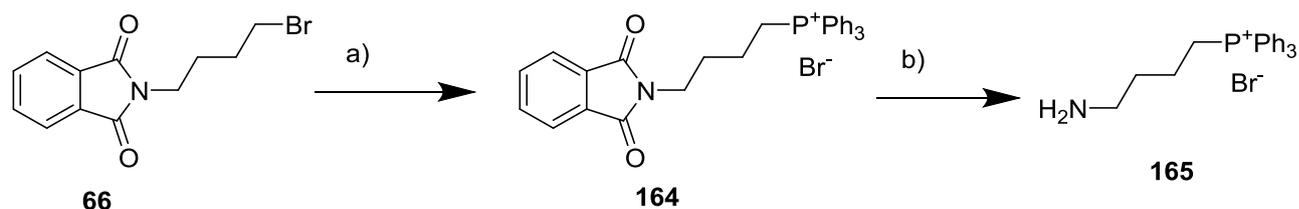
Scheme 3.13 Synthesis of amine for triphenylphosphonium mitochondria-targeting probes. Reagents and conditions: a) PPh_3, CH_3CN, MW, 200ºC, 3x10 min; b) N_2H_4, CH_3NH_2, EtOH, MW 160ºC 3x10 min.

Conveniently, this synthesis used the same starting phthalimide **66** as that of the alkyne (**Scheme 3.12**). A microwave reaction with triphenylphosphine formed the triphenylphosphonium salt **164** in 98% yield. Microwave-assisted hydrazinolysis under the optimized conditions determined in section **3.3.3.3** for 30 minutes removed the phthalimide protecting group to release the free amine **165**. The amine was used in a one pot azidation + "click" reaction to form the triphenylphosphonium probe **167** (**Scheme 3.14**).
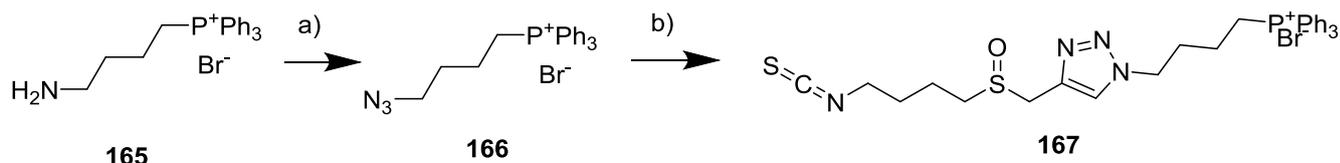
Scheme 3.14 One pot azidation and "click" reaction. Reagents and conditions: a) **160**, CuSO$_4$, NaHCO$_3$, CH$_3$OH, rt, 3h; b) **156**, TBTA, sodium ascorbate, MW 80 °C, 30 min.

3.5. Biological testing

3.5.1 Assessment of apoptosis

As with the fluorinated compounds in **Chapter 2**, we used flow cytometry to compare the effects of both compounds that would be administered in cells, the alkyne probe **156** and the mitochondria-targeting TPP$^+$ "click" probe **167** to those of sulforaphane **1**. Cells incubated with either low (10 µM) or high (40 µM) concentration of ITC were stained with JC-1 to assess the mitochondrial membrane depolarization associated with apoptosis.

Table 3.5 Effects of **1** and "click" probes on cell apoptosis

Concentration	% Apoptotic Cells (Normalized vs untreated cells) induced by			
	SF (1)	**Alkyne (156)**	**TPP probe (167)**	**DMSO**
10 µM	13.95 ± 1.36	54.44 ± 4.47	1.69 ± 1.50	1.24 ± 1.51
40 µM	51.63 ± 5.44	92.74 ± 1.58	3.68 ± 1.47	1.77 ± 1.50

Disappointingly, the mitochondria-targeting triphenylphosphonium probe **167** had very little effect on apoptosis induction, barely distinguishable from that induced by the vehicle even at the higher concentration (3.68 ± 1.47 vs 1.77 ± 1.50 % apoptotic cells). One explanation could

be that the modifications to the sulforaphane structure have been too drastic to maintain a similar apoptotic activity – as seen above (section **3.3.2**), the TPP$^+$ probe is considerably more lipophilic than **1**, with a molecular weight above 500 Da. Another possibility is that triphenylphosphonium moiety directs the molecule to the mitochondria with priority over the isothiocyanate, and prevents the normal interactions responsible for the induction of apoptosis, raising the possibility that mitochondria are not the organelles directly responsible for the proapoptotic activity of **1**. Remarkably, on the other hand, the alkyne **156** was found to exhibit a proapoptotic activity exceeding that of **1**, with the levels of apoptotic cells induced at the lower 10 µM concentration similar to those induced by 40 µM **1**. When using 40 µM alkyne, more than 90% of the cells became apoptotic.
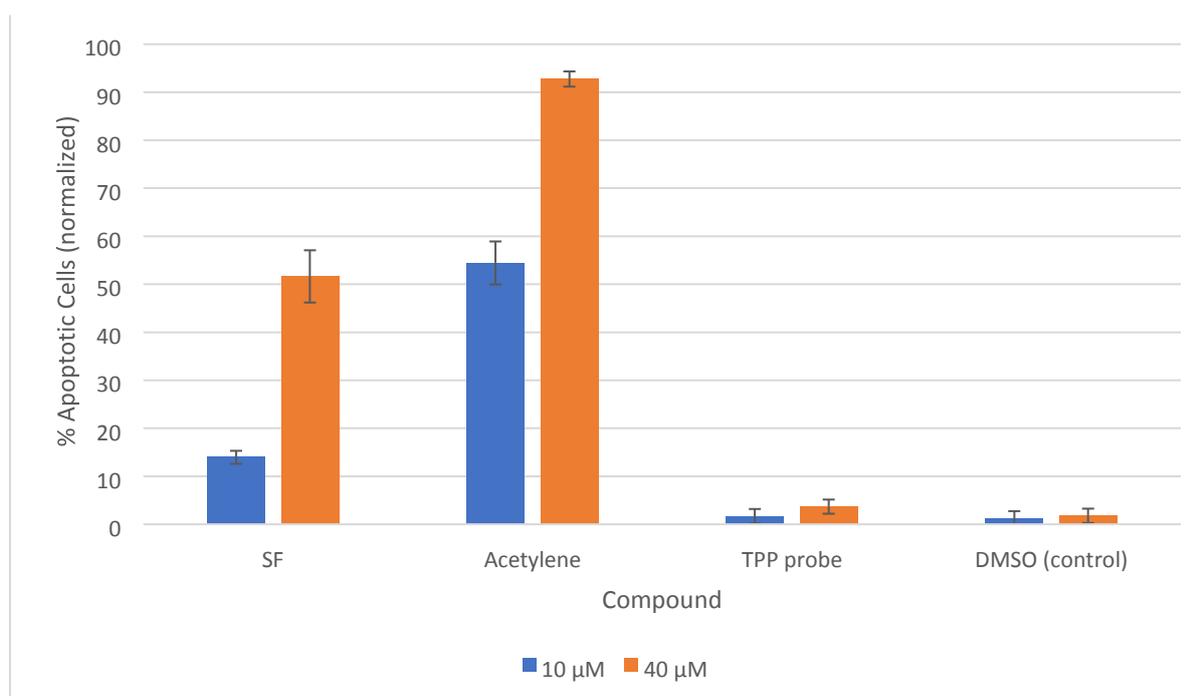
Fig. 3.11 Effects of **1**, alkyne probe **156** and the TPP+ probe **167** on apoptosis. Data obtained from 4 separate experiments.

Conclusions

In a second approach to developing probes useful for investigating the interactions of sulforaphane, we designed and synthesized alkyne probe 15**6** in 40% overall yield. Through "click" reactions with corresponding azides, this probe allows access to a variety of "warheads", moieties that can be used either to identify the interactions of **1** (e.g. using a fluorescent azide), or to modify its activity. In an attempt to design a mitochondria-targetting probe, we synthesized TPP$^+$ azide **166**. In a one pot azidation plus "click" reaction using azidation reagent **160**, we obtained TPP$^+$ probe **167** as a proof of concept for our approach. Surprisingly, alkyne **156** appeared more potent in the induction of apoptosis than sulforaphane, possibly due to increased stability and/or availability. Conversely, the TPP$^+$ probe **167** showed little activity. We speculate that the reduced pro-apoptotic activity could be owed to preferential direction by the TPP$^+$ moiety preventing interaction with normal targets of **1**.

CHAPTER 4

DISCUSSION AND FUTURE WORK

4.1.Discussion

4.1.1 Sulforaphane as a therapeutic agent

As shown in **Chapter 1**, sulforaphane exerts an influence in several important cell processes, including apoptosis, inflammation, and cell cycle arrest. Moreover, the fact that **1** is available through diet qualifies it as a nutraceutical, a term devised by Stephen De Felice to describe "any substance that may be considered a food or part of a food and that provides medical or health benefits, including the prevention and treatment of disease". Consequently, it has been a target of investigations regarding its potential as a therapeutic agent, with dozens of finished and ongoing clinical trials (**Section 1.3**) studying safety and effectiveness in diseases such as various types of cancer, diabetes, Alzheimer's disease, COPD, and autism spectrum disorders. Furthermore, having been considered safe, several health supplements containing either sulforaphane, glucoraphanin, or broccoli sprouts extracts (e.g., Prostaphane®, Broccomax®, Brokkoli®, Sulforaphane) are already commercially available. Evgen Pharma's Sulforadex® technology uses an α-cyclodextrin to stabilize sulforaphane or its synthetic derivatives, focusing on the up-regulation of Nrf2 and on the inhibition of pSTAT3. A stage II clinical trial using Sulforadex to reverse resistance to tamoxifen, fulvestrant, or an aromatase inhibitor on patients with metastatic breast cancer was completed in 2019. The results claim that Sulforadex could be used with generally mild side effects (mostly gastrointestinal), and that the combination treatment had a clinical benefit rate of 26%, with the median duration of clinical benefit extending to 9 months.

4.1.2 Current challenges in investigating sulforaphane metabolism/biomolecule interactions

The development of sulforaphane-based strategies would benefit from a better understanding of the underlying biological mechanisms (**Table 4.1**). However, there are important challenges to overcome in order to determine the complement of biomolecule interactions behind the bioactivity of SF.

One challenge stems from the low stability and availability of sulforaphane. Under normal conditions, dietary **1** will form in the gut as glucoraphanin is hydrolysed by myrosinase, and it will quickly be conjugated by glutathione, leading to a short period spent as actual SF. The sulforaphane molecule is itself not shelf stable, with some decomposition happening in less than 24 hours at room temperature.

A second challenge, derived from the first one, refers to timing – sulforaphane is involved in several pathways, interacting with different target molecules, and may target specific molecules at specific times after administration; furthermore, at lower concentrations SF may interact with a reduced set of targets, while at higher concentrations a wider number of interactions may be observed.

Finally, it is crucial to be able to detect sulforaphane during its activity. Compared to many medicinal compounds, sulforaphane is a small molecule, without features that allow tracking after its administration. Usual detection strategies, based on fluorescence, or the presence of unusual atoms (such as fluorine), cannot be directly employed to follow the metabolism of sulforaphane. For this reason, we have suggested the development of derivatives based on sulforaphane, which would retain or improve on its biological activity, as well as add detectable moieties that can help identify specific biomolecular interactions. The two specific strategies

we targeted involved the incorporation of fluorine atoms, and the use of "click" chemistry to attach azides with a fluorescent or isolatable load.

4.1.3 Fluorinated derivatives as tools to investigate sulforaphane metabolism

Concept

Fluorine atoms (particularly as trifluoromethyl $-CF_3$ groups) can be used to obtain derivatives of **1**. As the $-CF_3$ groups should theoretically neither be providing additional reactivity, (trifluoromethyl groups are typically used as bioisosteres of methyl groups) (O'Hagan 2008), nor prevent existing reactions, we would expect these molecules to show reactivity sufficiently close to that of **1**. If the fluorinated derivatives interact with the same biological targets as **1**, they will be attaching a $-CF_3$ group to these molecules, which can be employed as a ^{19}F-NMR tracker (Papeo et al. 2007; Mishra et al. 2014).

Discussion of results

In **Chapter 2** we showed the synthesis of a library of fluorinated derivatives of sulforaphane developed to help investigate the importance of molecular structural features, i.e., the length of the carbon linker, the state of oxidation on the sulfur atom, and the presence/absence of a spacer methylene unit between the trifluoromethyl and the sulfur atom.

The trifluoroethyl and trifluoromethyl derivatives required different initial methods for introducing fluorine in the molecule, while the latter parts of the synthetic pathways proceeded in a similar fashion. Computational analysis using the Molinspiration software suggested that the trifluoromethyl derivatives would have a larger cLogP than the trifluoroethyl derivatives, and the latter would more closely resemble the properties of natural ITCs (including a low cLogP). In the oxidation series (sulfide – sulfoxide – sulfone), the sulfoxide had the lowest

cLogP, while that of the sulfide was much higher, and that of the sulfone was of an intermediate value.

These results were corroborated with those obtained on THP-1 cells, where sulfoxides outperformed sulfides in increasing the levels of apoptotic cells (**Fig. 4.2**).
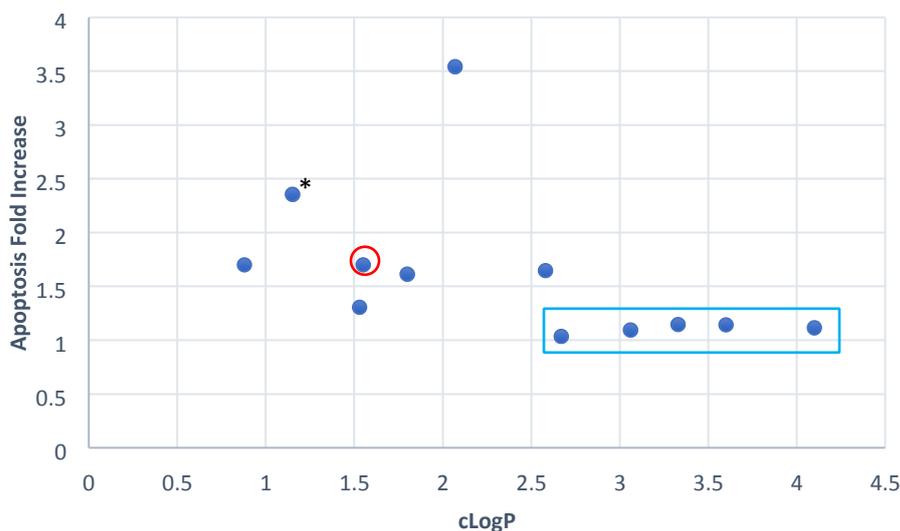
Fig. 4.2 Comparison of tested trifluoroethyl derivatives and natural ITCs, showing the induced fold increase of apoptosis compared to control, including the calculated LogP data. The blue rectangle delimits the sulfides **3** and **76-79**, while the red circle corresponds to erysolin **4**, the sulfone. * denotes sulforaphane **1**.

^{19}F-NMR experiments (**Section 2.4**) following the fluorinated trifluoroethyl derivatives suggested an explanation for the lack of activity observed from the sulfides, whose fluorine signal quickly disappeared upon dissolving in RPMI media. One possibility is that their relatively higher lipophilicity leads to aggregation into liposome like particles or micelles in the aqueous media, rather than a homogeneous distribution (though the use of DMSO as a vehicle should work to prevent this from happening). Another possibility is that they can react with one or more components of the media, and thus never reach the intended cellular targets.

4.1.4 "Click" compounds as tools to investigate sulforaphane metabolism

Concept

If an alkyne or azide derivative of sulforaphane can interact similarly with biomolecular targets of **1**, "click" reactions with compounds containing a moiety that can be either easily detected (e.g., a fluorescent group) or that can be recognized for affinity purification (biotin) will allow the identification of these biomolecules . Furthermore, the "click" reaction can also be employed to create targeted probes, which could potentially offer improved or altered reactivity compared to sulforaphane.

Discussion of results

In **Chapter 3** we showed the synthesis of an alkyne derivative of sulforaphane with a propargyl residue replacing the terminal methyl group, which we obtained in 40% overall yield over six steps. In parallel, we obtained an azide with a TPP$^+$ warhead intended to target mitochondria. Using a CuAAC reaction, we succeeded in coupling the alkyne with the TPP$^+$ azide, showing that the alkyne is a suitable coupling partner (**Section 3.4**).

Remarkably, in THP-1 cells, the alkyne derivative showed improved pro-apoptotic activity compared to **1**, while the mitochondria-targeted TPP$^+$ probe had very little activity (**Section 3.5**). While further investigations into reactivity are required, a possible explanation for the reduced activity is preferential targeting directed by the TPP$^+$ moiety, resulting in lack of interaction with the molecular targets of SF responsible for induction of apoptosis.

4.2 Conclusions

Our approach to the design of chemical probes for investigations into the metabolism of sulforaphane was focused on creating molecules that help solve the major issue in identifying the molecular targets of SF: the low visibility of SF in a biological environment and therefore its interactions with these targets. We addressed this issue by building two types of probes, modifying the molecular structure of **1** with moieties that can be detected using two different techniques.

The library of fluorinated probes was an expansion of those obtained by Kielbasinski *et al.* (Kiełbasiński *et al.*, 2014), however employing a different method of installing the trifluoromethyl group. Our investigations showed that some of these fluorinated compounds show similar pro-apoptotic activity to the parent natural ITCs and identified a basic hydrolysis reaction in trifluoroethyl derivatives, which had not been described previously for sulfoxides. Coupled with a potentially easy to induce decarboxylation, this reaction or a derivative could form the basis using sulforaphane derivatives as pro-drugs, with a simple reaction allowing access to the desired compound.

Our work with "click" probes lead to the synthesis of an alkyne derivative of SF, and proved its suitability in "click" reactions with selected azides. Considering that the alkyne showed improved pro-apoptotic activity compared to SF, it may in itself be a potentially interesting compound, beyond its applicability in "click" reactions. Separately, we optimized the microwave-assisted hydrazinolysis reaction, investigating the influence of temperature, molar ratios and of the addition of methyl amine, showing the importance of methyl amine in the formation of intermediates opening the phthalimide ring.

Compared to the previous existing Ahn and Clulow probes, the alkyne probe we designed has the following features:

i. The alkyne retains the original ITC group, unlike the sulfoxythiocarbamates employed in the other probes ii. The alkyne also retains the sulfoxide present in **1** – although previous research suggests that the Ahn and Clulow substitution of sulfoxide with a ketone seemed to have no effects on reactivity.

iii. Unlike the Ahn and Clulow probes, where the alkyne group branches off, our alkyne retains the linear structure of SF, at the cost of the terminal methyl group. This could allow **66** to interact in protein pockets where bulkier probes cannot reach due to steric hindrance.

Overall, the alkyne should prove a useful alternative to the Ahn and Clulow probes, and future work employing it should confirm some of the known biological interactions of **1** and potentially help identify additional molecules of interest.

4.3.Future Work

Future work will likely focus on using the probes to investigate the biomolecule interactions of sulforaphane and develop improved therapies based on sulforaphane.

4.3.1 Use fluorinated derivatives to determine organelle localization of fluorinated ITCs

Continuing our work with fluorinated ITCs, these will be administered in THP-1/Jurcat cells, established leukemic monocyte/T-cell lines, which will then undergo cell fractionation. Lysed cells are centrifuged at progressively increased rpm, leading to the sedimentation of increasingly smaller cell organelles: nuclei, mitochondria, microsomes, etc. Samples of the isolated fractions can then be analysed using ^{19}F-NMR, which will allow us to detect changes in the chemical shift associated with reactions with biomolecules, as well as to identify the main organelle targets of F-ITCs. Altering incubation times could help determine whether FITCs prioritize organelles differently as they accumulate in the cell.

4.3.2 Use "click" derivatives of SF to investigate biomolecule interactions of ITCs

4.3.2.1 "Click" reactions in cell lysate

An immediate next step is to use the newly obtained SF-based alkyne in "click" reactions performed after incubation inside cells. Given that CuAAC reactions are incompatible with living cells, this step will be performed in cell lysate. As detailed below, different types of azides can be used to achieve specific desired goals.

4.3.2.2 Imaging

Principle: A fluorescent compound transformed into an azide will undergo a "click" reaction with the alkyne, forming a fluorescent triazole that will tag any biomolecule that the alkyne is covalently bonded with. The triazole tag can aid in identifying these biomolecules following a separation procedure such as SDS-PAGE (**Fig. 4.1**).
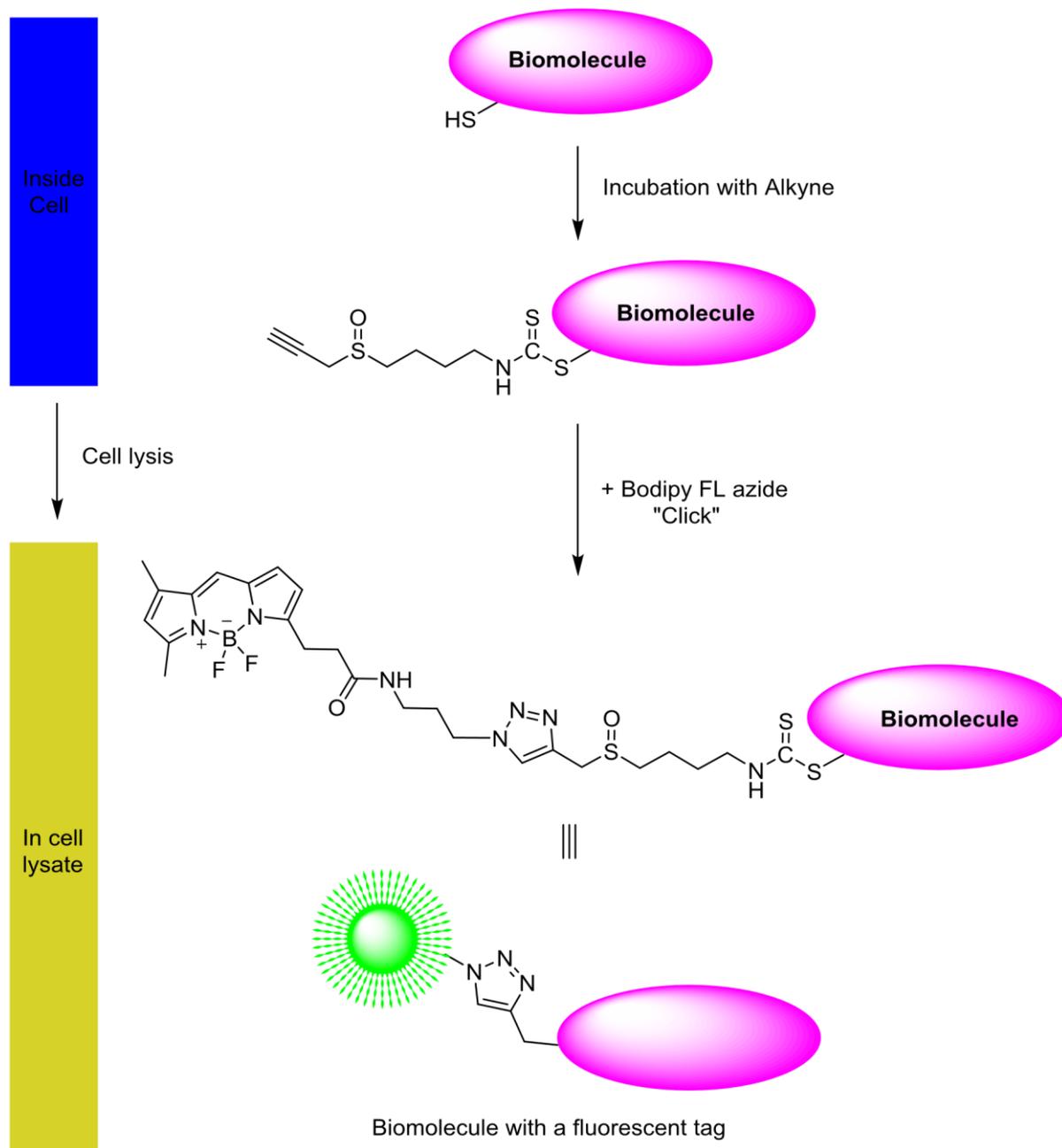
Fig. 4.1 Fluorescent tagging of relevant biomolecules using "click" chemistry

4.3.2.3 Affinity purification

Principle

One of the azides that were chosen for "click" reaction is functionalized with a biotin residue. Biotin, also known as vitamin B7 or vitamin H, forms high affinity non-covalent complexes with streptavidin, a protein that forms tetramers. These complexes, obtained through a combination of several hydrogen bonds, van der Waals and hydrophobic interactions, are characterized by the strongest non-covalent protein-ligand interaction. Streptavidin Dynabeads, magnetic beads with streptavidin, can be used for the affinity purification of biotinylated biomolecules, while unattached molecules can be washed away.

Attached proteins will then be identified using LCMS or SDS-PAGE.

4.3.3 Development of improved therapies based on sulforaphane

One manner of addressing the issues related to using sulforaphane as a therapeutic agent, particularly its low stability, would be the development of new molecules based on **1**. A number of derivatives (**Section 1.5**) have already been synthesised. Considering the structure of the sulforaphane molecule, we discern four molecular features where modifications can be made: 1. The terminal methyl group; 2. The sulfoxide group; 3. The carbon linker between the sulfoxide and the ITC; 4. The isothiocyanate group. Indeed, each of these features has been altered in the various synthetic SF derivatives (**Fig. 4.2**).
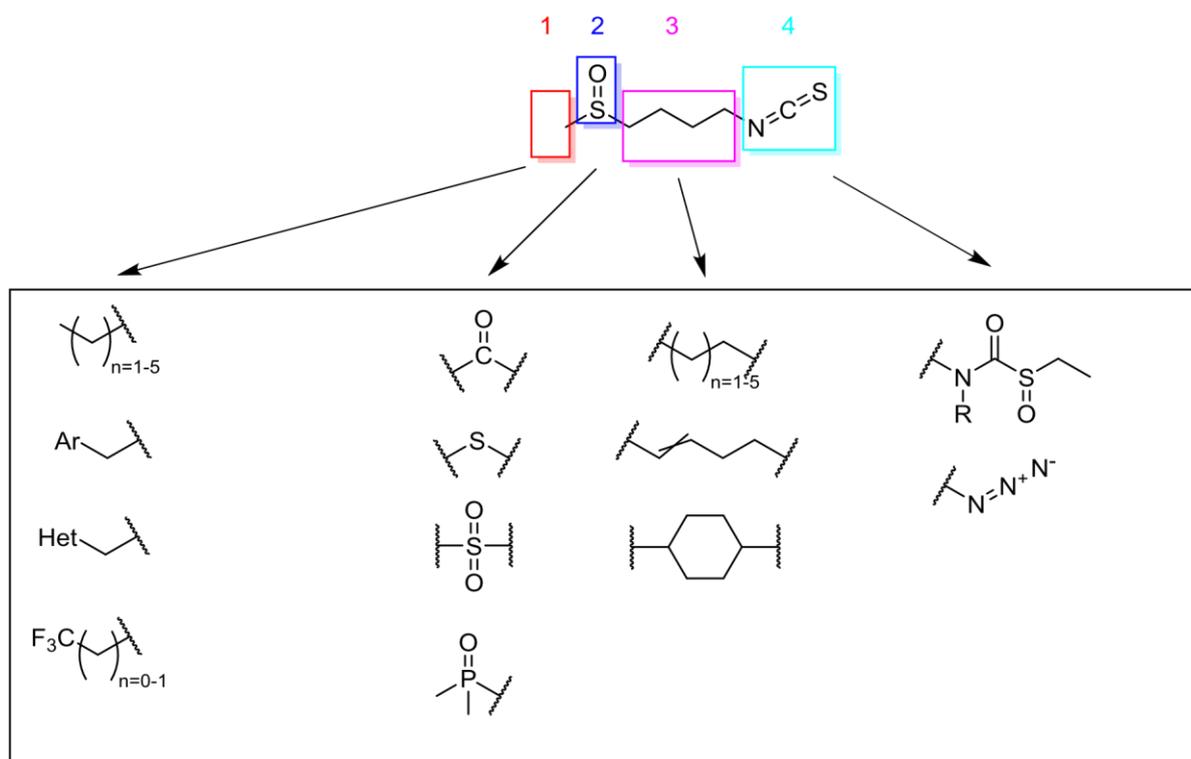
Fig. 4.2 Diversity in the known synthetic derivatives of sulforaphane, separated based on the structural features that are modified: 1. Terminal methyl 2. Sulfoxide 3. Carbon linker 4. Isothiocyanate.

The isothiocyanate group is vital for interactions with –SH and –NH$_2$ groups on biomolecules, and has therefore seen the least derivatisation; conceptually it is also more difficult to identify ITC derivatives where it is the ITC group that has been modified. Nonetheless, an alternative sulfoxythiocarbamate group was used in the two studies that created "click" probes based on **1** (Ahn et al. 2010; Clulow et al. 2017). An azide group would maintain some of the features of the ITC group (linearity, roughly similar polarity among the atoms in the group), but would not be expected to maintain the same reactivity.

The sulfoxide would logically be considered the other important molecular feature in **1**. Modifications have generally tried to keep the double bond with an oxygen atom, using ketones or dimethylphosphine to replace the sulfoxide.

In most synthetic derivatives we identified, the variability, therefore, comes in features 1 and 3, the terminal methyl and the carbon linker. The terminal methyl is arguably the easiest to modify while maintaining the core features of **1**, and a variety of such derivatives have been synthesised, using longer alkyl chains, adding (poly)cycloalkyl, aromatic or heterocyclic moieties. In the linker region, beyond modifications to the length and saturation (sulforaphene, the alkene derivative of **1** can occur naturally), a notable idea was to use a disubstituted cyclohexyl as a skeleton, leading to a less flexible frame on which the sulfoxide and the isothiocyanate can be grafted. Considering that the linker region seems to be the most sensitive to degradation, we speculate that modifications to this region are the most likely to lead to derivatives of **1** with improved stability that can maintain similar levels of cancer preventive activity.

CHAPTER 5

EXPERIMENTAL

5.1. Materials

All chemicals were purchased from commercial providers. Phthalimides **64-67** were purchased

from Acros Organics. Most other compounds, including 2,2,2-trifluoroethanethiol,

thiophosgene, hydrazine hydrate, sodium, Ruppert's Reagent **40**, sodium thiocyanate, mCPBA,

triphenyl phosphine, potassium thioacetate and propargyl bromide were purchased from

Sigma. Solvents were purchased from commercial providers such as Alfa Aesar and Sigma.

5.2. Chromatography

Reactions were monitored using thin-layer chromatography (TLC) on aluminum plates with

silica gel coating. Product separation and purification was achieved using "flash" column

chromatography with silica gel as a stationary phase. Eluents for both TLC and "flash"

chromatography included mixtures of hexanes, ethyl acetate, dichloromethane and methanol.

5.3. NMR

^{1}H-NMR and ^{13}C-NMR spectra were acquired on 300 MHz and 600 MHz Bruker

spectrometers. ^{19}F-NMR and ^{31}P-NMR spectra were acquired on a 600 MHz Bruker

spectrometer (resonance frequency of 565 MHz for fluorine). For most NMR experiments,

solutions were prepared by dissolving ~5 mg compound into 700 µL of the appropriate

deuterated solvent, typically CDCl$_3$, D$_2$O, or DMSO-d_6. Chemical shifts are reported in parts

per million (ppm) and coupling constants (J) in Hertz (Hz). Peak spin multiplicity is

abbreviated as follows: s (singlet), d (doublet), t (triplet), q (quartet), and m (multiplet), with

combinations possible (e.g. *dt* represents a doublet of triplets). Spectra wre processed and analysed using TopSpin and MestReNova software.

5.3.1. ^{19}F-NMR stability studies

Given the lack of competing signals present in ^{1}H-NMR, it is possible to use non-deuterated solvents for ^{19}F-NMR. The experiments investigating the stability of the trifluoroethyl derivatives of sulforaphane were performed in either de-ionized (DI) water, PBS, or RPMI media. An initial serial dilution of 39 in DI water (1 mg/mL, 0.1 mg/mL, 0.01 mg/mL, 1 µg/mL) was prepared to investigate LOD and LOQ. Further experiments were run using 10-100 µM solutions prepared from a 5 mM stock solution. 2,2,2-Trifluoroethanol (~-76.5 ppm) was added and used as fluorinated chemical shift reference. Experiments were run at 300 K, using the pulse sequence zgfhigqn30.2, 256 scans and a pulse width of 12.

5.4. General Methods

General method A: Synthesis of ω-N-phthalimido-1-alkyl-2',2',2'-trifluoroethyl sulfides

Adapted from (Kiełbasiński et al. 2014): Sodium methoxide was prepared by adding sodium metal (1.05 eq.) to anhydrous methanol, at 0 °C under argon, then a solution of 2,2,2-trifluoroethanethiol (1 eq.) in methanol was added dropwise. After 1h stirring, the methanol was removed under vacuum to leave the solid sodium 2,2,2-trifluoroethanethiolate, which was then redissolved in dimethoxyethane (25 mL). A solution of N-(ω-bromoalkyl)phthalimide (1 eq) in dimethoxyethane was added under argon at 0 °C, then the reaction was left to stir overnight, warming up to room temperature. Water (25 mL) was added to the mixture and the

organic fraction was extracted with DCM (3x25 mL). The combined organic layers were washed with water, dried with magnesium sulfate, then the solvent was removed under reduced pressure to give the crude product as a colourless oil.

General method B: Preparation of ω-N-phthalimido-1-alkyl-trifluoromethyl sulphides

Adapted from (Matheis et al. 2015): Cesium carbonate (1 eq), sodium thiocyanate (1.2 eq) and the bromoalkylphthalimide (1 eq) were placed in an oven-dried flask under argon, then acetonitrile (20 mL) and TMSCF$_3$ (1.2 eq) were added using a syringe. The suspension was heated to 60 °C and allowed to stir overnight. After completion was determined by TLC, diethyl ether was added to the reaction mixture, which was then washed with water and brine. The organic layer was dried with magnesium sulfate, filtered, and concentrated under reduced pressure.

General method C1: Removal of the phthalimide protecting group

Adapted from (Kiełbasiński et al. 2014): An ethanol solution of hydrazine hydrate (4 eq) was added under argon to an ethanol solution of fluorinated phthalimide (1 eq). The solution was refluxed for 3h, then allowed to stir overnight at room temperature. Concentrated HCl was added to the mixture and the solution was refluxed for 1.5 h. Water was added to the solution and the fine precipitate was filtered off over celite. The filtrate was evaporated under reduced pressure to give the crude amine hydrochloride, which was taken into the next step without further purification.

General method C2: Microwave removal of the phthalimide group

An ethanol solution of hydrazine hydrate (4 eq.) was added to a solution of phthalimide (1 eq.), followed by methylamine (1 eq.). The resulting solution was then microwaved at 160 °C until TLC showed consumption of starting material (3 x 10 min.). Concentrated (36.5%) HCl was added and the solution was microwaved again (2 x 10 min.). The reaction mixture was poured

in water and the phthalhydrazide precipitate was filtered off. Water and ethanol were removed under vacuum to give the crude amine hydrochlorate.

General method D: Preparation of isothiocyanate sulphides

Adapted from (Kiełbasiński et al. 2014): The amine hydrochloride was dissolved in chloroform, then thiophosgene (1.3 eq) and 5% NaOH (aq) were added at 0 ºC. The reaction was allowed to stir for 1.5 h, with more NaOH solution being added dropwise to the mixture in order to maintain the pH above 7. The layers were separated and the aqueous layer was washed with chloroform. The combined organic layers were then washed with water and dried with magnesium sulfate, then evaporated under reduced pressure to give the crude isothiocyanate. This was then purified using column chromatography on silica, using DCM as eluent.

General method E: Oxidation of sulphides to sulfoxides

Adapted from (Kiełbasiński et al. 2014): The sulfide was dissolved in DCM, then a DCM solution of mCPBA (1 eq) was added dropwise while stirring at 0 ºC. After TLC showed complete consumption of starting material, a 5% $NaHCO_3$ solution was added over the reaction mixture, continuing stirring for 30 minutes. The layers were then separated and the aqueous layer was extracted with DCM, then the combined organic layers were then washed with water and dried with magnesium sulfate, then evaporated under reduced pressure to give the crude sulfoxide, which was then purified using column chromatography on silica, using DCM with 2% methanol as eluent.

General method F: Oxidation of sulfoxides to sulfones

The sulfoxide was dissolved in DCM, then a DCM solution of mCPBA (1 eq) was added dropwise while stirring at room temperature. After TLC showed complete consumption of

starting material, a 5% NaHCO₃ solution was added over the reaction mixture, continuing stirring for 30 minutes. The layers were then separated and the aqueous layer was extracted with DCM, and the combined organic layers were washed with water and dried with magnesium sulfate, then evaporated under reduced pressure to give the crude sulfone.

5.5 Trifluoroethyl Sulforaphane Derivatives

2-(2-((2,2,2-trifluoroethyl)thio)ethyl)isoindoline-1,3-dione (68)
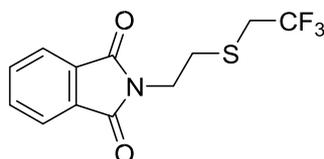
The compound was synthesised according to general procedure A from 2-(2-bromoethyl)isoindoline-1,3-dione **64** − (1.06 g, 4.09 mmol), using 2,2,2-trifluoroethanol (0.5 g, 4.09 mmol) and sodium (0.1 g, 4.30 mmol). The crude product was redissolved in DCM and purified through flash chromatography on silica using DCM as eluent. White solid, 85% conversion, 76% yield. ¹H NMR (600 MHz, CDCl₃) δ 7.91 − 7.70 (m, 4H - arom), 3.8 (t, $J = 6.8$ Hz, 2H − **CH₂**N), 3.17 (q, $J = 9.9$ Hz, 2H − **CH₂**CF₃), 2.98 (t, $J = 6.8$ Hz, 2H − **CH₂**S).

2-(3-((2,2,2-trifluoroethyl)thio)propyl)isoindoline-1,3-dione (69)
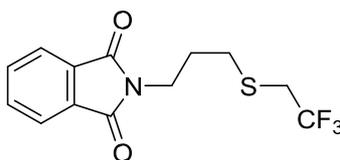
The compound was synthesised according to general procedure A from 2-(3-

bromopropyl)isoindoline-1,3-dione (**65**) – (1.12 g, 4.09 mmol), using 2,2,2-trifluoroethanol (0.5 g, 4.09 mmol) and sodium (0.1 g, 4.30 mmol). The crude product was redissolved in DCM and purified through flash chromatography on silica using DCM as eluent. Off-white solid, 70% conversion, 54% yield. ^{1}H NMR (300 MHz, CDCl$_3$) δ 7.91 – 7.64 (m, 4H - arom), 3.80 (t, J = 6.9 Hz 2H – C**H$_2$**N), 3.09 (q, J = 9.9 Hz, 2H – C**H$_2$**CF$_3$), 2.71 (t, J = 7.3 Hz, 2H – C**H$_2$**S), 2.06 – 1.90 (m, 2H – CH$_2$C**H$_2$**CH$_2$).

2-(4-((2,2,2-trifluoroethyl)thio)butyl)isoindoline-1,3-dione (70)
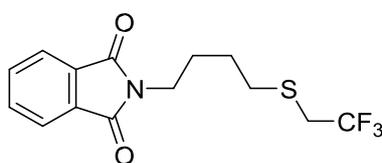
The compound was synthesised according to general procedure A from 2-(4-bromobutyl)isoindoline-1,3-dione (**66**) – (1.18 g, 4.09 mmol), using 2,2,2-trifluoroethanol (0.5 g, 4.09 mmol) and sodium (0.1 g, 4.30 mmol). The crude product was redissolved in DCM and purified through flash chromatography on silica using DCM as eluent. Off-white solid, 86% yield, ^{1}H NMR (300 MHz, CDCl$_3$) δ 7.89 – 7.64 (m, 4H - arom), 3.70 (t, J = 6.9 Hz, 2H – C**H$_2$**N), 3.05 (q, J = 9.9 Hz, 2H – C**H$_2$**CF$_3$), 2.70 (t, J = 7.2 Hz, 2H – C**H$_2$**S), 1.89 – 1.38 (m, 4H – CH$_2$C**H$_2$**C**H$_2$**CH$_2$). Compared to lit. ^{1}H NMR (CDCl$_3$): δ 1.58-1.85 (m, 4H, CH$_2$CH$_2$), 2.69 (t, 2H, J = 7.07 Hz, CH$_2$S), 3.04 (q, 2H, J = 9.33 Hz, CH$_2$CF$_3$), 3.69 (t, 2H, J = 6.81 Hz, CH$_2$N), 7.67-7.86 (m, 4H – arom) (Kiełbasiński et al. 2014).

2-(5-((2,2,2-trifluoroethyl)thio)pentyl)isoindoline-1,3-dione (71)
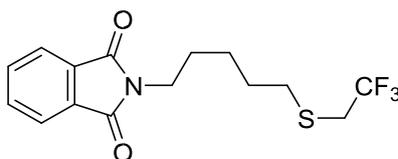
The compound was synthesised according to general procedure A from 2-(5-bromopentyl)isoindoline-1,3-dione (**67**) – (1.24 g, 4.09 mmol), using 2,2,2-trifluoroethanol (0.5 g, 4.09 mmol) and sodium (0.1 g, 4.30 mmol). The crude product was redissolved in DCM and purified through flash chromatography on silica using DCM as eluent. Off white solid, 71% conversion, 60% yield, ^{1}H NMR (300 MHz, CDCl3) δ 7.91 – 7.60 (m, 4H - arom), 3.68 (t, J = 7.2 Hz, 2H – **CH₂**N), 3.04 (q, J = 10.0 Hz, 2H - **CH₂**CF₃), 2.64 (t, J = 7.3 Hz, 2H – **CH₂**S), 1.78 – 1.57 (m, 4H - CH₂**CH₂**CH₂**CH₂**CH₂), 1.57 – 1.36 (m, 2H – CH₂CH₂**CH₂**CH₂CH₂). Compared to lit. ^{1}H NMR (CDCl₃): δ 1.41-1.50 (m, 2H), 1.58-1.77 (m, 4H), 2.65 (t, 2H, J = 7.07 Hz, CH₂S), 3.05 (q, 2H, J = 9.33 Hz, CH₂CF₃), 3.69 (t, 2H, J = 6.81 Hz, CH₂N), 7.67-7.82 (m, 4H – arom) (Kiełbasiński et al. 2014).

2-((2,2,2-trifluoroethyl)thio)ethan-1-aminium chloride (72)
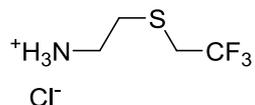
The compound was synthesised according to general procedure C1 from 2-(2-((2,2,2trifluoroethyl)thio)ethyl)isoindoline-1,3-dione (**68**) (0.867 g, 3.00 mmol) dissolved in ethanol

(50 mL), and hydrazine hydrate (0.768 g, 12.00 mmol). The crude 2-((2,2,2-trifluoroethyl)thio)ethan-1-aminium chloride was telescoped into the next reaction.

3-((2,2,2-trifluoroethyl)thio)propan-1-aminium chloride (73)
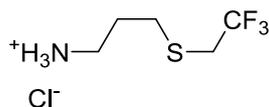
The compound was synthesised according to general procedure C1 from 2-(3-((2,2,2trifluoroethyl)thio)propyl)isoindoline-1,3-dione (**69**) (0.606 g, 2.00 mmol) dissolved in ethanol

(50 mL), and hydrazine hydrate (0.512 g, 8.00 mmol). The crude 3-((2,2,2-trifluoroethyl)thio)propan-1-aminium chloride was telescoped into the next reaction.

4-((2,2,2-trifluoroethyl)thio)butan-1-aminium chloride (74)

$^+$H$_3$N—／＼／＼—S—／CF$_3$
Cl$^-$
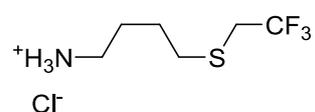
The compound was synthesised according to general procedure C1 from 2-(4-((2,2,2trifluoroethyl)thio)butyl)isoindoline-1,3-dione (**70**) (0.750 g, 2.36 mmol) dissolved in ethanol (50 mL), and hydrazine hydrate (0.606 g, 9.45 mmol). The crude 4-((2,2,2-trifluoroethyl)thio)butan-1-aminium chloride was telescoped into the next reaction.

5-((2,2,2-trifluoroethyl)thio)pentan-1-aminium chloride (75)

$^+$H$_3$N—／＼／＼／—S—＼CF$_3$
Cl$^-$
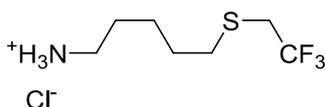
The compound was synthesised according to general procedure C1 from 2-(5-((2,2,2trifluoroethyl)thio)pentyl)isoindoline-1,3-dione (**71**) (0.750 g, 2.26 mmol) dissolved in ethanol (50 mL), and hydrazine hydrate (0.586 g, 9.06 mmol). The crude 5-((2,2,2-trifluoroethyl)thio)pentan-1-aminium chloride was telescoped into the next reaction.

(2-isothiocyanatoethyl)(2,2,2-trifluoroethyl)sulfane (76)
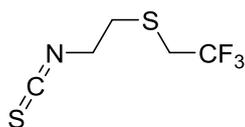
The compound was obtained according to general procedure D from 2-((2,2,2trifluoroethyl)thio)ethan-1-aminium chloride (**72**) (0.587 g, 3.00 mmol), used without purification after procedure C1, and thiophosgene (0.448 g, 0.300 mL, 3.9 mmol). The aqueous layer was washed with 3x25 mL chloroform and the combined organic layers were washed with water (3x50 mL) and dried (MgSO$_4$). The crude compound was purified using flash chromatography on silica with DCM as eluent. Yellow oil, 37% yield over two steps. ^{1}H NMR (300 MHz, CDCl$_3$) δ 3.74 (t, J = 6.6 Hz, 2H – **CH$_2$N**), 3.15 (q, J = 9.7 Hz, 2H – **CH$_2$CF$_3$**), 2.96 (t, J = 6.6 Hz, 2H – **CH$_2$S**).

(3-isothiocyanatopropyl)(2,2,2-trifluoroethyl)sulfane (77)
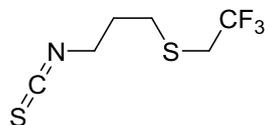
The compound was obtained according to general procedure D from 3-((2,2,2trifluoroethyl)thio)propan-1-aminium chloride (**73**) (0.419 g, 2.00 mmol), used without purification after procedure C1, and thiophosgene (0.299 g, 0.200 mL, 2.6 mmol). The aqueous layer was washed with 3x25 mL chloroform and the combined organic layers were washed with water (3x50 mL) and dried (MgSO$_4$). The crude compound was purified using flash chromatography on silica with DCM as eluent. Yellow oil. ^{1}H NMR, 53% yield over two steps, (300 MHz, CDCl$_3$) δ 3.68 (t, J = 6.3 Hz 2H – **CH$_2$N**), 3.09 (q, J = 9.8 Hz, 2H – **CH$_2$CF$_3$**), 2.80 (t, J = 7.0 Hz, 2H – **CH$_2$S**), 2.07 – 1.91 (m, 2H – **CH$_2$CH$_2$CH$_2$**); proton decoupled ^{19}F-NMR (565 MHz, CDCl$_3$): δ -66.40 (s)

**(4-isothiocyanatobutyl)(2,2,2-trifluoroethyl)sulfane (78)**
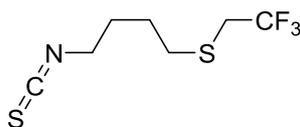
The compound was obtained according to general procedure D from 4-((2,2,2trifluoroethyl)thio)butan-1-aminium chloride (**74**) (0.524 g, 2.36 mmol), used without purification after procedure C1, and thiophosgene (0.354 g, 0.236 mL, 3.07 mmol). The aqueous layer was washed with 3x25 mL chloroform and the combined organic layers were washed with water (3x50 mL) and dried ($MgSO_4$). The crude compound was purified using flash chromatography on silica with DCM as eluent. Light yellow oil, 49% yield over two steps, ^1H NMR (300 MHz, $CDCl_3$) δ 3.56 (t, J = 6.2 Hz, 2H − **CH₂N**), 3.08 (q, J = 9.9 Hz, 2H − **CH₂CF₃**), 2.72 (t, J = 6.7 Hz, 2H − **CH₂S**), 1.92 − 1.66 (m, 4H − CH₂**CH₂CH₂**CH₂); proton decoupled ^{19}F-NMR (565 MHz, H_2O): δ -66.17 (s). Compared to lit. ^1H NMR ($CDCl_3$): δ 1.66-1.90 (m, 4H, CH₂CH₂), 2.72 (t, 2H, J = 6.55 Hz, CH₂S), 3.08 (q, J = 9.91 Hz, CH₂CF₃), 3.56 (t, 2H, J = 6.05 Hz, CH₂N). ^{19}F NMR ($CDCl_3$): δ -65.76 (t, 3F, J_{H-F} = 9.81 Hz) (Kiełbasiński et al. 2014).

**(5-isothiocyanatopentyl)(2,2,2-trifluoroethyl)sulfane** (**79**)
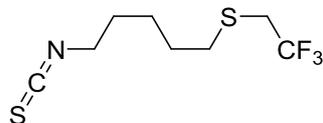
The compound was obtained according to general procedure D from 5-((2,2,2trifluoroethyl)thio)pentan-1-aminium chloride (**75**) (0.53 g, 2.26 mmol), used without purification after procedure C1, and thiophosgene (0.338 g, 0.225 mL, 2.94 mmol). The aqueous layer was washed with 3x25 mL chloroform and the combined organic layers were washed with water (3x50 mL) and dried ($MgSO_4$). The crude compound was purified using

flash chromatography on silica with DCM as eluent. Yellow oil, 42% yield over two steps, ^{1}H NMR (300 MHz, CDCl$_3$) δ 3.53 (t, J = 6.5 Hz, 2H – **CH$_2$N**), 3.07 (q, 2H, J = 9.9 Hz – **CH$_2$CF$_3$**), 2.69 (t, J = 7.1 Hz, 2H – **CH$_2$S**), 1.79 – 1.46 (m, 6H – CH$_2$**CH$_2$CH$_2$CH$_2$**CH$_2$); proton decoupled ^{19}F NMR (565 MHz, CDCl$_3$) δ -66.41 (s). Compared to lit. ^{1}H NMR (CDCl$_3$): δ 1.52-1.79 (m, 6H), 2.69 (t, 2H, J = 6.87 Hz, CH$_2$S), 3.07 (q, J = 9.92 Hz, CH$_2$CF$_3$), 3.53 (t, 2H, J = 6.38 Hz, CH$_2$N). ^{19}F NMR (CDCl$_3$): δ -65.8 (t, 3F, $J_{H\text{-}F}$ = 9.80 Hz) (Kiełbasiński et al. 2014).

1,1,1-trifluoro-2-((2-isothiocyanatoethyl)sulfinyl)ethane (80)
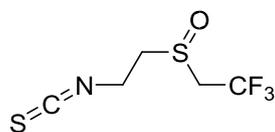
The compound was prepared according to general procedure E from (2-isothiocyanatoethyl)(2,2,2-trifluoroethyl)sulfane (**76**) (0.101 g, 0.50 mmol) and mCPBA (65% concentration, 0.133 g , 0.50 mmol). After adding a 5% aqueous NaHCO$_3$ solution (25 mL), to neutralize the resulting meta-chlorobenzoic acid, the aqueous phase was extracted with 3x25 mL DCM. The combined organic layers were washed with water (3x50) ml, dried (MgSO$_4$) and the solvent was removed under vacuum. After purification (chromatography on silica, 2% methanol in DCM as eluent), the compound was isolated in 88% as an off-white solid. ^{1}H NMR (300 MHz, CDCl$_3$) δ 4.21 – 4.06 (m, 2H – **CH$_2$N**), 3.57 (q, J = 9.9 Hz, 2H – **CH$_2$CF$_3$**), 3.24 – 3.04 (m, 2H – **CH$_2$S**); proton decoupled ^{19}F NMR (565 MHz, CDCl$_3$) δ -60.54 (s).

(3-isothiocyanatopropyl)(2,2,2-trifluoroethyl)sulfoxide (81)
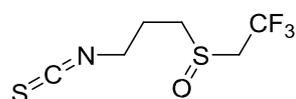
The compound was prepared according to general procedure E from (3-isothiocyanatopropyl)(2,2,2-trifluoroethyl)sulfane (**77**) (0.150 g, 0.70 mmol) and mCPBA (65% concentration, 0.185 g , 0.70 mmol). After adding a 5% aqueous NaHCO$_3$ solution (25 mL), to neutralize the resulting meta-chlorobenzoic acid, the aqueous phase was extracted with 3x25 mL DCM. The combined organic layers were washed with water (3x50) ml, dried (MgSO$_4$) and the solvent was removed under vacuum. After purification (chromatography on silica, 2% methanol in DCM as eluent), the compound was isolated in 83% yield as an off-white solid. ^{1}H-NMR (600 MHz, CDCl$_3$) δ 3.82 – 3.73 (m, 2H – **CH$_2$**N), 3.58 – 3.45 (m, 2H – **CH$_2$**CF$_3$), 3.06 – 2.93 (m, 2H – **CH$_2$**S), 2.34 – 2.20 (m, 2H – CH$_2$**CH$_2$**CH$_2$); proton decoupled ^{19}F NMR (565 MHz, CDCl$_3$) δ -60.65 (s).

## (4-isothiocyanatobutyl)(2,2,2-trifluoroethyl)sulfoxide (82)
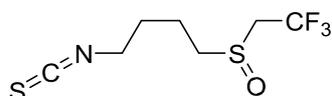
The compound was prepared according to general procedure E from (4-isothiocyanatobutyl)(2,2,2-trifluoroethyl)sulfane (**78**) (0.177 g, 0.77 mmol) and mCPBA (65% concentration, 0.205 g , 0.77 mmol). After adding a 5% aqueous NaHCO$_3$ solution (25 mL), to neutralize the resulting meta-chlorobenzoic acid, the aqueous phase was extracted with 3x25 mL DCM. The combined organic layers were washed with water (3x50) ml, dried (MgSO$_4$) and the solvent was removed under vacuum. After purification (chromatography on silica, 2% methanol in DCM as eluent), the compound was isolated in 85% yield as an off-white solid. ^{1}H NMR (600 MHz, CDCl$_3$) δ 3.66 – 3.58 (m, 2H – **CH$_2$**N), 3.55 – 3.42 (m, 2H – **CH$_2$**CF$_3$), 2.99 – 2.84 (m, 2H – **CH$_2$**S), 2.08 – 1.84 (m, 4H – CH$_2$**CH$_2$CH$_2$**CH$_2$); proton decoupled ^{19}F NMR (565 MHz, CDCl$_3$) δ -60.68 (s). LC-MS m/z calculated for [M+H$^+$] C$_7$H$_{11}$NS$_2$OF$_3$: 246.0229 found 246.0235. Compared to lit. ^{1}H NMR (CDCl$_3$): δ 1.80-2.07 (m, 4H, CH$_2$CH$_2$), 2.78-3.01

(m, 2H, CH$_2$S), 3.47 (q, J = 10.07 Hz, CH$_2$CF$_3$), 3.61 (t, 2H, J = 6.01 Hz, CH$_2$N). ^{19}F NMR (CDCl$_3$): δ -60.08 (t, 3F, $J_{H\text{-}F}$ = 9.77 Hz) (Kiełbasiński et al. 2014).

(5-isothiocyanatopentyl)(2,2,2-trifluoroethyl)sulfoxide (83)
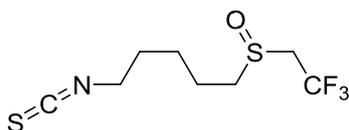
The compound was prepared according to general procedure E from (5-isothiocyanatopentyl)(2,2,2-trifluoroethyl)sulfane (**79**) (0.150 g, 0.62 mmol) and mCPBA (65% concentration, 0.164 g , 0.62 mmol). After adding a 5% aqueous NaHCO$_3$ solution (25 mL), to neutralize the resulting meta-chlorobenzoic acid, the aqueous phase was extracted with 3x25 mL DCM. The combined organic layers were washed with water (3x50) ml, dried (MgSO$_4$) and the solvent was removed under vacuum. After purification (chromatography on silica, 2% methanol in DCM as eluent), the compound was isolated in 80% yield as a pale yellow solid. ^{1}H NMR (600 MHz, CDCl$_3$) δ 3.57 (t, J = 6.1 Hz, 2H – **CH$_2$N**), 3.53 – 3.40 (m, 2H – **CH$_2$CF$_3$**), 2.96 – 2.80 (m, 2H – **CH$_2$S**), 1.97 – 1.85 (m, 2H – NCH$_2$**CH$_2$**CH$_2$CH$_2$CH$_2$), 1.78 (p, J = 6.6 Hz, 2H – NCH$_2$CH$_2$**CH$_2$**CH$_2$CH$_2$), 1.72 – 1.54 (m, 2H NCH$_2$CH$_2$CH$_2$**CH$_2$**CH$_2$); ^{19}F NMR (565 MHz, CDCl$_3$) δ -60.73 (s). Compared to lit. ^{1}H NMR (CDCl$_3$): δ 1.61-1.71 (m, 2H, CH$_2$), 1.78 (p, J = 7.03 Hz), 1.84-1.97 (m, 2H) 2.81-2.96 (m, 2H, CH$_2$SO), 3.42-3.51 (m, 2H, CH$_2$CF$_3$), 3.56 (t, 2H, J = 6.38 Hz, CH$_2$N). ^{19}F NMR (CDCl$_3$): δ -60.11 (t, 3F, $J_{H\text{-}F}$ = 9.79 Hz) (Kiełbasiński et al. 2014).

(4-isothiocyanatobutyl)(2,2,2-trifluoroethyl)sulfone (82)
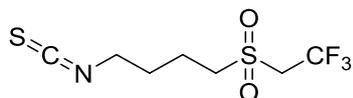
The compound was prepared according to general procedure F from (4-

isothiocyanatobutyl)(2,2,2-trifluoroethyl)sulfoxide (**82**) (0.050 g, 0.2 mmol) and mCPBA (65% concentration, 0.053 g , 0.2 mmol). After adding a 5% aqueous $NaHCO_3$ solution (15 mL), to neutralize the resulting meta-chlorobenzoic acid, the aqueous phase was extracted with 3x25 mL DCM. The combined organic layers were washed with water (3x30) ml, dried ($MgSO_4$) and the solvent was removed under vacuum. After purification (chromatography on silica, 2% methanol in DCM as eluent), the compound was isolated in 72% yield as an off-white solid. ^{1}H NMR (600 MHz, $CDCl_3$) δ 3.81 (q, *J* = 9.2 Hz, 2H – **CH₂**CF₃), 3.61 (t, *J* = 6.3 Hz, 2H – **CH₂**N), 3.25 − 3.18 (t. *J* = 6.9 Hz, 2H – **CH₂**S), 2.08 − 1.84 (m, 4H - CH₂**CH₂CH₂**CH₂).; proton decoupled ^{19}F NMR (565 MHz, $CDCl_3$) δ -61.17 (s).

5.6. Trifluoromethyl derivatives

2-(2-((trifluoromethyl)thio)ethyl)isoindoline-1,3-dione (92)
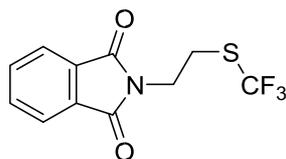
The compound was prepared according to general procedure B, using 2-(2-bromoethyl)isoindoline-1,3-dione **64** (0.950 g, 3.66 mmol), Cs_2CO_3 (1.194 g, 3.66 mmol), NaSCN (0.364 g, 4.40 mmol), and TMSCF₃ (0.66 mL, 0.631g, 4.40 mmol), using acetonitrile (25 mL) as solvent. After the reaction reached completion, diethyl ether (50 mL) was added to the mixture, which was washed with water (3x50 mL) and brine (3x50 mL), dried ($MgSO_4$), then the solvent was removed under reduced pressure. ^{1}H NMR (600 MHz, $CDCl_3$) δ 7.94 − 7.89 (m, 2H - arom), 7.81 − 7.77 (m, 2H - arom), 4.16 (t, *J* = 6.5 Hz, 2H – **CH₂**N), 3.32 (t, *J* = 6.5 Hz, 2H – **CH₂**S); ^{13}C NMR (151 MHz, $CDCl_3$) δ 134.41, 123.68, 37.30, 31.81). ^{19}F-NMR (565 MHz, $CDCl_3$): δ -41.16 (s)

2-(3-((trifluoromethyl)thio)propyl)isoindoline-1,3-dione (93)
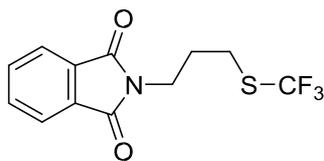
The compound was prepared according to general procedure B, using 2-(3-bromopropyl)isoindoline-1,3-dione **65** (1.000 g, 3.66 mmol), Cs_2CO_3 (1.194 g, 3.66 mmol), NaSCN (0.363 g, 4.39 mmol), and $TMSCF_3$ (0.66 mL, 0.630 g, 4.76 mmol), using acetonitrile (25 mL) as solvent. After the reaction reached completion, diethyl ether (50 mL) was added to the mixture, which was washed with water (3x50 mL) and brine (3x50 mL), dried ($MgSO_4$), then the solvent was removed under reduced pressure. ^1H NMR (600 MHz, $CDCl_3$) δ 7.96 – 7.84 (m, 2H - arom), 7.82 – 7.69 (m, 2H - arom), 3.84 (t, J = 6.8 Hz, 2H – **CH₂**N), 2.94 (t, J = 7.4 Hz, 2H – **CH₂**S), 2.12 (p, J = 7.0 Hz, 2H - CH₂**CH₂**CH₂). ^{19}F-NMR (565 MHz, $CDCl_3$): δ -41.16 (s); ^{13}C NMR (151 MHz, $CDCl_3$) δ 168.29, 134.27, 131.87, 123.48, 111.85, 35.86, 31.55, 29.30.

2-(4-((trifluoromethyl)thio)butyl)isoindoline-1,3-dione (94)
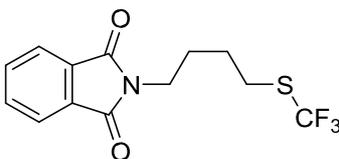
The compound was prepared according to general procedure B, using 2-(4-bromobutyl)isoindoline-1,3-dione **66** (1.000 g, 3.47 mmol), Cs_2CO_3 (1.132 g, 3.47 mmol), NaSCN (0.345 g, 4.17 mmol), and $TMSCF_3$ (0.62 mL, 0.599 g, 4.17 mmol), using acetonitrile (25 mL) as solvent. After the reaction reached completion, diethyl ether (50 mL) was added to

the mixture, which was washed with water (3x50 mL) and brine (3x50 mL), dried (MgSO$_4$), then the solvent was removed under reduced pressure. ^{1}H NMR (600 MHz, CDCl$_3$) δ 7.92 – 7.84 (m, 2H - arom), 7.79 – 7.71 (m, 2H - arom), 3.75 (t, J = 6.9 Hz, 2H – **CH$_2$N**), 2.96 (t, J = 7.2 Hz, 2H – **CH$_2$S**), 1.89 – 1.73 (m, 4H – **CH$_2$CH$_2$**); ^{19}F-NMR (565 MHz, CDCl$_3$): δ -41.14 (s). Compared with lit. 1H NMR (CDCl$_3$): δ 1.70-1.87 (m, 4H, CH$_2$CH$_2$), 2.91 (t, 2H, J = 6.66 Hz, CH$_2$S), 3.70 (t, 2H, J = 6.60 Hz, CH$_2$N), 7.68-7.85 (m, 4H, arom). 19F NMR (CDCl$_3$): δ -40.51.

2-(5-((trifluoromethyl)thio)pentyl)isoindoline-1,3-dione (95)
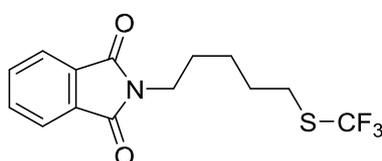
The compound was prepared according to general procedure B, using 2-(3-bromopentyl)isoindoline-1,3-dione **67** (1.200 g, 3.97 mmol), Cs$_2$CO$_3$ (1.294 g, 3.97 mmol), NaSCN (0.394 g, 4.76 mmol), and TMSCF$_3$ (0.71 mL, 0.684 g, 4.76 mmol), with acetonitrile (25 mL) as solvent. After the reaction reached completion, diethyl ether (50 mL) was added to the mixture, which was washed with water (3x50 mL) and brine (3x50 mL), dried (MgSO$_4$), then the solvent was removed under reduced pressure. ^{1}H NMR (600 MHz, CDCl$_3$) δ 7.89 – 7.83 (m, 2H - arom), 7.77 – 7.70 (m, 2H - arom), 3.73 (t, J = 7.1 Hz, 2H - **CH$_2$N**), 2.96 (t, J = 7.2 Hz, 2H – **CH$_2$S**), 1.91 (dt, J = 15.0, 7.4 Hz, 2H – NCH$_2$**CH$_2$**CH$_2$CH$_2$CH$_2$)), 1.76 (dt, J = 15.0, 7.4 Hz, 2H – NCH$_2$CH$_2$**CH$_2$**CH$_2$CH$_2$), 1.53 (dq, J = 15.4, 7.7 Hz, 2H NCH$_2$CH$_2$CH$_2$**CH$_2$**CH$_2$); ^{13}C NMR (151 MHz, CDCl$_3$) δ 168.41, 134.00, 132.07, 123.27, 112.15, 77.25, 77.03, 76.82, 37.48, 33.78, 29.38, 27.90, 25.21; ^{19}F-NMR (565 MHz, CDCl$_3$): δ -41.19 (s)

2-((trifluoromethyl)thio)ethan-1-aminium chloride (96)
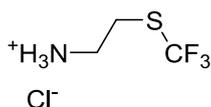
$$^+H_3N \diagup \diagdown S \diagdown CF_3$$

$$Cl^-$$

The compound was synthesised according to general procedure C1, using 2-(2((trifluoromethyl)thio)ethyl)isoindoline-1,3-dione (**92**) (0.500 g, 1.82 mmol) dissolved in ethanol (50 mL) and hydrazine hydrate (0.466 g, 7.27 mmol). The crude 2-((trifluoromethyl)thio)ethan-1-aminium chloride was telescoped into the next reaction.

3-((trifluoromethyl)thio)propan-1-aminium chloride (97)

$$^+H_3N \diagup \diagdown S-CF_3$$

$$Cl^-$$
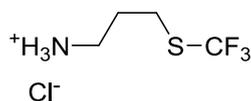
The compound was synthesised according to general procedure C1, using 2-(3((trifluoromethyl)thio)propyl)isoindoline-1,3-dione (**93**) (0.500 g, 1.73 mmol) dissolved in ethanol (50 mL) and hydrazine hydrate (0.444 g, 6.92 mmol). The crude 3-((trifluoromethyl)thio)propan-1-aminium chloride was telescoped into the next reaction.

4-((trifluoromethyl)thio)butan-1-aminium chloride (98)

$$^+H_3N \diagup \diagdown \diagup S \diagdown CF_3$$

$$Cl^-$$
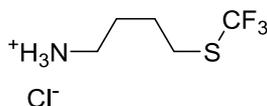
The compound was synthesised according to general procedure C1, using 2-(4((trifluoromethyl)thio)butyl)isoindoline-1,3-dione (**94**) (0.500 g, 1.65 mmol) dissolved in ethanol (50 mL) and hydrazine hydrate (0.423 g, 6.59 mmol). The crude 4-((trifluoromethyl)thio)butan-1-aminium chloride was telescoped into the next reaction.

5-((trifluoromethyl)thio)pentan-1-aminium chloride (99)

^+H_3N —／＼／— S—CF$_3$

Cl$^-$
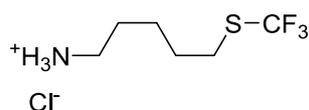
The compound was synthesised according to general procedure C1, using 2-(5((trifluoromethyl)thio)pentyl)isoindoline-1,3-dione (**95**) (0.500 g, 1.58 mmol) dissolved in ethanol (50 mL) and hydrazine hydrate (0.404 g, 6.32 mmol). The crude 5-((trifluoromethyl)thio)pentan-1-aminium chloride was telescoped into the next reaction.

(2-isothiocyanatoethyl)(trifluoromethyl)sulfane (100)

S=C=N—／— S—CF$_3$
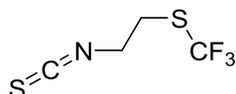
The compound was obtained according to general procedure D from 5-((2,2,2trifluoroethyl)thio)pentan-1-aminium chloride (**96**) (0.53 g, 2.26 mmol), used without purification after procedure C1, and thiophosgene (0.338 g, 0.225 mL, 2.94 mmol). The aqueous layer was washed with 3x25 mL chloroform and the combined organic layers were washed with water (3x50 mL) and dried (MgSO$_4$). The crude compound was purified using "flash" chromatography on silica with DCM as eluent.

(3-isothiocyanatopropyl)(trifluoromethyl)sulfane (101)
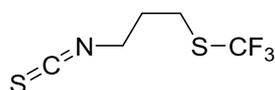
S=C=N—／＼— S—CF$_3$

The compound was obtained according to general procedure D from 5-((2,2,2trifluoroethyl)thio)pentan-1-aminium chloride (**97**) (0.53 g, 2.26 mmol), used without purification after procedure C1, and thiophosgene (0.338 g, 0.225 mL, 2.94 mmol). The aqueous layer was washed with 3x25 mL chloroform and the combined organic layers were

washed with water (3x50 mL) and dried (MgSO$_4$). The crude compound was purified using "flash" chromatography on silica with DCM as eluent. ^{1}H NMR (600 MHz, CDCl$_3$) δ 3.71 (dd, J = 11.3, 5.0 Hz, 2H), 2.82 (t, J = 6.9 Hz, 2H), 2.16 – 2.10 (m, 2H); ^{19}F NMR (565 MHz, CDCl$_3$) δ -40.90 (s).

(4-isothiocyanatobutyl)(trifluoromethyl)sulfane (102)
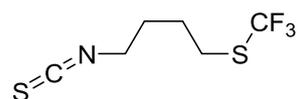
The compound was obtained according to general procedure D from 5-((2,2,2trifluoroethyl)thio)pentan-1-aminium chloride (**98**) (0.53 g, 2.26 mmol), used without purification after procedure C1, and thiophosgene (0.338 g, 0.225 mL, 2.94 mmol). The aqueous layer was washed with 3x25 mL chloroform and the combined organic layers were washed with water (3x50 mL) and dried (MgSO$_4$). The crude compound was purified using "flash" chromatography on silica with DCM as eluent. ^{1}H NMR (600 MHz, CDCl$_3$) δ 3.60 (dd, J = 7.1, 5.2 Hz, 2H), 2.99 – 2.93 (m, 2H), 1.91 – 1.81 (m, 4H); ^{19}F NMR (565 MHz, CDCl$_3$) δ -41.07 (s). Compared with lit. ^{1}H-NMR (CDCl$_3$): δ 1.70-1.87 (m, 4H, CH2CH2), 2.90 (t, 2H, J = 6.6 Hz, CH2S), 3.60 (t, 2H, J = 6. 0 Hz, CH2N) ^{19}F NMR (CDCl$_3$) δ -40.4 (s).

(5-isothiocyanatopentyl)(trifluoromethyl)sulfane (103)
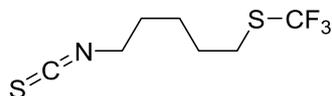
The compound was obtained according to general procedure D from 5-((2,2,2trifluoroethyl)thio)pentan-1-aminium chloride (**99**) (0.53 g, 2.26 mmol), used without purification after procedure C1, and thiophosgene (0.338 g, 0.225 mL, 2.94 mmol). The

aqueous layer was washed with 3x25 mL chloroform and the combined organic layers were washed with water (3x50 mL) and dried (MgSO$_4$). The crude compound was purified using "flash" chromatography on silica with DCM as eluent.

1-isothiocyanato-2-((trifluoromethyl)sulfinyl)ethane (104)
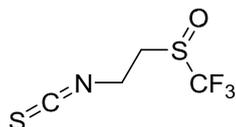
The compound was prepared according to general procedure E from (2-isothiocyanatoethyl)(trifluoromethyl)sulfane (**100**) (0.101 g, 0.50 mmol) and mCPBA (65% concentration, 0.133 g , 0.50 mmol). After adding a 5% aqueous NaHCO$_3$ solution (10 mL), to neutralize the resulting meta-chlorobenzoic acid, the aqueous phase was extracted with 3x10 mL DCM. The combined organic layers were washed with water (3x25 ml), dried (MgSO$_4$) and the solvent was removed under vacuum. After purification (chromatography on silica, 2% methanol in DCM as eluent), the compound was isolated in 68% as an off-white solid.

1-isothiocyanato-3-((trifluoromethyl)sulfinyl)propane (105)
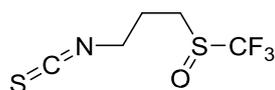
The compound was prepared according to general procedure E from (3-isothiocyanatopropyl)(trifluoromethyl)sulfane (**101**) (0.035 g, 0.17 mmol) and mCPBA (65% concentration, 0.045 g , 0.17 mmol). After adding a 5% aqueous NaHCO$_3$ solution (10 mL), to neutralize the resulting meta-chlorobenzoic acid, the aqueous phase was extracted with 3x10 mL DCM. The combined organic layers were washed with water (3x25 ml), dried (MgSO$_4$)

and the solvent was removed under vacuum. After purification (chromatography on silica, 2% methanol in DCM as eluent), the compound was isolated in 63% yield as an off-white solid

1-isothiocyanato-4-((trifluoromethyl)sulfinyl)butane (106)
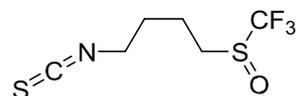
The compound was prepared according to general procedure E from (4-isothiocyanatobutyl)(2,2,2-trifluoroethyl)sulfane (**102**) (0.177 g, 0.77 mmol) and mCPBA (65% concentration, 0.205 g , 0.77 mmol). After adding a 5% aqueous $NaHCO_3$ solution (25 mL), to neutralize the resulting meta-chlorobenzoic acid, the aqueous phase was extracted with 3x25 mL DCM. The combined organic layers were washed with water (3x50 ml), dried ($MgSO_4$) and the solvent was removed under vacuum. After purification (chromatography on silica, 2% methanol in DCM as eluent), the compound was isolated in 78% yield as an off-white solid. ^1H NMR (600 MHz, $CDCl_3$) δ 3.60 (m, 2H), 3.09 – 2.93 (m, 2H), 2.11 – 1.81 (m, 4H); ^{19}F NMR (565 MHz, $CDCl_3$) δ -73.12 (s). Compared with lit. ^1H NMR ($CDCl_3$): δ 1.88-2.09 (m, 4H, CH2CH2), 2.94-3.09 (m, 2H, CH2SO), 3.60 (t, 2H, J = 6.2 Hz, CH2N). 19F NMR (CDCl3): δ - 72.9.

1-isothiocyanato-5-((trifluoromethyl)sulfinyl)pentane (107)
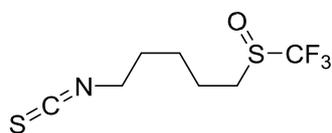
The compound was prepared according to general procedure E from (2-isothiocyanatoethyl)(2,2,2-trifluoroethyl)sulfane (**103**) (0.150 g, 0.62 mmol) and mCPBA (65% concentration, 0.164 g , 0.62 mmol). After adding a 5% aqueous $NaHCO_3$ solution (25

mL), to neutralize the resulting meta-chlorobenzoic acid, the aqueous phase was extracted with 3x25 mL DCM. The combined organic layers were washed with water (3x50 ml), dried (MgSO$_4$) and the solvent was removed under vacuum. After purification (chromatography on silica, 2% methanol in DCM as eluent), the compound was isolated in 65% yield as an off-white solid.

5.7."Click" probe synthesis

S-(4-(1,3-dioxoisoindolin-2-yl)butyl) ethanethioate (151)
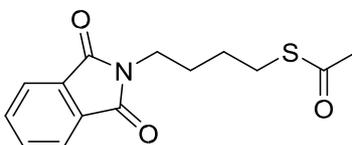
The compound was obtained from 2-(4-bromobutyl)isoindoline-1,3-dione **66** (2.015 g, 7.00 mmol) and potassium thioacetate (2.447 g, 21.00 mmol). The potassium acetate was added to a solution of **66** in THF (80 mL), and the reaction mixture was heated to reflux for 4 h. The solvent was removed under reduced pressure, then water (40 mL) was added and ethyl acetate (3x40 mL) was used to extract the product. The combined organic fractions were washed with water (3x50 mL) and brine (3x50 mL), dried (MgSO$_4$), and the solvent was removed under reduced pressure. ^{1}H NMR (600 MHz, CDCl$_3$) δ 7.88 – 7.83 (m, 2H - arom), 7.75 – 7.69 (m, 2H – arom), 3.71 (t, *J* = 7.1 Hz, 2H – **CH$_2$N**), 2.92 (t, *J* = 7.2 Hz, 2H – **CH$_2$S**), 2.33 (s, 3H, **CH$_3$**), 1.81 – 1.73 (m, 2H – **CH$_2$CH$_2$N**), 1.65 (ddd, *J* = 17.8, 9.1, 5.7 Hz, 2H, **CH$_2$CH$_2$S**). ^{13}C NMR (151 MHz, CDCl$_3$) δ 195.64, 168.34, 133.91, 132.10, 123.22, 37.38, 30.60, 28.49, 27.68, 26.90 MS (ESI, *m/z*): [M+1]$^+$ C$_{14}$H$_{16}$NO$_3$S calculated 278.0845, found 278.0864. Compared with lit. ^{1}H NMR (CDCl$_3$, 500 MHz): δ 1.61-1.66 (m, 2H), 1.72-1.77 (m, 2H), 2.31 (s, 3H), 2.91 (t, 2H, J = 7.0 Hz), 3.69 (t, 2H, J = 7.0 Hz), 7.72 (dd, 2H, J = 3.0, 5.5 Hz), 7.85 (dd, 2H, J = 3.0, 5.5 Hz); ^{13}C NMR (CDCl$_3$, 125 MHz): δ 26.93, 27.70, 28.52, 30.60, 37.42,

123.24, 132.17, 133.93, 168.35, 195.60 (Hu et al. 2013).

2-(4-mercaptobutyl)isoindoline-1,3-dione (152)
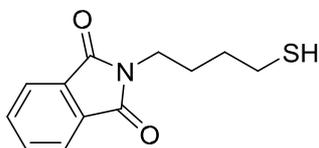
This compound was obtained from S-(4-(1,3-dioxoisoindolin-2-yl)butyl) ethanethioate **151** (0.282 g, 1.02 mmol), which was dissolved in methanol (15 mL) and degassed by purging with nitrogen. 36% HCl (0.43 mL, 5.08 mmol) was added, then the mixture was microwaved at 100 ºC until TLC control showed complete consumption of starting material. The reaction mixture was diluted into water (30 mL), then ethyl acetate (3x25 mL) was used to extract the product. The combined organic fractions were washed with water and brine, dried with $MgSO_4$ and the solvent was removed under reduced pressure. ^{1}H NMR (600 MHz, CDCl$_3$) δ 7.89 – 7.83 (m, 2H - arom), 7.77 – 7.70 (m, 2H - arom), 3.73 (t, J = 7.1 Hz, 2H – **CH$_2$**N), 2.59 (dd, J = 15.0, 7.2 Hz, 2H – **CH$_2$**SH), 1.86 – 1.65 (m, 4H – **CH$_2$CH$_2$**), 1.37 (t, J = 7.9 Hz, 1H - **SH**); ^{13}C NMR (151 MHz, CDCl$_3$) δ 168.38, 133.94, 132.10, 123.23, 37.33, 31.09, 27.31, 24.09, 24.08. MS (ESI, m/z): [M+1]$^+$ C$_{12}$H$_{14}$NO$_2$S calculated 236.07398, found 236.0758. Compared with lit. ^{1}H NMR (CDCl$_3$, 500 MHz): δ 1.26 (t, 1H, J = 7.0 Hz), 1.63-1.69 (m, 2H), 1.77-1.83 (m, 2H), 2.55-2.59 (dd, 2H, J = 7.0 Hz), 3.70 (t, 2H, J = 7.0 Hz), 7.72 (dd, 2H, J = 3.0, 5.5 Hz), 7.84 (dd, 2H, J = 3.0, 5.5 Hz); ^{13}C NMR (CDCl$_3$, 125 MHz): d 24.09, 27.31, 31.10, 37.33, 123.24, 132.11, 133.95, 168.39 (Hu et al. 2013).

2-(4-(prop-2-yn-1-ylthio)butyl)isoindoline-1,3-dione (153)
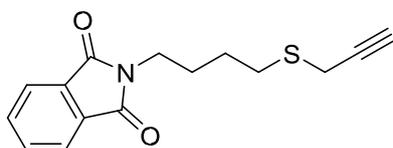
A methanol solution of 2-(4-mercaptobutyl)isoindoline-1,3-dione **152** (0.200 g, 0.085 mmol) was degassed and treated with NaOH (0.041 g, 1.02 mmol) at 0 °C. After 10 minutes, propargyl bromide (0.14 mL, 0.190 g, 1.27 mmol) was added and the solution was stirred overnight, warming up to room temperature. After the reaction was completed, the methanol was removed under reduced pressure, then water (25 mL) was added and the product was extracted with ethyl acetate (3x25 mL). The organic fractions were combined, dried and the solvent was removed under reduced pressure. ^{1}H NMR (300 MHz, CDCl$_3$) δ 7.92 − 7.80 (m, 2H), 7.78 − 7.68 (m, 2H), 3.74 (t, J = 7.0 Hz, 2H), 3.25 (d, J = 2.6 Hz, 2H), 2.81 − 2.69 (m, 2H), 2.22 (t, J = 2.6 Hz, 1H), 1.90 − 1.63 (m, 4H). ^{13}C NMR (151 MHz, CDCl$_3$) δ 168.39, 133.93, 132.11, 123.22, 70.97, 37.47, 31.04, 27.72, 26.23, 19.17. MS (ESI, *m/z*): [M+1]$^+$ C$_{15}$H$_{16}$NO$_2$S calculated 274.08963, found 274.0906.

4-(prop-2-yn-1-ylthio)butan-1-aminium chloride (154)
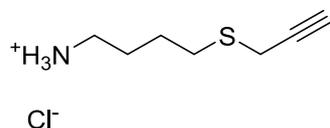
The compound was obtained according to general procedure C2, using 2-(4-(prop-2-yn-1ylthio)butyl)isoindoline-1,3-dione (**153**) dissolved in ethanol (15 mL) and placed in a microwave vessel, hydrazine hydrate and methylamine. The crude 4-(prop-2-yn-1ylthio)butan-1-aminium chloride (**154**) was telescoped into the next reaction. MS (ESI, *m/z*): [M+1]$^+$ C$_7$H$_{14}$NS calculated 144.0841, found 144.0857

(4-isothiocyanatobutyl)(prop-2-yn-1-yl)sulfane (155)
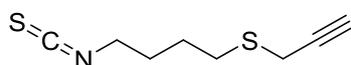
The compound was obtained according to general procedure D from 5-((2,2,2trifluoroethyl)thio)pentan-1-aminium chloride (**154**) (0.53 g, 2.26 mmol), used without purification after procedure C1, and thiophosgene (0.338 g, 0.225 mL, 2.94 mmol). The aqueous layer was washed with 3x25 mL chloroform and the combined organic layers were washed with water (3x50 mL) and dried (MgSO$_4$). The crude compound was purified using flash chromatography on silica with DCM as eluent. ^{1}H NMR (600 MHz, CDCl$_3$) δ 3.59 (t, *J* = 6.4 Hz, 2H), 3.28 (dd, *J* = 4.0, 2.6 Hz, 2H), 2.76 (t, *J* = 6.9 Hz, 2H), 2.28 (t, *J* = 2.6 Hz, 1H), 1.89 – 1.72 (m, 4H). ^{13}C NMR (151 MHz, CDCl$_3$) δ 71.19, 31.18, 30.69, 28.89, 25.80, 19.28, 19.19. MS (ESI, *m/z*): [M+1]$^+$ C$_{15}$H$_{16}$NO$_2$S calculated 186.04056, found 186.0409

1-isothiocyanato-4-(prop-2-yn-1-ylsulfinyl)butane (156)
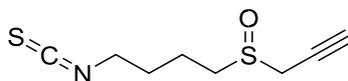
The compound was synthesised according to general procedure E, using (4isothiocyanatobutyl)(prop-2-yn-1-yl)sulfane (**155**) (0.200 g, 1.08 mmol), using 65% mCPBA (0.191 g, 1.08 mmol). After adding a 5% aqueous NaHCO$_3$ solution (20 mL), to neutralize the resulting meta-chlorobenzoic acid, the aqueous phase was extracted with 3x20 mL DCM. The combined organic layers were washed with water (3x50) ml, dried (MgSO$_4$) and the solvent was removed under vacuum. ^{1}H NMR (600 MHz, CDCl$_3$) δ 3.67 (t, *J* = 5.2 Hz, 2H), 3.31 – 3.26 (m, 2H), 2.77 (t, *J* = 6.8 Hz, 2H), 2.28 (dd, *J* = 5.5, 2.9 Hz, 1H), 1.88 – 1.69 (m, 4H). MS (ESI, *m/z*): [M+1]$^+$ C$_8$H$_{12}$NOS$_2$ calculated 202.03548, found 202.0357

Imidazole-1-sulfonyl azide hydrosulphate (160)
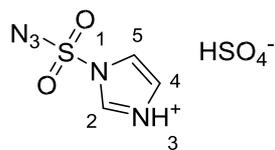
Based on (Potter et al. 2016), sodium azide (1.300 g, 20.00 mmol) was suspended in acetonitrile (50 mL), then the sulfuryl chloride (2.782 g, 20.00 mmol) was added dropwise at 0-5 ℃. The mixture was allowed to warm up, stirring overnight at room temperature. Imidazole (2.750 g, 40.00 mmol) was added in portions (5x0.550 g) at 0-5 ℃ and the resulting slurry was stirred for 3h at room temperature. The mixture was diluted with ethyl acetate (100 mL), washed with water, (3x100 mL) then saturated sodium bicarbonate (3x100 mL), dried over magnesium sulfate and filtered. A solution of sulfuric acid (2.063 g, 20.00 mmol) in ethyl acetate (50 mL) was added slowly at 0 ℃, and the mixture was allowed to warm up to room temperature stirring for 1h. The precipitate was filtered, washed, and dried to obtain the pure imidazole-1-sulfonyl azide hydrosulphate as clear white crystals (88% yield), which was stored at -20 ℃ and used for azidation reactions. ^{1}H NMR (300 MHz, D$_2$O) δ 13.28 – 13.24 (m, 1H HSO$_4$$^-$), 9.25 – 9.21 (m, 1H CH), 8.01 (dd, J = 2.1, 1.6 Hz, 1H - CH), 7.60 (dd, J = 2.1, 1.2 Hz, 1H - CH). Compared with lit. ^{1}H NMR (DMSO-d6, 400 MHz) δ14.29 (s, br, NH$^+$), 13.11 (s,HSO4$^-$), 9.08 (s, CH), 8.08 (t, J= 1.7 Hz, CH), 7.52 (dd, J= 1.7, 0.8Hz, CH) (Potter et al. 2016).

Benzyl azide (162)
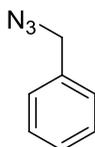
Benzylamine **161** (0.080 g, 0.74 mmol), imidazole-sulfonyl azide hydrosulphate **160** (0.240 g, 0.89 mmol), copper sulfate (0.002 g, 0.001 mmol) and potassium carbonate (0.224 g. 1.62 mmol) are suspended in methanol (10 mL). After the reaction is finished, the mixture is

concentrated, diluted with water (20 mL), acidified with HCl and extracted with ethyl acetate (3x20 mL). The combined organic fractions are dried with magnesium sulfate, filtered and the solvent is removed under vacuum. ^{1}H NMR (600 MHz, CDCl$_3$) δ 7.41 (t, J = 7.2 Hz, 2H – arom), 7.39 – 7.32 (m, 3H – arom), 4.37 (s, 2H – CH$_2$). ^{13}C NMR (151 MHz, CDCl$_3$) δ 135.37, 128.83, 128.31, 128.21, 54.82. Compared with lit. ^{1}H NMR (400 MHz, CDCl$_3$) δ 7.43–7.30 (m, 5H), 4.35 (s, 2H). ^{13}C NMR (101 MHz, Chloroform–d) δ 135.5, 129.0, 128.5, 128.4, 55.0 (Rabet et al. 2016).

Benzyl propargyl amine (168)
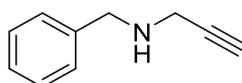
The propargyl bromide solution (0.595 mL, 0.472 g, 4.00 mmol) was added to a solution of benzylamine (2.599 g, 24.01 mmol) in toluene (50 mL) and stirred at rt. Solvent was removed under vacuum, then the product was purified using flash chromatography. ^{1}H NMR (600 MHz, CDCl$_3$) δ 7.43 – 7.23 (m, 5H – arom.), 3.91 (s, 2H – CH$_2$), 3.50 – 3.40 (d, J = 1.8 Hz, 2H – CH$_2$), 2.28 (dd, J = 2.4, 1.9 Hz, 1H CH), 1.56 (s, 1H NH). Compared with lit. ^{1}H NMR (400 MHz, CDCl$_3$): δ = 1.71 (s, 1H, NH); 2.29 (d, $^3J_{HH}$ = 1.6 Hz, 1H, CH); 3.46 (s, 2H, CH$_2$); 3.92 (s, 2H, CH$_2$); 7.28-7.39 (m, 5H, Ar-H) ppm (Gao et al. 2012).

Benzyl[(1-benzyl-1H-1,2,3-triazol-4-yl)methyl]amine (169)
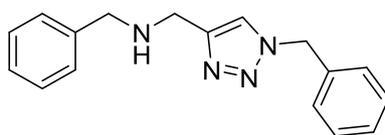
Benzylamine **161** (0.034 g, 0.31 mmol), CuSO$_4$ (0.001 g, 0.01 mmol), and NaHCO$_3$ (0.026g, 0.31 mmol) were suspended in methanol (5 mL), then a methanol (10 mL) solution of imidazolium sulfonyl azide hydrosulphate **160** (0.084 g, 0.31 mmol) was added and the mixture was stirred at rt until complete consumption of the amine. Benzyl propargyl amine (**168**) (0.045 g, 0.31 mmol), TBTA (0.008 g, 0.02 mmol) and sodium ascorbate (0.006 g, 0.03 mmol) were added and the mixture was microwaved at 80 ºC for 30 minutes. Water (15 mL) was added and the product was extracted using ethyl acetate (3x20 mL). The combined organic fractions were dried with magnesium sulfate, filtered and the solvent was removed under vacuum. ^{1}H NMR (600 MHz, CDCl$_3$) δ 7.48 − 7.16 (m, 10H), 5.52 (dd, J = 19.0, 12.1 Hz, 1H), 4.36 (s, 1H), 3.97 − 3.81 (m, 2H), 3.60 (s, 1H), 3.33 (d, J = 2.4 Hz, 1H), 2.34 − 2.27 (m, 1H). MS (ESI, m/z): [M+1]$^+$ C$_{17}$H$_{19}$N$_4$ calculated 279.16042, found 279.16126.

4-(N-phthalimido)-aminobutyl triphenyl phosphonium bromide (164)
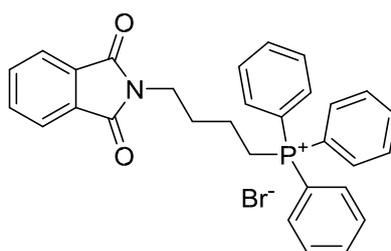
The 2-(4-bromobutyl)isoindoline-1,3-dione (**66**) (1.200 g, 4.17 mmol) and triphenylphosphine (1.104 g, 4.17 mmol) were suspended in acetonitrile (15 mL) and microwaved at 200 ºC for 3x10 minutes until reaction was complete, then solvent was removed under vacuum. The compound was obtained in 98% yield. ^{1}H NMR (600 MHz, CDCl$_3$) δ 7.89 − 7.81 (m, 6H), 7.80 − 7.65 (m, 13H), 4.01 − 3.92 (m, 2H), 3.78 (t, J = 6.4 Hz, 2H), 2.18 − 2.10 (m, 2H), 1.69 − 1.60

(m, 2H). ^{31}P-NMR (243 MHz, CDCl$_3$) δ 24.75 (bs) Compared with lit. 1H NMR (400 MHz; CDCl3): δ 7.92−7.81 (m, 6H), 7.78−7.61 (m, 13H) (PPh3 and 4 × ArH), 4.16−3.99 (m, 2H, PCH2), 3.76 (t, J = 6.5 Hz, 2H, NCH2), 2.16 (p, J = 7.0 Hz, 2H), 1.66−1.53 (m, 2H) (NCH2CH2CH2) (Gaiser et al. 2019).

4-aminobutyl triphenyl phosphonium bromide (165)
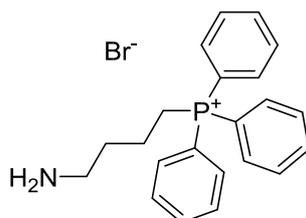
The compound was obtained according to general procedure C2 from 4-(N-phthalimido)aminobutyl triphenyl phosphonium bromide (**164**) (2.270 g, 4.09 mmol), using 50% hydrazine hydrate (1.048 g, 16.34 mmol) and methylamine (0.385 g, 4.09 mmol). Concentrated HCl was added and the mixture was microwaved again. Water was added and the precipitate was filtered off. The filtrate was evaporated under vacuum. ^{1}H NMR (600 MHz, D$_2$O) δ 7.93 – 7.88 (m, 3H), 7.83 – 7.71 (m, 12H), 3.40 (ddd, J = 13.6, 9.9, 6.7 Hz, 2H), 3.03 – 2.98 (m, 2H), 1.96 – 1.88 (m, 2H), 1.85 – 1.77 (m, 2H). ^{31}P-NMR (243 MHz, CDCl$_3$) δ 25.51 (bs)

(4-(4-((((4-isothiocyanatobutyl)sulfinyl)methyl)-1H-1,2,3-triazol-1yl)butyl)triphenylphosphonium bromide – TPP$^+$ sulforaphane probe (167)
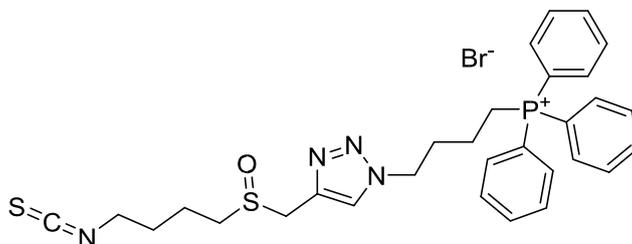
Procedure 1

165, copper sulfate, and NaHCO$_3$ were suspended in methanol, then a methanol solution of imidazole sulfonyl azide was added and the mixture was stirred at rt until complete consumption of amine. **156**, TBTA and sodium ascorbate were added and the mixture was microwaved at 80 °C for 30 minutes. Water was added and the product is extracted using ethyl acetate. The combined organic fractions were dried with magnesium sulfate, filtered and the solvent was removed under vacuum.

Procedure 2

Sodium azide was dissolved in water (20 mL), then an equal volume of DCM was added, followed by triflic anhydride at 0 °C. After stirring for 2h at 0 °C, the aqueous phase was extracted with DCM. The combined organic phases were extracted with NaHCO$_3$. **165**, copper sulfate, and NaHCO$_3$ were suspended in water, then the DCM solution of triflic azide was added, followed by methanol to create a homogeneous mixture, which was stirred at rt until complete consumption of amine. **156**, TBTA and sodium ascorbate were added and the mixture was microwaved at 80 °C for 30 minutes. Water was added and the product was extracted using ethyl acetate. The combined organic fractions were dried with magnesium sulfate, filtered and the solvent was removed under vacuum. MS (ESI, *m/z*): [M]$^+$ C$_{30}$H$_{34}$N$_4$OS$_2$P calculated 561.190616, found 561.1906.

5.8. Biological methods

Cell culture:

THP-1 cells were cultured in RPMI 1640 media supplemented with 2 mM glutamine, 10% foetal bovine serum and 1% penicillin/streptomycin [100units/100□g per mL, respectively], and maintained at 37 °C in a humidified atmosphere with 5% CO$_2$.

F-ITC treatment:

The cells were collected and spun at 300g for 5 minutes to form a pellet, which was then dispersed in fresh RPMI media. Cells were plated in 96-well plates at a density of 5×10^5 cells/mL in the presence of 1 µM, 2.5 µM, 5 µM, 10 µM, 20 µM, 40 µM or 80 µM isothiocyanate solutions (subsequent experiments focused only on a low dose of 10 µM and a high dose of 40 µM), or vehicle (DMSO), or PBS, and cultured overnight as above. Each dose was applied in triplicate and used in the subsequent experiments.

Mitochondrial depolarisation

To assess apoptosis-related mitochondrial depolarisation, 45 µL cells were taken from culture after 24 h incubation with the isothiocyanate solutions and stained using mitochondrial dye JC1 at a final concentration of 2 µM. Treated cells were incubated for 30 minutes at 37 ℃ with JC-1, followed by flow cytometric analysis of the JC-1 monomer and polymer formation using a BD Accuri C6 flow cytometer.

MitoTracker Green staining

MitoTracker Green (MTG) is a mitochondrial dye that localises in the mitochondria regardless of the mitochondrial membrane potential. 45 µL cells were taken from culture after 24 h incubation with the isothiocyanate solutions and stained using MTG at a final concentration of 200 nM. Treated cells were incubated for 1 h at 37 ℃, followed by flow cytometric analysis.

Flow Cytometry

Flow cytometry data were acquired on a BD Accuri C6 flow cytometer with the FL-1 channel based on 488 nm excitation and 533/30nm band pass emission detection while FL-2 was based on 488 nm excitation and 585/20nm band pass emission detection. Analysis was attained using the BD Accuri® software version 1.0.264.21 and Flowing Software version 2.5.1. The stained

cells were homogenized by pipetting up and down, transferred into 1 mL Eppendorf tubes and acquired at 66 µL/min. A custom gate defined as "Cells" was created in the SSC-A vs FSC-A dot plot, excluding the low granularity/low size debris, and acquisition was performed with limits of 5000 events in "Cells" or 30 µL. Using untreated cells as control, a second custom gate was created to delimitate the population of normal presenting cells ("Normal"). For JC-1 experiments, stained untreated cells were used to create a custom gate in the FL1-A vs FL2-A dot plot surrounding the compact group containing the majority of cells and defined as "Non-apoptotic".

Calibration of the flow cytometer was certified by routine 6 and 8 peak bead analysis as per manufacturer's instructions.

BIBLIOGRAPHY

Ahn, Y.-H., Hwang, Y., Liu, H., Wang, X. J., Zhang, Y., Stephenson, K. K., Boronina, T. N., Cole, R. N., Dinkova-Kostova, A. T., Talalay, P., & Cole, P. A. (2010). Electrophilic tuning of the chemoprotective natural product sulforaphane. *Proceedings of the National Academy of Sciences*, *107*(21), 9590–9595. https://doi.org/10.1073/pnas.1004104107

Akiyama, H., Barger, S., Barnum, S., Bradt, B., Bauer, J., Cole, G. M., Cooper, N. R., Eikelenboom, P., Emmerling, M., Fiebich, B. L., Finch, C. E., Frautschy, S., Griffin, W. S. T., Hampel, H., Hull, M., Landreth, G., Lue, L. F., Mrak, R., MacKenzie, I. R., … Wyss-Coray, T. (2000). Inflammation and Alzheimer's disease. In *Neurobiology of Aging* (Vol. 21, Issue 3, pp. 383–421). Elsevier Inc. https://doi.org/10.1016/S0197-4580(00)00124-X

Ames, B. N. (1983). Dietary carcinogens and anticarcinogens oxygen radicals and degenerative diseases. *Science*, *221*(4617), 1256–1264. https://doi.org/10.1126/science.6351251

Baena, R., & Salinas, P. (2015). Diet and colorectal cancer. In *Maturitas* (Vol. 80, Issue 3, pp. 258–264). Elsevier Ireland Ltd. https://doi.org/10.1016/j.maturitas.2014.12.017

Baier, S. R., Zbasnik, R., Schlegel, V., & Zempleni, J. (2014). Off-target effects of sulforaphane include the derepression of long terminal repeats through histone acetylation events. *Journal of Nutritional Biochemistry*, *25*(6), 665–668. https://doi.org/10.1016/j.jnutbio.2014.02.007

Beckmann, H. S. G., & Wittmann, V. (2007). One-pot procedure for diazo transfer and azidealkyne cycloaddition: Triazole linkages from amines. *Organic Letters*, *9*(1), 1–4. https://doi.org/10.1021/ol0621506

Bernard, W. S., & Christopher, P. W. (2020). World cancer report 2020. In *World Health Organization*. http://publications.iarc.fr/Non-Series-Publications/World-Cancer-Reports/World-Cancer-Report-2014

Bertl, E., Bartsch, H., & Gerhäuser, C. (2006). Inhibition of angiogenesis and endothelial cell functions are novel sulforaphane-mediated mechanisms in chemoprevention. *Molecular Cancer Therapeutics*, *5*(3), 575–585. https://doi.org/10.1158/1535-7163.mct-05-0324

Bhatnagar, P., Wickramasinghe, K., Wilkins, E., & Townsend, N. (2016). Trends in the epidemiology of cardiovascular disease in the UK. In *Heart* (Vol. 102, Issue 24, pp. 1945–1952). BMJ Publishing Group. https://doi.org/10.1136/heartjnl-2016-309573

Biasutto, Lucia, Andrea Mattarei, Ester Marotta, Alice Bradaschia, Nicola Sassi, Spiridione Garbisa, Mario Zoratti, and Cristina Paradisi. 2008. "Development of Mitochondria-Targeted Derivatives of Resveratrol." *Bioorganic & Medicinal Chemistry Letters* 18 (20): 5594–97. https://doi.org/https://doi.org/10.1016/j.bmcl.2008.08.100.

Black, P. H., & Garbutt, L. D. (2002). Stress, inflammation and cardiovascular disease. In *Journal of Psychosomatic Research* (Vol. 52, Issue 1, pp. 1–23). https://doi.org/10.1016/S0022-3999(01)00302-6

Brandon, M., Baldi, P., & Wallace, D. C. (2006). Mitochondrial mutations in cancer. In *Oncogene* (Vol. 25, Issue 34, pp. 4647–4662). Nature Publishing Group. https://doi.org/10.1038/sj.onc.1209607

Carmeliet, P., & Jain, R. K. (2000). Angiogenesis in cancer and other diseases. In *Nature* (Vol. 407, Issue 6801, pp. 249–257). Nature Publishing Group. https://doi.org/10.1038/35025220

Castro, C. I., & Briceno, J. C. (2010). Perfluorocarbon-Based Oxygen Carriers: Review of Products and Trials. *Artificial Organs*, *34*(8), no-no. https://doi.org/10.1111/j.1525-1594.2009.00944.x

Cavell, B. E., Syed Alwi, S. S., Donlevy, A., & Packham, G. (2011). Anti-angiogenic effects of dietary isothiocyanates: Mechanisms of action and implications for human health. In *Biochemical Pharmacology* (Vol. 81, Issue 3, pp. 327–336). Elsevier Inc. https://doi.org/10.1016/j.bcp.2010.10.005

Charpentier, J., Früh, N., & Togni, A. (2015). Electrophilic trifluoromethylation by use of hypervalent iodine reagents. In *Chemical Reviews* (Vol. 115, Issue 2, pp. 650–682). American Chemical Society. https://doi.org/10.1021/cr500223h

Chen, H., Landen, C. N., Li, Y., Alvarez, R. D., & Tollefsbol, T. O. (2013). Epigallocatechin gallate and sulforaphane combination treatment induce apoptosis in paclitaxel-resistant ovarian cancer cells through hTERT and Bcl-2 down-regulation. *Experimental Cell Research*. https://doi.org/10.1016/j.yexcr.2012.12.026

Chiao, J. W., Chung, F. L., Kancherla, R., Ahmed, T., Mittelman, A., & Conaway, C. C. (2002). Sulforaphane and its metabolite mediate growth arrest and apoptosis in human prostate cancer cells. *International Journal of Oncology*, *20*(3), 631–636. https://doi.org/10.3892/ijo.20.3.631

Chicco, A. J., & Sparagna, G. C. (2007). Role of cardiolipin alterations in mitochondrial dysfunction and disease. In *American Journal of Physiology - Cell Physiology* (Vol. 292, Issue 1, pp. 33–44). American Physiological Society. https://doi.org/10.1152/ajpcell.00243.2006

Chou, T. C. (2010). Drug combination studies and their synergy quantification using the chou-talalay method. In *Cancer Research* (Vol. 70, Issue 2, pp. 440–446). American Association for Cancer Research. https://doi.org/10.1158/0008-5472.CAN-09-1947

Clarke, J. D., Dashwood, R. H., & Ho, E. (2008). Multi-targeted prevention of cancer by sulforaphane. In *Cancer Letters* (Vol. 269, Issue 2, pp. 291–304). https://doi.org/10.1016/j.canlet.2008.04.018

Clarke, J. D., Hsu, A., Williams, D. E., Dashwood, R. H., Stevens, J. F., Yamamoto, M., & Ho, E. (2011). Metabolism and tissue distribution of sulforaphane in Nrf2 knockout and wild-type mice. *Pharmaceutical Research*, *28*(12), 3171–3179. https://doi.org/10.1007/s11095-011-0500-z

Clarke, J. D., Hsu, A., Yu, Z., Dashwood, R. H., & Ho, E. (2011). Differential effects of sulforaphane on histone deacetylases, cell cycle arrest and apoptosis in normal prostate cells versus hyperplastic and cancerous prostate cells. *Molecular Nutrition & Food Research*, *55*(7), 999–1009. https://doi.org/10.1002/mnfr.201000547

Clulow, J. A., Storck, E. M., Lanyon-Hogg, T., Kalesh, K. A., Jones, L. H., & Tate, E. W. (2017a). Competition-based, quantitative chemical proteomics in breast cancer cells identifies new target profiles for sulforaphane. *Chemical Communications*, *53*(37), 5182–5185. https://doi.org/10.1039/c6cc08797c

Clulow, J. A., Storck, E. M., Lanyon-Hogg, T., Kalesh, K. A., Jones, L., & Tate, E. W. (2017b). *Competition-based, quantitative chemical proteomics in breast cancer cells identifies new target profiles for sulforaphane Electronic Supplementary Material (ESI) for*.

Cobb, S. L., & Murphy, C. D. (2009). 19F NMR applications in chemical biology. In *Journal of Fluorine Chemistry* (Vol. 130, Issue 2, pp. 132–143). https://doi.org/10.1016/j.jfluchem.2008.11.003

Cohen, S. S., Flaks, J. G., Barner, H. D., Loeb, M. R., & Lichtenstein, J. (1958). THE MODE

OF ACTION OF 5-FLUOROURACIL AND ITS DERIVATIVES. *Proceedings of the*

National Academy of Sciences, *44*(10), 1004–1012.

https://doi.org/10.1073/pnas.44.10.1004

Dalvit, C., & Vulpetti, A. (2019). Ligand-Based Fluorine NMR Screening: Principles and
Applications in Drug Discovery Projects. In *Journal of Medicinal Chemistry* (Vol. 62,

Issue 5, pp. 2218–2244). American Chemical Society.

https://doi.org/10.1021/acs.jmedchem.8b01210

Du, G.-J., Zhang, Z., Wen, X.-D., Yu, C., Calway, T., Yuan, C.-S., & Wang, C.-Z. (2012).

Epigallocatechin Gallate (EGCG) Is the Most Effective Cancer Chemopreventive

Polyphenol in Green Tea. *Nutrients*, *4*(11), 1679–1691.

https://doi.org/10.3390/nu4111679

Fahey, J. W., Haristoy, X., Dolan, P. M., Kensler, T. W., Scholtus, I., Stephenson, K. K.,

Talalay, P., & Lozniewski, A. (2002). Sulforaphane inhibits extracellular, intracellular,

and antibiotic-resistant strains of Helicobacter pylori and prevents

benzo[a]pyreneinduced stomach tumors. *Proceedings of the National Academy of*

Sciences of the

United States of America, *99*(11), 7610–7615. https://doi.org/10.1073/pnas.112203099

Fahey, J. W., Zhang, Y., & Talalay, P. (1997). Broccoli sprouts: An exceptionally rich source

of inducers of enzymes that protect against chemical carcinogens. *Proceedings of the*

National Academy of Sciences of the United States of America, *94*(19), 10367–10372.

https://doi.org/10.1073/pnas.94.19.10367

Farinetti, A., Zurlo, V., Manenti, A., Coppi, F., & Mattioli, A. V. (2017). Mediterranean diet

and colorectal cancer: A systematic review. In *Nutrition* (Vols. 43–44, pp. 83–88).

Elsevier Inc. https://doi.org/10.1016/j.nut.2017.06.008

Finichiu, Peter G, David S Larsen, Cameron Evans, Lesley Larsen, Thomas P Bright, Ellen L
Robb, Jan Trnka, et al. 2015. "A Mitochondria-Targeted Derivative of Ascorbate: MitoC."
Free Radical Biology & Medicine 89 (December): 668–78.
https://doi.org/10.1016/j.freeradbiomed.2015.07.160.

Gaiser, Birgit I, Mia Danielsen, Emil Marcher-Rørsted, Kira Røpke Jørgensen, Tomasz M
Wróbelwróbel, Mikael Frykman, Henrik Johansson, et al. 2019. "Probing the Existence
of a Metastable Binding Site at the B2-Adrenergic Receptor with Homobivalent Bitopic
Ligands." *Journal of Medicinal Chemistry* 62 (17): 7806–39.
https://doi.org/10.1021/acs.jmedchem.9b00595.

Gamet-Payrastre, L. (2006). Signaling Pathways and Intracellular Targets of Sulforaphane
Mediating Cell Cycle Arrest and Apoptosis. *Current Cancer Drug Targets*, *6*(2), 135–
145. https://doi.org/10.2174/156800906776056509

Gamet-Payrastre, Laurence, Li, P., Lumeau, S., Cassar, G., Dupont, M. A., Chevolleau, S.,
Gasc, N., Tulliez, J., & Tercé, F. (2000). Sulforaphane, a naturally occurring
isothiocyanate, induces cell cycle arrest and apoptosis in HT29 human colon cancer
cells. *Cancer Research*, *60*(5), 1426–1433.
http://cancerres.aacrjournals.org/cgi/content/full/60/5/1426

Gao, Jian, Qing-Wen Song, Liang-Nian He, Chang Liu, Zhen-Zhen Yang, Xu Han, Xue-Dong
Li, and Qing-Chuan Song. 2012. "Preparation of Polystyrene-Supported Lewis Acidic
Fe(III) Ionic Liquid and Its Application in Catalytic Conversion of Carbon Dioxide."
Tetrahedron 68 (20): 3835–42. https://doi.org/https://doi.org/10.1016/j.tet.2012.03.048.

Gasper, A. V., Al-Janobi, A., Smith, J. A., Bacon, J. R., Fortun, P., Atherton, C., Taylor, M.

A., Hawkey, C. J., Barrett, D. A., & Mithen, R. F. (2005). Glutathione S-transferase M1 polymorphism and metabolism of sulforaphane from standard and high-glucosinolate broccoli. *American Journal of Clinical Nutrition*, *82*(6), 1283–1291. https://doi.org/10.1093/ajcn/82.6.1283

Gee, C. T., Arntson, K. E., Urick, A. K., Mishra, N. K., Hawk, L. M. L., Wisniewski, A. J., & Pomerantz, W. C. K. (2016). Protein-observed 19F-NMR for fragment screening, affinity quantification and druggability assessment. *Nature Protocols*, *11*(8), 1414–1427. https://doi.org/10.1038/nprot.2016.079

Gillis, E. P., Eastman, K. J., Hill, M. D., Donnelly, D. J., & Meanwell, N. A. (2015). Applications of Fluorine in Medicinal Chemistry. *Journal of Medicinal Chemistry*, *58*(21), 8315–8359. https://doi.org/10.1021/acs.jmedchem.5b00258

Gilmore, T. D. (2006). Introduction to NF-κB: Players, pathways, perspectives. In *Oncogene* (Vol. 25, Issue 51, pp. 6680–6684). https://doi.org/10.1038/sj.onc.1209954

Goddard-Borger, E. D., & Stick, R. V. (2007). An efficient, inexpensive, and shelf-stable diazotransfer reagent: Imidazole-1-sulfonyl azide hydrochloride. *Organic Letters*, *9*(19), 3797–3800. https://doi.org/10.1021/ol701581g

Golia, E., Limongelli, G., Natale, F., Fimiani, F., Maddaloni, V., Pariggiano, I., Bianchi, R., Crisci, M., D'Acierno, L., Giordano, R., Di Palma, G., Conte, M., Golino, P., Russo, M. G., Calabrò, R., & Calabrò, P. (2014). Inflammation and cardiovascular disease: From pathogenesis to therapeutic target. In *Current Atherosclerosis Reports* (Vol. 16, Issue 9). Current Medicine Group LLC 1. https://doi.org/10.1007/s11883-014-0435-z

Gräff, J., & Tsai, L. H. (2013). Histone acetylation: Molecular mnemonics on the chromatin. In *Nature Reviews Neuroscience* (Vol. 14, Issue 2, pp. 97–111). Nature Publishing

Group. https://doi.org/10.1038/nrn3427

Greaney, A. J., Maier, N. K., Leppla, S. H., & Moayeri, M. (2016). Sulforaphane inhibits multiple inflammasomes through an Nrf2-independent mechanism. *Journal of Leukocyte Biology*, *99*(1), 189–199. https://doi.org/10.1189/jlb.3a0415-155rr

Grunstein, M. (1997). Histone acetylation in chromatin structure and transcription. In *Nature* (Vol. 389, Issue 6649, pp. 349–352). Nature Publishing Group. https://doi.org/10.1038/38664

Han, Min, Mohammad Reza Vakili, Hoda Soleymani Abyaneh, Ommoleila Molavi, Raymond Lai, and Afsaneh Lavasanifar. 2014. "Mitochondrial Delivery of Doxorubicin via Triphenylphosphine Modification for Overcoming Drug Resistance in MDA-MB-435/DOX Cells." https://doi.org/10.1021/mp500038g.

Hanahan, D., & Weinberg, R. A. (2011). Hallmarks of cancer: The next generation. In *Cell* (Vol. 144, Issue 5, pp. 646–674). Cell Press. https://doi.org/10.1016/j.cell.2011.02.013

Heiss, E., Herhaus, C., Klimo, K., Bartsch, H., & Gerhäuser, C. (2001). Nuclear Factor κB Is a Molecular Target for Sulforaphane-mediated Anti-inflammatory Mechanisms. *Journal of Biological Chemistry*, *276*(34), 32008–32015. https://doi.org/10.1074/jbc.M104794200

Holmes, C. (2013). Review: Systemic inflammation and Alzheimer's disease. In *Neuropathology and Applied Neurobiology* (Vol. 39, Issue 1, pp. 51–68). Neuropathol Appl Neurobiol. https://doi.org/10.1111/j.1365-2990.2012.01307.x

Hoogewijs, Kurt, Andrew M. James, Robin A.J. Smith, Michael J. Gait, Michael P. Murphy, and Robert N. Lightowlers. 2016. "Assessing the Delivery of Molecules to the

Mitochondrial Matrix Using Click Chemistry." ChemBioChem, July, 1312–16. https://doi.org/10.1002/CBIC.201600188.

Hotchkiss, R. S., & Nicholson, D. W. (2006). Apoptosis and caspases regulate death and inflammation in sepsis. In *Nature Reviews Immunology* (Vol. 6, Issue 11, pp. 813–822). https://doi.org/10.1038/nri1943

Houtkooper, R. H., & Vaz, F. M. (2008). Cardiolipin, the heart of mitochondrial metabolism. In *Cellular and Molecular Life Sciences* (Vol. 65, Issue 16, pp. 2493–2506). Springer. https://doi.org/10.1007/s00018-008-8030-5

Hu, C., Eggler, A. L., Mesecar, A. D., & Van Breemen, R. B. (2011). Modification of Keap1 cysteine residues by sulforaphane. *Chemical Research in Toxicology*, *24*(4), 515–521. https://doi.org/10.1021/tx100389r

Hu, K., Qi, Y. J., Zhao, J., Jiang, H. F., Chen, X., & Ren, J. (2013). Synthesis and biological evaluation of sulforaphane derivatives as potential antitumor agents. *European Journal of Medicinal Chemistry*, *64*, 529–539. https://doi.org/10.1016/j.ejmech.2013.03.045

Huisgen, R. (1963). 1.3-Dipolare Cycloadditionen Rückschau und Ausblick. *Angewandte Chemie*, *75*(13), 604–637. https://doi.org/10.1002/ange.19630751304

Huisgen, R., Szeimies, G., & Möbius, L. (1967). 1.3-Dipolare Cycloadditionen, XXXII. Kinetik der Additionen organischer Azide an CC-Mehrfachbindungen. *Chemische Berichte*, *100*(8), 2494–2507. https://doi.org/10.1002/cber.19671000806

Hung, C.-N., Huang, H.-P., Wang, C.-J., Liu, K.-L., & Lii, C.-K. (2014). Sulforaphane Inhibits TNF-α-Induced Adhesion Molecule Expression Through the Rho A/ROCK/NFκB Signaling Pathway. *Journal of Medicinal Food*, *17*(10), 1095–1102. https://doi.org/10.1089/jmf.2013.2901

Jelley, Edwin E. 1936. "Spectral Absorption and Fluorescence of Dyes in the Molecular State."
Nature 138 (3502): 1009–10. https://doi.org/10.1038/1381009a0.

Jewett, J. C., & Bertozzi, C. R. (2010). Cu-free click cycloaddition reactions in chemical
biology. In *Chemical Society Reviews* (Vol. 39, Issue 4, pp. 1272–1279).
https://doi.org/10.1039/b901970g

Jiang, H., Shang, X., Wu, H., Huang, G., Wang, Y., Al-Holou, S., Gautam, S. C., & Chopp,
M. (2010). Combination treatment with resveratrol and sulforaphane induces apoptosis
in human U251 Glioma cells. *Neurochemical Research*, *35*(1), 152–161.
https://doi.org/10.1007/s11064-009-0040-7

Johnson, D. G., & Walker, C. L. (1999). CYCLINS AND CELL CYCLE CHECKPOINTS.
Annual Review of Pharmacology and Toxicology, *39*(1), 295–312.
https://doi.org/10.1146/annurev.pharmtox.39.1.295

Juge, N., Mithen, R. F., & Traka, M. (2007). Molecular basis for chemoprevention by
sulforaphane: A comprehensive review. In *Cellular and Molecular Life Sciences* (Vol.
64, Issue 9, pp. 1105–1127). https://doi.org/10.1007/s00018-007-6484-5

Kallifatidis, G., Labsch, S., Rausch, V., Mattern, J., Gladkich, J., Moldenhauer, G., Büchler,
M. W., Salnikov, A. V., & Herr, I. (2011). Sulforaphane increases drug-mediated
cytotoxicity toward cancer stem-like cells of pancreas and prostate. *Molecular Therapy*,
19(1), 188–195. https://doi.org/10.1038/mt.2010.216

Kamal, M. M., Akter, S., Lin, C. N., & Nazzal, S. (2020). Sulforaphane as an anticancer
molecule: mechanisms of action, synergistic effects, enhancement of drug safety, and
delivery systems. In *Archives of Pharmacal Research* (Vol. 43, Issue 4, pp. 371–384).
Pharmaceutical Society of Korea. https://doi.org/10.1007/s12272-020-01225-2

Kang, Byoung Heon, Markus D Siegelin, Janet Plescia, Christopher M Raskett, David S Garlick, Takehiko Dohi, Jane B Lian, Gary S Stein, Lucia R Languino, and Dario C Altieri. 2010. "Preclinical Characterization of Mitochondria-Targeted Small Molecule Hsp90 Inhibitors, Gamitrinibs, in Advanced Prostate Cancer." *Clinical Cancer Research : An Official Journal of the American Association for Cancer Research* 16 (19): 4779–88. https://doi.org/10.1158/1078-0432.CCR-10-1818.

Kassahun, K., Davis, M., Hu, P., Martin, B., & Baillie, T. (1997). Biotransformation of the naturally occurring isothiocyanate sulforaphane in the rat: Identification of phase I metabolites and glutathione conjugates. *Chemical Research in Toxicology*, *10*(11), 1228–1233. https://doi.org/10.1021/tx970080t

Kelso, Geoffrey F, Carolyn M Porteous, Carolyn V Coulter, Gillian Hughes, William K Porteous, Elizabeth C Ledgerwood, Robin A J Smith, and Michael P Murphy. 2000. "Selective Targeting of a Redox-Active Ubiquinone to Mitochondria within Cells ANTIOXIDANT AND ANTIAPOPTOTIC PROPERTIES*." https://doi.org/10.1074/jbc.M009093200.

Kensler, T. W., Egner, P. A., Agyeman, A. S., Visvanathan, K., Groopman, J. D., Chen, J. G., Chen, T. Y., Fahey, J. W., & Talalay, P. (2013). Keap1-Nrf2 signaling: A target for cancer prevention by sulforaphane. *Topics in Current Chemistry*, *329*, 163–178. https://doi.org/10.1007/128-2012-339

Kerr, J. F. R., Wyllie, A. H., & Curriet, A. R. (1972). APOPTOSIS: A BASIC BIOLOGICAL PHENOMENON WITH WIDE-RANGING IMPLICATIONS IN TISSUE KINETICS. In *Br. J. Cancer* (Vol. 26).

Keum, Y. S. (2011). Regulation of the Keap1/Nrf2 system by chemopreventive sulforaphane:

Implications of posttranslational modifications. *Annals of the New York Academy of Sciences*, *1229*(1), 184–189. https://doi.org/10.1111/j.1749-6632.2011.06092.x

Keum, Y. S., Jeong, W. S., & Tony Kong, A. N. (2004). Chemoprevention by isothiocyanates and their underlying molecular signaling mechanisms. In *Mutation Research - Fundamental and Molecular Mechanisms of Mutagenesis* (Vol. 555, Issues 1-2 SPEC. ISS., pp. 191–202). Elsevier. https://doi.org/10.1016/j.mrfmmm.2004.05.024

Kiełbasiński, P., Łuczak, J., Cierpiał, T., Błaszczyk, J., Sieroń, L., Wiktorska, K., Lubelska, K., Milczarek, M., & Chilmończyk, Z. (2014). New enantiomeric fluorine-containing derivatives of sulforaphane: Synthesis, absolute configurations and biological activity. *European Journal of Medicinal Chemistry*, *76*, 332–342. https://doi.org/10.1016/j.ejmech.2014.02.036

King, J. F., & Gill, M. S. (2002). Alkyl 2,2,2-Trifluoroethanesulfonates (Tresylates): Elimination−Addition vs Bimolecular Nucleophilic Substitution in Reactions with Nucleophiles in Aqueous Media 1 . *The Journal of Organic Chemistry*, *61*(21), 7250–7255. https://doi.org/10.1021/jo9610366

Ko, J.-H., Sethi, G., Um, J.-Y., Shanmugam, M. K., Arfuso, F., Kumar, A. P., Bishayee, A., & Ahn, K. S. (2017). The Role of Resveratrol in Cancer Therapy. *International Journal of Molecular Sciences*, *18*(12), 2589. https://doi.org/10.3390/ijms18122589

Kolb, H. C., Finn, M. G., & Sharpless, K. B. (2001). Click Chemistry: Diverse Chemical Function from a Few Good Reactions. In *Angewandte Chemie - International Edition* (Vol. 40, Issue 11, pp. 2004–2021). John Wiley & Sons, Ltd. https://doi.org/10.1002/1521-3773(20010601)40:11<2004::AID-ANIE2004>3.0.CO;2-5

Kotecha, R., Takami, A., & Espinoza, J. L. (2016). *Dietary phytochemicals and cancer chemoprevention : a review of the clinical evidence An Overview of Carcinogenesis*. *7*(32).

Kovarova, Jaromira, Martina Bajzikova, Magdalena Vondrusova, Jan Stursa, Jacob Goodwin, Maria Nguyen, Renata Zobalova, et al. 2014. "Mitochondrial Targeting of α-Tocopheryl Succinate Enhances Its Anti-Mesothelioma Efficacy." *Redox Report* 19 (1): 16–25. https://doi.org/10.1179/1351000213Y.0000000064.

Landis-piwowar, K. R., & Iyer, N. R. (2014). *Cancer Growth and Metastasis Cancer Chemoprevention : Current State of the Art*. 19–25. https://doi.org/10.4137/CGM.S11288.RECEIVED

Larsen, G. L., & Henson, P. M. (1983). Mediators of inflammation. In *Annual review of immunology* (Vol. 1, Issue 1, pp. 335–359). Annual Reviews 4139 El Camino Way, P.O. Box 10139, Palo Alto, CA 94303-0139, USA. https://doi.org/10.1146/annurev.iy.01.040183.002003

Li, Y., Zhang, T., Schwartz, S. J., & Sun, D. (2011). Sulforaphane Potentiates the Efficacy of 17-Allylamino 17-Demethoxygeldanamycin Against Pancreatic Cancer Through Enhanced Abrogation of Hsp90 Chaperone Function. *Nutrition and Cancer*, *63*(7), 1151–1159. https://doi.org/10.1080/01635581.2011.596645

Liang, H., & Yuan, Q. (2012). Natural sulforaphane as a functional chemopreventive agent: Including a review of isolation, purification and analysis methods. In *Critical Reviews in Biotechnology* (Vol. 32, Issue 3, pp. 218–234). https://doi.org/10.3109/07388551.2011.604838

Liu, X., Xu, C., Wang, M., & Liu, Q. (2015). Trifluoromethyltrimethylsilane: Nucleophilic trifluoromethylation and beyond. In *Chemical Reviews* (Vol. 115, Issue 2, pp. 683–730). American Chemical Society. https://doi.org/10.1021/cr400473a

Logan, Angela, Victoria R Pell, Karl J Shaffer, Cameron Evans, Nathan J Stanley, Ellen L Robb, Tracy A Prime, et al. 2016. "Assessing the Mitochondrial Membrane Potential in Cells and In Vivo Using Targeted Click Chemistry and Mass Spectrometry." *Cell Metabolism* 23 (2): 379–85. https://doi.org/10.1016/j.cmet.2015.11.014.

Lontchi-Yimagou, E., Sobngwi, E., Matsha, T. E., & Kengne, A. P. (2013). Diabetes mellitus and inflammation. *Current Diabetes Reports*, *13*(3), 435–444. https://doi.org/10.1007/s11892-013-0375-y

Luengo-Fernandez, R., Leal, J., Gray, A., & Sullivan, R. (2013). Economic burden of cancer across the European Union: A population-based cost analysis. *The Lancet Oncology*, *14*(12), 1165–1174. https://doi.org/10.1016/S1470-2045(13)70442-X

Martincorena, I., & Campbell, P. J. (2015). Somatic mutation in cancer and normal cells. In *Science* (Vol. 349, Issue 6255, pp. 1483–1489). American Association for the Advancement of Science. https://doi.org/10.1126/science.aab4082

Martínez, M. D., Luna, L., Tesio, A. Y., Feresin, G. E., Durán, F. J., & Burton, G. (2016). Antioxidant properties in a non-polar environment of difluoromethyl bioisosteres of methyl hydroxycinnamates. *Journal of Pharmacy and Pharmacology*, *68*(2), 233–244. https://doi.org/10.1111/jphp.12507

Matheis, Christian, Minyan Wang, Thilo Krause, and Lukas J. Goossen. 2015. "Metal-Free Trifluoromethylthiolation of Alkyl Electrophiles via a Cascade of Thiocyanation and Nucleophilic Cyanide-CF_3 Substitution." *Synlett* 26 (11): 1628–32. https://doi.org/10.1055/s-0034-1378702.

Mazarakis, N., Snibson, K., Licciardi, P. V., & Karagiannis, T. C. (2020). The potential use

of L-sulforaphane for the treatment of chronic inflammatory diseases: A review of the

clinical evidence. In *Clinical Nutrition* (Vol. 39, Issue 3, pp. 664–675). Churchill

Livingstone. https://doi.org/10.1016/j.clnu.2019.03.022

McKay, C. S., & Finn, M. G. (2014). Click chemistry in complex mixtures: Bioorthogonal

bioconjugation. In *Chemistry and Biology* (Vol. 21, Issue 9, pp. 1075–1101). Elsevier

Ltd. https://doi.org/10.1016/j.chembiol.2014.09.002

Mentella, Scaldaferri, Ricci, Gasbarrini, & Miggiano. (2019). Cancer and Mediterranean

Diet: A Review. *Nutrients*, *11*(9), 2059. https://doi.org/10.3390/nu11092059

Middleton, W. J. (1975). New Fluorinating Reagents. Dialkylaminosulfur Fluorides. *Journal

of Organic Chemistry*, *40*(5), 574–578. https://doi.org/10.1021/jo00893a007

Mishra, N. K., Urick, A. K., Ember, S. W. J., Schonbrunn, E., & Pomerantz, W. C. (2014).

Fluorinated aromatic amino acids are sensitive 19 f NMR probes for

bromodomainligand interactions. *ACS Chemical Biology*, *9*(12), 2755–2760.

https://doi.org/10.1021/cb5007344

Mitsiogianni, M., Trafalis, D. T., Franco, R., Zoumpourlis, V., Pappa, A., & Panayiotidis, M.

I. (2021). Sulforaphane and iberin are potent epigenetic modulators of histone

acetylation and methylation in malignant melanoma. *European Journal of Nutrition*,

60(1), 147–158. https://doi.org/10.1007/s00394-020-02227-y

Moon, D. O., Kim, M. O., Kang, S. H., Choi, Y. H., & Kim, G. Y. (2009). Sulforaphane

suppresses TNF-α-mediated activation of NF-κB and induces apoptosis through

activation of reactive oxygen species-dependent caspase-3. *Cancer Letters*, *274*(1), 132–

142. https://doi.org/10.1016/j.canlet.2008.09.013

Mykhailiuk, P. K., Kubyshkin, V., Bach, T., & Budisa, N. (2017). Peptidyl-Prolyl Model
Study: How Does the Electronic Effect Influence the Amide Bond Conformation?
Journal   of   Organic   Chemistry,   *82*(17),   8831–8841.
https://doi.org/10.1021/acs.joc.7b00803

Myzak, M. C., Dashwood, W. M., Orner, G. A., Ho, E., & Dashwood, R. H. (2006).
Sulforaphane inhibits histone deacetylase in vivo and suppresses tumorigenesis in Apc
min mice . *The FASEB Journal*, *20*(3), 506–508. https://doi.org/10.1096/fj.05-4785fje

Negi, G., Kumar, A., & S. Sharma, S. (2011). Nrf2 and NF-κB Modulation by
Sulforaphane Counteracts Multiple Manifestations of Diabetic Neuropathy in Rats and
High Glucose-Induced Changes. *Current Neurovascular Research*, *8*(4), 294–304.
https://doi.org/10.2174/156720211798120972

Nyffeler, P. T., Durón, S. G., Burkart, M. D., Vincent, S. P., & Wong, C. H. (2004).
Selectfluor: Mechanistic insight and applications. In *Angewandte Chemie - International
Edition* (Vol. 44, Issue 2, pp. 192–212). https://doi.org/10.1002/anie.200400648

O'Hagan, D. (2008). Understanding organofluorine chemistry. An introduction to the C-F
bond. *Chemical Society Reviews*, *37*(2), 308–319. https://doi.org/10.1039/b711844a

Otrock, Z. K., Mahfouz, R. A. R., Makarem, J. A., & Shamseddine, A. I. (2007).
Understanding the biology of angiogenesis: Review of the most important molecular
mechanisms. In *Blood Cells, Molecules, and Diseases* (Vol. 39, Issue 2, pp. 212–220).
Academic Press. https://doi.org/10.1016/j.bcmd.2007.04.001

Ouyang, L., Shi, Z., Zhao, S., Wang, F.-T., Zhou, T.-T., Liu, B., & Bao, J.-K. (2012).
Programmed cell death pathways in cancer: a review of apoptosis, autophagy and
programmed necrosis. *Cell Proliferation*, *45*(6), 487–498.
https://doi.org/10.1111/j.1365-2184.2012.00845.x

Pandey, P., Singh, A. K., Singh, M., Tewari, M., Shukla, H. S., & Gambhir, I. S. (2017). The

see-saw of Keap1-Nrf2 pathway in cancer. In *Critical Reviews in Oncology/Hematology*

(Vol. 116, pp. 89–98). Elsevier Ireland Ltd.

https://doi.org/10.1016/j.critrevonc.2017.02.006

Papa, S., Choy, P. M., & Bubici, C. (2019). The ERK and JNK pathways in the regulation of

metabolic reprogramming. In *Oncogene* (Vol. 38, Issue 13, pp. 2223–2240). Nature

Publishing Group. https://doi.org/10.1038/s41388-018-0582-8

Papeo, G., Giordano, P., Brasca, M. G., Buzzo, F., Caronni, D., Ciprandi, F., Mongelli, N.,

Veronesi, M., Vulpetti, A., & Dalvit, C. (2007). Polyfluorinated amino acids for

sensitive 19F NMR-based screening and kinetic measurements. *Journal of the American

Chemical Society*, *129*(17), 5665–5672. https://doi.org/10.1021/ja069128s

Parnaud, G., Li, P. F., Cassar, G., Rouimi, P., Tulliez, J., Combaret, L., & Gamet-Payrastre,

L. (2004). Mechanism of sulforaphane-induced cell cycle arrest and apoptosis in human

colon cancer cells. *Nutrition and Cancer*, *48*(2), 198–206.

https://doi.org/10.1207/s15327914nc4802_10

Pericleous, M., Mandair, D., & Caplin, M. E. (2013). Diet and supplements and their impact

on colorectal cancer. *Journal of Gastrointestinal Oncology*, *4*(4), 409–423.

https://doi.org/10.3978/j.issn.2078-6891.2013.003

Picard, M., Taivassalo, T., Gouspillou, G., & Hepple, R. T. (2011). Mitochondria: isolation,

structure and function. *The Journal of Physiology*, *589*(18), 4413–4421.

https://doi.org/10.1113/jphysiol.2011.212712

Poltronieri, J., Becceneri, A., Fuzer, A., Filho, J., Martin, A., Vieira, P., Pouliot, N., &

Cominetti, M. (2014). [6]-gingerol as a Cancer Chemopreventive Agent: A Review of

Its Activity on Different Steps of the Metastatic Process. *Mini-Reviews in Medicinal*

Chemistry, *14*(4), 313–321. https://doi.org/10.2174/1389557514666140219095510

Posner, G. H., Cho, C. G., Green, J. V., Zhang, Y., & Talalay, P. (1994). Design and

Synthesis of Bifunctional Isothiocyanate Analogs of Sulforaphane: Correlation between

Structure and Potency as Inducers of Anticarcinogenic Detoxication Enzymes. *Journal

of Medicinal Chemistry*, *37*(1), 170–176. https://doi.org/10.1021/jm00027a021

Potter, Garrett T, Gordon C Jayson, Gavin J Miller, and John M Gardiner. 2016. "An Updated

Synthesis of the Diazo-Transfer Reagent Imidazole-1-Sulfonyl Azide Hydrogen Sulfate."

The Journal of Organic Chemistry 81 (8): 3443–46.

https://doi.org/10.1021/acs.joc.6b00177.

Pradhan, S. J., Mishra, R., Sharma, P., & Kundu, G. C. (2010). Quercetin and sulforaphane in

combination suppress the progression of melanoma through the down-regulation of

matrix metalloproteinase-9. *Experimental and Therapeutic Medicine*, *1*(6), 915–920.

https://doi.org/10.3892/etm.2010.144

Presolski, S. I., Hong, V. P., & Finn, M. G. (2011). Copper-Catalyzed Azide-Alkyne Click

Chemistry for Bioconjugation. In *Current Protocols in Chemical Biology*. John Wiley &
Sons, Inc. https://doi.org/10.1002/9780470559277.ch110148

Psurski, M., Janczewski, Ł., Świtalska, M., Gajda, A., Goszczyński, T. M., Oleksyszyn, J.,

Wietrzyk, J., & Gajda, T. (2017). Novel phosphonate analogs of sulforaphane:

Synthesis, in vitro and in vivo anticancer activity. *European Journal of Medicinal

Chemistry*, *132*, 63–80. https://doi.org/10.1016/j.ejmech.2017.03.028

Rabet, Pauline T G, Gabriele Fumagalli, Scott Boyd, and Michael F Greaney. 2016. "Benzylic

C–H Azidation Using the Zhdankin Reagent and a Copper Photoredox Catalyst." *Organic

Letters* 18 (7): 1646–49. https://doi.org/10.1021/acs.orglett.6b00512.

Rajendran, P., Kidane, A. I., Yu, T. W., Dashwood, W. M., Bisson, W. H., Löhr, C. V., Ho, E., Williams, D. E., & Dashwood, R. H. (2013). HDAC turnover, CtIP acetylation and dysregulated DNA damage signaling in colon cancer cells treated with sulforaphane and related dietary isothiocyanates. *Epigenetics*, *8*(6). https://doi.org/10.4161/epi.24710

Rostovtsev, V. V., Green, L. G., Fokin, V. V., & Sharpless, K. B. (2002). A Stepwise Huisgen Cycloaddition Process: Copper(I)-Catalyzed Regioselective "Ligation" of Azides and Terminal Alkynes. *Angewandte Chemie*, *114*(14), 2708–2711. https://doi.org/10.1002/1521-3757(20020715)114:14<2708::AID-ANGE2708>3.0.CO;2-0

Shang, H. S., Shih, Y. L., Lee, C. H., Hsueh, S. C., Liu, J. Y., Liao, N. C., Chen, Y. L., Huang, Y. P., Lu, H. F., & Chung, J. G. (2017). Sulforaphane-induced apoptosis in human leukemia HL-60 cells through extrinsic and intrinsic signal pathways and altering associated genes expression assayed by cDNA microarray. *Environmental Toxicology*, *32*(1), 311–328. https://doi.org/10.1002/tox.22237

Shi, Y. H., Dai, D. F., Li, J., Dong, Y. W., Jiang, Y., Li, H. G., Gao, Y., Chong, C. K., Li, H. Y., Chu, X. Q., Yang, C., Zhang, Q., Tong, Z. S., Bai, C. G., & Chen, Y. (2016). Sulforaphane analogues with heterocyclic moieties: Syntheses and inhibitory activities against cancer cell lines. *Molecules*, *21*(4). https://doi.org/10.3390/molecules21040514

Su, S. (2008). *Fluorination of Organic Com pounds*.

Szeto, Hazel H, and Peter W Schiller. 2011. "Novel Therapies Targeting Inner Mitochondrial Membrane--from Discovery to Clinical Development." *Pharmaceutical Research* 28 (11): 2669–79. https://doi.org/10.1007/s11095-011-0476-8.

Taguchi, K., Motohashi, H., & Yamamoto, M. (2011). Molecular mechanisms of the Keap1Nrf2 pathway in stress response and cancer evolution. In *Genes to Cells* (Vol. 16, Issue 2, pp. 123–140). https://doi.org/10.1111/j.1365-2443.2010.01473.x

Talmadge, J. E., & Fidler, I. J. (2010). AACR centennial series: The biology of cancer metastasis: Historical perspective. In *Cancer Research* (Vol. 70, Issue 14, pp. 5649–5669). Cancer Res. https://doi.org/10.1158/0008-5472.CAN-10-1040

Tatum, N. J., Yufit, D. S., Cobb, S. L., & Coxon, C. R. (2015). Synthesis, Ni(II) Schiff base complexation and structural analysis of fluorinated analogs of the ligand (S)-2-[N-(N′benzylprolyl)amino]benzophenone (BPB). *Journal of Fluorine Chemistry*, *173*, 77–83. https://doi.org/10.1016/j.jfluchem.2015.02.007

Thangapazham, R. L., Sharma, A., & Maheshwari, R. K. (2006). Multiple molecular targets in cancer chemoprevention by curcumin. In *AAPS Journal* (Vol. 8, Issue 3, pp. E443–E449). Springer. https://doi.org/10.1208/aapsj080352

Thiehoff, C., Rey, Y. P., & Gilmour, R. (2017). The Fluorine Gauche Effect: A Brief History. In *Israel Journal of Chemistry* (Vol. 57, Issue 1, pp. 92–100). Wiley-VCH Verlag. https://doi.org/10.1002/ijch.201600038

Thirumurugan, P., Matosiuk, D., & Jozwiak, K. (2013). Click chemistry for drug development and diverse chemical-biology applications. In *Chemical Reviews* (Vol. 113, Issue 7, pp. 4905–4979). https://doi.org/10.1021/cr200409f

Townsend, B. E., & Johnson, R. W. (2016). Sulforaphane induces Nrf2 target genes and attenuates inflammatory gene expression in microglia from brain of young adult and aged mice. *Experimental Gerontology*, *73*, 42–48.

https://doi.org/10.1016/j.exger.2015.11.004

Tsao, A. S., Kim, E. S., & Hong, W. K. (2004). Chemoprevention of Cancer. *CA: A Cancer Journal for Clinicians*, *54*(3), 150–180. https://doi.org/10.3322/canjclin.54.3.150

Vanduchova, A., Anzenbacher, P., & Anzenbacherova, E. (2019). Isothiocyanate from Broccoli, Sulforaphane, and Its Properties. In *Journal of Medicinal Food* (Vol. 22, Issue 2). https://doi.org/10.1089/jmf.2018.0024

Vargas, A. J., & Thompson, P. A. (2012). Diet and nutrient factors in colorectal cancer risk. In *Nutrition in Clinical Practice* (Vol. 27, Issue 5, pp. 613–623). https://doi.org/10.1177/0884533612454885

Verhoork, S. J. M., Killoran, P. M., & Coxon, C. R. (2018). Fluorinated Prolines as Conformational Tools and Reporters for Peptide and Protein Chemistry. In *Biochemistry* (Vol. 57, Issue 43, pp. 6132–6143). American Chemical Society. https://doi.org/10.1021/acs.biochem.8b00787

Vermeulen, Martijn, Binne Zwanenburg, Gordon J.F. Chittenden, and Hans Verhagen. 2003. "Synthesis of Isothiocyanate-Derived Mercapturic Acids." *European Journal of Medicinal Chemistry* 38 (7–8): 729–37. https://doi.org/10.1016/S0223-5234(03)00141-7.

Wang, C., & Wang, C. (2017). Anti-nociceptive and anti-inflammatory actions of sulforaphane in chronic constriction injury-induced neuropathic pain mice. *Inflammopharmacology*, *25*(1), 99–106. https://doi.org/10.1007/s10787-016-0307-y

Wang, J., Sánchez-Roselló, M., Aceña, J. L., Del Pozo, C., Sorochinsky, A. E., Fustero, S., Soloshonok, V. A., & Liu, H. (2014). Fluorine in pharmaceutical industry: Fluorinecontaining drugs introduced to the market in the last decade (2001-2011). In *Chemical Reviews* (Vol. 114, Issue 4, pp. 2432–2506). https://doi.org/10.1021/cr4002879

Wang, X., Li, Y., Dai, Y., Liu, Q., Ning, S., Liu, J., Shen, Z., Zhu, D., Jiang, F., Zhang, J., & Li, Z. (2016). Sulforaphane improves chemotherapy efficacy by targeting cancer stem cell-like properties via the miR-124/IL-6R/STAT3 axis. *Scientific Reports*, *6*. https://doi.org/10.1038/srep36796

Wattenberg, L. W. (1985). Chemoprevention of Cancer. *Cancer Research*, *45*(1).

Wiberg, K. B., Murcko, M. A., Laidig, K. E., & MacDougall, P. J. (1990). Origin of the "gauche effect" in substituted ethanes and ethenes. *Journal of Physical Chemistry*, *94*(18), 6956–6959. https://doi.org/10.1021/j100381a008

Wiseman, M. J. (2018). *Nutrition and cancer: prevention and survival*. https://doi.org/10.1017/S0007114518002222

Wolfe, S. (1972). The Gauche Effect. Some Stereochemical Consequences of Adjacent Electron Pairs and Polar Bonds. *Accounts of Chemical Research*, *5*(3), 102–111. https://doi.org/10.1021/ar50051a003

Wu, S., Powers, S., Zhu, W., & Hannun, Y. A. (2016). Substantial contribution of extrinsic risk factors to cancer development. *Nature*, *529*(7584), 43–47. https://doi.org/10.1038/nature16166

Yanaka, A., Fahey, J. W., Fukumoto, A., Nakayama, M., Inoue, S., Zhang, S., Tauchi, M., Suzuki, H., Hyodo, I., & Yamamoto, M. (2009). Dietary sulforaphane-rich broccoli sprouts reduce colonization and attenuate gastritis in Helicobacter pylori-infected mice and humans. *Cancer Prevention Research*, *2*(4), 353–360. https://doi.org/10.1158/1940-6207.CAPR-08-0192

Yang, X. Z., Chang, Y., & Wei, W. (2016). Endothelial Dysfunction and Inflammation: Immunity in Rheumatoid Arthritis. In *Mediators of Inflammation* (Vol. 2016). Hindawi

Limited. https://doi.org/10.1155/2016/6813016

Yao, H., Wang, H., Zhang, Z., Jiang, B., Luo, J., & Shi, X. (2008). Sulforaphane inhibited expression of hypoxia-inducible factor-1α in human tongue squamous cancer cells and prostate cancer cells. *International Journal of Cancer*, *123*(6), 1255–1261. https://doi.org/10.1002/ijc.23647

Yearn, S. C., & Katzenellenbogen, J. A. (1993). Tetrabutylammonium fluoride-induced conversion of tresylates to mesylates. *Tetrahedron Letters*, *34*(10), 1579–1580. https://doi.org/10.1016/0040-4039(93)85011-K

Zhang, J. M., & An, J. (2007). Cytokines, inflammation, and pain. In *International Anesthesiology Clinics* (Vol. 45, Issue 2, pp. 27–37). NIH Public Access. https://doi.org/10.1097/AIA.0b013e318034194e

Zhang, Y., Talalay, P., Cho, C. G., & Posner, G. H. (1992). A major inducer of anticarcinogenic protective enzymes from broccoli: Isolation and elucidation of structure. *Proceedings of the National Academy of Sciences of the United States of America*, *89*(6), 2399–2403. https://doi.org/10.1073/pnas.89.6.2399

Zhang, Z., Atwell, L. L., Farris, P. E., Ho, E., & Shannon, J. (2016). Associations between cruciferous vegetable intake and selected biomarkers among women scheduled for breast biopsies. *Public Health Nutrition*, *19*(7), 1288–1295. https://doi.org/10.1017/S136898001500244X

Zhao, Zuoquan, Qian Yu, Tiantian Mou, Chang Liu, Wenjiang Yang, Wei Fang, Cheng Peng, Jie Lu, Yu Liu, and Xianzhong Zhang. 2014. "Highly Efficient One-Pot Labeling of New Phosphonium Cations with Fluorine-18 as Potential PET Agents for Myocardial

Perfusion Imaging." *Molecular Pharmaceutics* 11 (11): 3823–31. https://doi.org/10.1021/mp500216g.

Zielonka, J., Joseph, J., Sikora, A., Hardy, M., Ouari, O., Vasquez-Vivar, J., Cheng, G., Lopez, M., & Kalyanaraman, B. (2017). Mitochondria-Targeted Triphenylphosphonium-Based Compounds: Syntheses, Mechanisms of Action, and Therapeutic and Diagnostic Applications. In *Chemical Reviews* (Vol. 117, Issue 15, pp. 10043–10120). American Chemical Society. https://doi.org/10.1021/acs.chemrev.7b00042

APPENDIX 1

Table: Completed clinical trials involving sulforaphane (reproduced from (Mazarakis *et al.*, 2020)) – Next pages

Population Cohort	Study Design	Study Arms	Results
Healthy	Randomised n = 17 (adults)	Topical application of LSF on days 1-3; i. 0.534 and 5.34 nM ii. 10.7 and 21.4 nM iii. 42.7 and 85.4 nM iv. 170 and 340 nM v. 681 nM Skin biopsies (3 mm diameter) taken 24hrs after last treatment.	NQO1 enzyme activity increased to 1.5 and 4.5 fold after a single and triple application of 150 nmol of LSF. Non-significant adverse reactions.
Healthy	Randomised Parallel assignment n = 24 (adults)	Days 1-3 received either; i. 200 nmol/cm^2 GRR, or ii. 200 nmol/cm^2 LSF On day 4, 1 cm^2 of the treated area was exposed to monochromatic UV radiation and visible light, and erythema-induced solarstimulated UV radiation.	LSF topical application reduced skin erythema by 35%, from a mean erythema sum of 91 to 59 (p = 0.02).
Healthy	Single-group assignment n = 6 (adults)	Consumed daily for 10 days; i. 300 mL of liquefied broccoli (22 mM of LSF)	1.5hrs after ingestion LSF plasma levels peaked, for both the single dose and repeated doses of LSFe indicative of no accumulation effect.
Healthy	Randomised Parallel assignment n = 291 (adults)	Taken daily for 12wks; i. Placebo of mango juice ii. 40 mmol of LSF þ600 mmol of GRR in pineapple juice	12wks of consistent dosing of LSF improved detoxification of pollutants compared to the placebo group: benzene (+54.7%), acrolein (+21.7%), and crotonaldehyde (+2.0%) all with p = 0.01.significant difference in adverse events Non-signi amongst control and treated groups. No severe adverse events recorded.
Healthy (upper airway)	Randomised Single-blind study n = 57 (adults)	3 consecutive days subjects ingested 25, 50, 75, 100, 125, 150, 175 or 200 g of either i. BroccoSprout® (89-102 mM of LSF) ii. Placebo: alfalfa sprouts	Doses >100g of BSE/day significantly increased phase II enzymes expressed from nasal lavage fluid compared to the pretreatment baseline; ranging from 13.86 to 198.81% and 15.32-120.86% for NQO1 and HO-1, respectively. 5 subjects reported some gastrointestinal discomfort at grade I and II.
Healthy	Single group assignment n = 3	Consumed BSE (100 mM) daily for 2 weeks.	Collection of PBMCs pre- and postBSE consumption resulted in an increase in MARCO expression, and Nrf2-regulated antioxidant genes NQO1, GCLM and HO-1.

| Healthy | Randomised Crossover assignment n = 20 (adults) | There are 2 interventions, with a 2wk wash period between interventions; i. A single dose of LSF (200 mM), ii. Consume LSF (100 mM) at 0hrs and 12hrs | 12hr dosing of 100 mM of LSF retained a higher LSF plasma level than the single LSF dose (200 mM), 0.12 ± 0.02 mM and 0.04 ± 0.01 mM, $p < 0.001$, respectively. Neither antioxidant (HO-1) nor epigenetic (HDAC activity and p21) markers were affected by LSF. |

Population Cohort	Study Design	Study Arms	Results
Healthy	Phase 1 Randomised Crossover assignment n = 50 (adults)	All individuals were given 5 days of placebo prior to treatment of either; i. Placebo of mango juice ii. 150 mmol of LSF in mango juice iii. 800 mmol of GRR in mango juice Followed by 5 days of placebo (washout) and subjects were returned for 7 days of the opposite supplement.	SF_T levels were 3.58 times higher in SFN compared to GRR supplemented beverages. Two non-significant grade I adverse events were reported.
Healthy	Pilot study Crossover assignment Open label n = 10 (adults)	A 3-day wash out period between each of the 3 interventions will occur. Each intervention will be conducted daily; i. Oral ingestion of GRR-BSE (600 mM of glucoraphanin) ii. Oral ingestion of LSF-BSE (150 mM of LSF)	LSF-BSE oral ingestion had significantly higher ($p = 0.0013$) bioavailability as compared to GRRBSE intervention. Buccal scrapings indicated a 2-fold upregulation of NQO1 mRNA was observed in 2/3rds (6 of 9) of GRR-BSE, and half of the LSF-BSE (3 of 6).
Mammoplasty reduction	Pilot study Singlegroup assignment n = 8 (female, adults)	Subjects drank 20 mL of liquidised broccoli samples (200 mM of LSF)	A single dose of LSF after the breast reduction increased NQO1 and OH-1 transcripts expressed in the breasts as well as NQO1 enzymatic activity at 0.21 ± 0.01mOD/mg/min and 0.20 ± 0.01mOD/mg/min in the right and the left breast, respectively.
Healthy	Non-randomised Single group assignment n = 3 (adults)	68g BroccoSprout (592.25 mM of LSF) was consumed with cream cheese in a bagel	After consumption of BroccoSprout, HDAC activity was significantly suppressed in PBMCs at 3 and 6hrs and returned back to baseline levels at 24 and 48hrs.
Environmental carcinogens	Randomised Parallel assignment n = 200 (adults)	3 day old BSE to be consumed daily for 2wks; i. BSE boiled once to create a broth ii. Placebo: an inactive BSE broth	In comparison to the placebo group, the BSE treated group had significantly increased ($p = 0.001$) excreted dithiocarbamatese an average of 49mmol/12hrs. No problems with safety or tolerance were noted.

| Bowel habit | Randomised Parallel assignment Semiopen label n = 58 (adults) | To ingestion daily for 4wks either; i. 20g of BSE, or ii. Placebo: 20g of alfalfa sprouts | A significant reduction of duration of defecation score (0.96 ± 0.62 to 0.58 ± 0.58, $p = 0.0077$) and constipation score (7.25 ± 2.83 to 5.17 ± 3.27, $p = 0.0017$) after BSE compared to the placebo group. BSE significantly ($p = 0.0498$) decreased the amount of Bifidobacterium in the stool after 4 weeks as compared to the placebo group. |

Population Cohort	Study Design	Study Arms	Results
Healthy	Phase 1 Randomised Double-blind Placebo controlled n = 10 (adults)	5-day wash out period, followed by 7days with treatment every 8hrs; i. Glucosinolate (25 mM) ii. Glucosinolate (100 mM) iii. ITCs (25 mM) iv. Placebo	The mean cumulative excretion of dithiocarbonates of $18.7 \pm 9.4\%$ ($\pm SD$), which has a 4-fold difference amongst individuals. No severe adverse events or intolerances were recorded.
Healthy	Crossover assignment n = 12 (male, adults)	Consumed either: i. 200g of fresh broccoli, or ii. 200g of steamed broccoli	The average cumulative ITCs excreted in the urine after 24hrs was significantly greater ($p < 0.001$) in the fresh broccoli compared to the steamed broccoli, with mean values of 68.1 ± 22.6 mM and 20.6 ± 12.8, respectively. It is estimated that 7.5% and 24.9% of the glucoraphanin was converted into LSF-NAC in the urine for steamed and fresh broccoli, respectively.
Healthy	Single-group assignment n = 4 (male, adults)	Single dose of 200 mM of broccoli sprout ITCs.	ITCs peaked in the plasma at 1hr after ingestion (ranged from 0.943 to 1.748 mmol/ l, mean: 1.18 ± 0.38 mmol/l), and 8hrs in the urinary samples with a cumulative mean excretion of 117 ± 6.18 mmol ($58.3 \pm 2.8\%$ of the original dose) and a clearance rate of 41.9 ± 5.31 mmol/l.
Cancer			
Prostate cancer	Randomised Parallel assignment n = 98 (male, adults)	Consumed daily for 4 weeks; i. 8 LSF capsules (4 capsules B.I.D, total of 169.21 mM of LSF) ii. Or 8 placebo (4 B.I.D)	Not yet reported

Prostate cancer	Single-arm study n = 20 (male, adults)	20wk trial of subjects consuming 4 capsules of LSF (200 mM) daily.	Only one patient resulted in >50% declines of PSA after LSF treatment. There was a significant increase in PSA doubling time from 6.1months to 9.6months while on treatment compared to pre-treatment (p = 0.044). Grade I and grade II events were recorded, yet no severe adverse effects from LSF.
Prostate cancer	Pilot study Randomised Double-blind study Placebocontrolled Parallel assignment n = 40 (male, adults)	15 capsules are to consumed daily during the course of their respective chemotherapy treatment: i. 90 mg of LSF (~507 mM) ii. Placebo: methylcellulose (90 mg)	Ongoing, results not yet reported

Population Cohort	Study Design	Study Arms	Results
Abnormal breast mammograms	Randomised Double-blinded Parallel assignment Placebo controlled n = 54 (female, adults)	8wk trial; i. BroccoMax ii. Placebo	A decrease in total cell proliferation in ductal carcinoma in situ tissue, with an inverse association of Ki67 (p=0.004, SE = 0.001 and FDR q value = 0.03), this was not observed in benign or invasive ductal carcinoma tissue after BroccoMax consumption.
Nasal allergic response to DEP	Single-arm n = 29 (adults)	4 day wash out period followed by 4 consecutive days of daily consumption of; i. LSF-BSE (100 mmol) in mango juice	BSE treatment significantly decreased the log total cell count of the nasal lavage compared to the control and screening phases (p < 0.01 and p < 0.001 at 6 and 12hrs, respectively). No severe adverse events recorded.
Asthma	Non-randomised Single group assignment n = 44 (adults)	Consumed i. 100 mM of BSE in mango juice daily for 2wks;	60% of the asthmatics blocked the bronchoconstriction effects (decreased the FEV_1 response by 13 ± 8%, p = 0.002) of Mch after BSE consumption of which increased NQO1 expression and bronchoprotection increased (20.6 ± 72.8%), while 20% of asthmatics increased Mch effects (11 ± 11%, p = 0.004) decreased NQO1 expression, bronchoprotection decreased (54.4 ± 78.3%).

COPD	Phase 2 Randomised Parallel assignment Placebocontrolled n = 89 (adults)	4wk trial of daily ingestion of either; i. Placebo (microcellulose) ii. LSF (25 mmol) iii. LSF (150 mmol)	No significant differences were found amongst group for antioxidants and inflammatory markers (Nrf2) nor pulmonary function. No treatment related severe adverse events were found.
Asthma	Randomised Double-blind Parallel assignment n = 40 (adults)	Ingest daily for 3 days; i. 100g of broccoli sprouts ii. Placebo: 100g of alfalfa sprouts	Ingestion of BSE did not improve overall experimental parameters (FENO, antioxidant biomarkers, inflammatory markers). Although a defined increase of LSF concentration within serum levels (21 vs 22 ppb, $p = 0.76$).
Diabetes			
Type 2 diabetes	Randomised Parallel assignment Double-blind study n = 97 (adults)	Consumed daily for 12wks; i. BSE powder (150 mM of LSF) ii. Placebo powder	BSE reduced HbA1c (0.2 mmol/mol reduction per 1 mmol/mol, $p = 0.004$) and reduced fasting glucose (8.3 ± 0.3 mM as compared to the placebo group 9±.4 mM, $p = 0.023$), while obese dysregulated patients significantly improved fasting glucose ($p = 0.036$) and change in HbA1c levels ($p = 0.034$) after BSE treatment. No severe adverse side effects.

Population Cohort	Study Design	Study Arms	Results
Type 2 diabetes	Randomised Double-blind Parallel assignment Placebocontrolled n = 72 (adults)	Consume daily for 4wks; i. 10g of BroccoPhane (~225 mM of LSF) ii. 5g of BroccoPhane (~112.5 mM of LSF) iii. Placebo: 5g of cornstarch powder	LSF consumption significantly decreased fasting glucosee 8.13-7.03 mmol/l and 9.38 -7.48 mmol/l for 5g and 10g of BroccoPhane as compared to baseline levels, respectively. 10g of BroccoPhane significantly reduced insulin resistance (2.21±1.55, $p < 0.05$) and insulin resistance index (5.20±4.35mU/l; $p < 0.05$) as compared to the controls and baseline levels. No severe adverse events were recorded.
Other			
Epidermolysis bullosa simplex	Pilot Randomised Splitbody assignment Single-blind study Placebo controlled n = 4 (adults)	Applied topically to the inner arm daily for 1wk: i. BSE (500 nmol of LSF/mL) ii. Vehicle alone	Topical treatment of BSE activated KRT17 significantly (mean increase 3.6- ±0.2-fold, $p = 0.0022$) in all patients, while nonsignificantly increased NQO1 in 3 of the 4 patients.

GSTM1 genotype	Randomised Crossover assignment n = 16 (adults)	21 day interval between the consumption of either; i. 150 mL of standard broccoli soup ii. 150 mL super broccoli soup, or iii. Placebo: 150 mL of water	Super broccoli consumption was found to have ~3 fold greater amounts of LSF than std broccoli in serum levels. GSTM1-null subjects had marginally higher, yet not significantly, LSF concentrations than GSTM1-positive subjects.
Helicobacter pylori infection	Randomised Double-blind Parallelassignment Placebocontrolled n = 48 (adults)	8wk trial: i. 70g of BSE (420 mM of LSF) ii. Placebo: 70g of alfalfa	LSF significantly reduced bacterial infection ($p < 0.05$). Inflammation (PGI and PGII) of the gastric lumen significantly ($p < 0.05$) reduced in the LSF treated group, and returned to baseline levels after the completion of the study. No adverse reactions to BSE were recorded.
Helicobacter pylori infection	Randomised Parallel assignment n = 9 (adults)	Patients consumes twice daily for 7 days: i. 14g BSE, ii. 28g BSE, or iii. 56g BSE	The Helicobacter pylori infection was completely eradicated in one patient from each of the intervention groups.
Osteoarthritis	Randomised Parallel assignment Double-blind study n = 40 (adults)	Patients were first subject to a 7 day wash out period, before consuming daily for 14 days either: i. 100g of low glucosinolate broccoli, or ii. 100g of high glucosinolate broccoli	Patients that ingested high glucosinolates compared to low glucosinolates had significantly higher detectable levels of LSF (0.320.02 mean change, respectively, $p < 0.0001$). High glucosinolates had detectable levels of ITCs in their synovial fluid of the knee (mean 496.6 nM).
Sickle Cell Disease	Phase 1 Randomised Parallel, and crossover assignment Open-label n = 15 (adults)	To be consumed daily for 21 days: i. 50g BSE ii. 100g BSE iii. 150g BSE	Significant increases in whole blood Nrf2 markers hmox1 ($p = 0.045$) and hgb1 ($p = 0.0253$) at doses of 100e150g of BSE were determined pre- and post-treatment. No severe adverse events were likely to be related to BSE consumption.